DOCTORAL DISSERTATION

Study on Microstructure Control and Thermoelectric Properties of β-$FeSi_2$/Si Composites

JULY, 2019

FARAH LIANA BINTI MOHD REDZUAN

Osaka University

Graduate School of Engineering

Abstract

Thermoelectricity is one of the promising concept significant to the waste heat recovery system towards managing issues on energy resources. It allows the wasted heat to be directly converted to electricity. This thesis focuses on the newly introduced semiconducting β-$FeSi_2$/Si based composites as a potential thermoelectric (TE) material. The new idea is initiated by utilizing eutectoid decomposition process of high temperature α-Fe_2Si_5 phase producing β-$FeSi_2$/Si duplex phase. This counters the issue on the long production process of β-$FeSi_2$ originated from the peritectoid reaction of α-Fe_2Si_5 and ε-FeSi phases. At the same time, the coexisting of Si is expected to precipitate finely, small enough to help reduce thermal conductivity (κ). The aim to clarify the process viable in improving both electrical and thermal properties is focused towards enhancing the thermoelectric (TE) performance of β-$FeSi_2$/Si based composites.

Chapter 1 introduces this work by discussing the (1) the fundamentals of TE, (2) selection of TE material and (3) strategies constructed towards enhancing TE performance value (ZT value).

Chapter 2 initiates the attempt of synthesizing β-$FeSi_2$/Si composite. The annealing conditions viable for decomposition of α-Fe_2Si_5 producing β-$FeSi_2$/Si composites is observed at 800℃ for 4 h. The evaluation from electrical and thermal properties of β-$FeSi_2$/Si composite shows a high value of electrical resistivity (ρ) and κ, unfavorable for TE performance enhancement. This is possibly due to the precipitations of Si. However, the ZT value is significantly enhanced when compared to the single phase β-$FeSi_2$ and Co doped β-$FeSi_2$ because of the scattering character in β-$FeSi_2$/Si composites. Furthermore,

Si phase itself has a high value of Seebeck coefficient (S).

Chapter 3 discusses the attempt to improve ρ of β-$FeSi_2$/Si composite by introducing Co as dopant within the main phase of β-$FeSi_2$. We found that doping of Co did not affect the fine precipitations of Si within the main β-$FeSi_2$ phase and Co helps reduce ρ value significantly. However, both ρ and κ values of composite are still higher than that of the Co doped β-$FeSi_2$ single phase ones.

Chapter 4 discusses the attempt to further improve ρ of Co doped β-$FeSi_2$/Si composite by doping of P in secondary phase Si. We found that P could not be distributed uniformly within the Si secondary phase. However, the ρ is greatly reduced when P is doped. The intervention of P in Si phase also helps reduce κ of this composite.

Then, efforts to further reduce κ of composite by minimizing the size of Si is discussed in **chapter 5**. We added Cu to Co doped β-$FeSi_2$/Si composite resulting to the reduction of Si size reaching less than 100 nm in size, thus reducing its κ value.

We tried to clarify the effects on annealing conditions towards phase transformation rate of β-$FeSi_2$/Si based composites in **chapter 6**. We found that composites with Cu transformed more rapidly than composites without Cu in them. These findings will be useful for future attempts in setting the best annealing conditions to obtain β-$FeSi_2$/Si based composite with the most significant microstructure towards enhancing its TE performance attributed by the distinct reduction of κ.

In **chapter 7**, we conclude that - (1) jointly doping of Co and P improves electrical properties, (2) adding Cu reduces κ from the reduction of Si size, (3) quantitative evaluation on annealing conditions may help achieve microstructure essential for further reduction of κ. This enables us to provide significant indications of the process achievable towards enhancing TE performance.

Acknowledgement

In the name of Allah, the most Gracious and the most Merciful

A special thanks to my family who has been very supportive and have not stopped praying and hoping for my success.

A very special appreciation and thanks to my supervisor, Assoc. Professor ITO MIKIO, you have been a tremendous mentor, supporter and advisor to me. I would like to say thank you for encouraging me throughout my research and gave me the chance and space to develop my thinking and working skills needed as a developed research student. I am also thankful for the flexibility you gave for me to balance my family-related matters.

I would also like to express my appreciation to Professor TAKEDA MASATOSHI from Nagaoka University of Technology for the continuous support, help and advices in realizing this research work, both directly and indirectly.

Next, I would like to thank all my lab members who have not only helped me to learn a lot of things but also tolerated to communicate with me despite my limited availability to converse in Japanese. Without these individuals, I may not have the ability to even start this research project.

Lastly I would also like to thank each and every individual who has been helping me throughout the completion of this thesis, directly or indirectly. I hope that this thesis can be a good reference and the research project itself can be part of the crucial development of energy-conserving related researches and projects.

Table of contents

Chapter 1 Managing energy issues via waste heat recovery

1.1 Background

Energy is an essential element of material, wealth and a fundamental source, contributing impacts to the human beings and the environment. When energy becomes insufficient due to limited sources and high costs, people suffer from lack of direct energy services to perform daily routines of cooking, washing, heating and others. On the other hand, lack of efficiency in handling energy sources and usage can lead to environmental problems, sinking economic benefit. Generally, population growth rates and geographic distribution of human populations influence the demands of energy and usage. However, the real global energy problem is that we nearly run out of the low cost energy that has been triggering most industrial development of today's rich countries, disadvantaging the poor ones [7].

Japan is a country with very little energy resources, and this situation continues to worsen due to the two oil crisis in the 1970's to the present day [18,22]. As a result, there are three main policies regarding energy management, set by the government to face this issue while maintaining its high growth and development in science and technology [18];

I to ensure economic growth that meets the need of Japan's population and labor activities

II to ensure the stability and security of energy

III to protect the environment responding to the growing problems and issues on global warming

Responding to these policies, Japan has been focusing their efforts in these four areas: the strengthening of energy conservation measures

I promotion of the introduction of new energy

II promotion of nuclear energy development;

III expansion of the use of natural gas.

Current situations highlight that with little natural energy resources, Japan relies on imported oil, natural gas, and coal to meet high energy demand [33]. Environmental issues occurred from the expansion of residues from these resources such as emission of CO_2 are also worrying. Furthermore, Japan is highly facilitated with over 50 nuclear power plants as their energy sources. Unfortunately, the tragic disaster of tsunami and earthquake that hits Japan caused severe damages to the Fukushima power plant in March 2011. This results in shutdown of 48 out of 50 power plants, increasing the spending of Japan to reach $250 billion per year on imported oil, gas, and coal [33].

Therefore, importance in expanding the development of renewable energy is getting essential. The Japanese government has set renewable energy targets between 25% and 35% of total power generation by 2030, where $700 billion needs to be invested in new, renewable energy development [33]. In this regard, the efforts towards developing renewable energy triggers the use of waste heat recovery systems.

Our environment encounters more than 60% of wasted heat released by human activities from industrial, transportation, residential and institutional area. For example, waste heat generated from industrial processes like heat conduction, convection and radiation via industrial products, equipment and systems [2,13]. Therefore, applying waste heat recovery system in industrial processes can help reduce fuel consumption, lower harmful emissions and improve production efficiency. Consequently, this work is

inspired by the need to recover wasted heat via the significant research in thermoelectric material, the most fundamental area in thermoelectricity [17].

1.2 Understanding thermoelectric

Thermoelectricity is a concept of applying direct conversion from heat to electricity. Exceptional benefits of thermoelectricity include [8] :

I Made of simple structure

II Small and lightweight

III Zero dependence on moving element resulting in high reliability and long lifetime.

IV Environmental friendly due to harmless generation output.

1.2.1 Thermoelectric history

There are three important individuals that contribute to the world of thermoelectricity initiated since the 18^{th} century. They are Thomas Johann Seebeck, Jean Charles Athanase Peltier and William Thomson, whom each discovered the Seebeck effect, Peltier effect and Thomson effect, respectively [6]. Both Seebeck effect and Peltier effect are the most basic principles of thermoelectricity, while Thomson effect has the mathematical relationship between the Seebeck and Peltier effects. In this study, we mainly focus on the principle of the Seebeck effect to discuss our findings.

1.2.2 Seebeck effect

Thomas Johann Seebeck discovered that a current will flow in a closed circuit when two dissimilar conductors with different temperatures are combined, that will be initiated by the Seebeck effect [6]. As shown in Fig. 1.1, consider a finite rod of a conducting material that is heated only on one end. The temperature gradient across the rod causes

diffusion of the charge carriers from the heated side to the cooler side. They will continue to move to the cooler side of the material until an equilibrium state is established. Increasing the temperature gradient between the two both ends will cause more charge carriers to move to the cooler side creating a new potential difference [6].

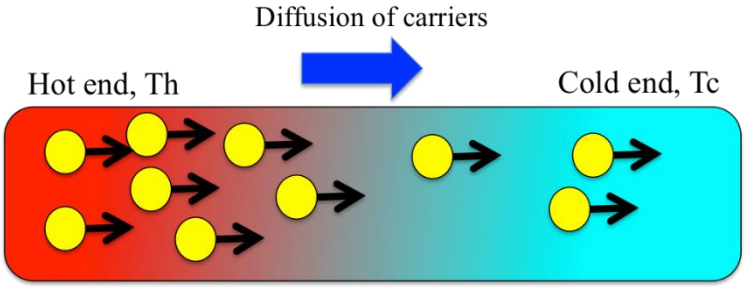

Figure 1.1 Illustration of Seebeck Effect's principle.

Therefore, as shown in Fig 1.2, if a temperature gradient exists at a junction of two dissimilar conductors connected electrically in series and thermally in parallel, a voltage is produced. This potential drop of $V = V_2 - V_1$ is the result of the of Seebeck effect.

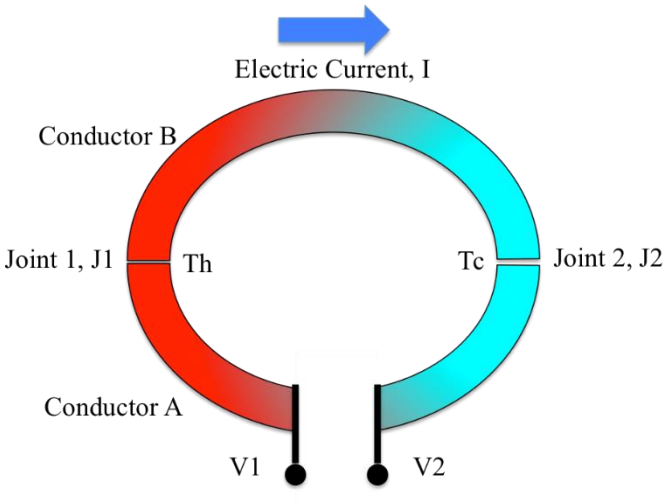

Figure 1.2 Schematic illustration of Seebeck effect's principle.

The voltage generated depends on the Seebeck coefficient, *S*, and the temperature difference, ΔT, between the two junctions in the thermocouple, as derived in Eq. 1.1.

$$S = \frac{V}{\Delta T} \quad \ldots \textbf{Equation 1.1}$$

1.2.3 Thermoelectric power generation

A thermoelectric power-generating module is constructed with *p*-type and *n*-type semiconductor elements [9]. The *p* and *n*-type elements are connected electrically in series and thermally in parallel [26]. The mechanism of thermoelectric power generation by applying the Seebeck effect in a π-type TE module is shown in Fig. 1.3.

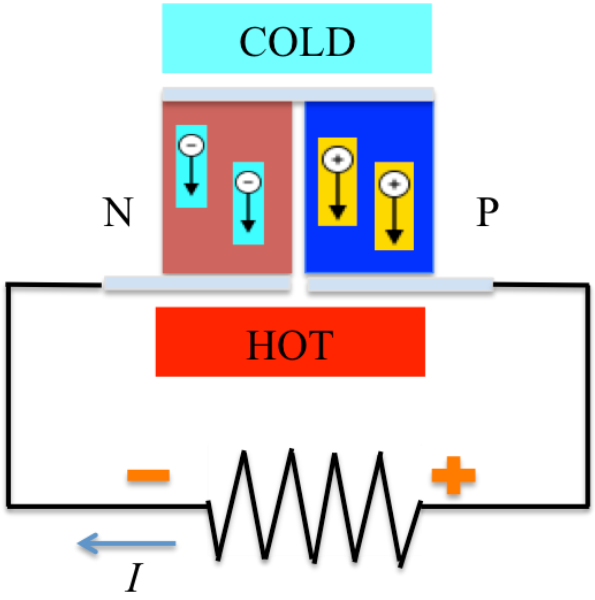

Figure 1.3 Schematic illustration of the π type thermoelectric module.

The electrons in the high temperature region of *n*-type semiconductor element, which are greater in number than holes are activated as heated. These electrons are diffused to the lower temperature region, generating thermal electromotive force, while the high

temperature side reaches a high electrical potential. On the other hand, higher amount of holes than that of electrons in the *p*-type semiconductor element causes the higher temperature region to be activated when heated. Then, these holes diffuse to the lower temperature region, generating thermal electromotive force while the lower temperature is maintained, which obtains a higher electrical potential [9]. When these two semiconductor elements are combined as shown in Fig. 1.3, electrical potential difference or voltage exists. As they are connected with a load resistance, electric current flows generating electrical power [9].

1.2.4 Performance evaluation of thermoelectric material

The development of thermoelectric material is the most fundamental effort in enhancing the performance and efficiency in thermoelectricity for wide usage and application. The power generating performance of thermoelectric conversion materials is expressed by the index Z, known as the figure of merit in the following Eq. 1.2.

$$\boldsymbol{Z = \frac{S^2}{\rho\kappa}} \quad \textbf{... Equation 1.2}$$

S, κ and *PF* are Seebeck coefficient, thermal conductivity and power factor respectively. *PF* is defined by S^2/ρ, generally known as the electrical property. Multiplying average absolute temperature of the thermoelectric system, *T* to both side of Eq. 1.2 develops to the definition of dimensionless figure of merit, *ZT*. Therefore, it is essential to identify thermoelectric material with high value of Seebeck coefficient and low value of both electrical resistivity and thermal conductivity.

1.3 β-$FeSi_2$ as the environmental friendly thermoelectric material

The development of thermoelectric material is the most fundamental effort in enhancing the performance and efficiency in thermoelectricity for wide usage and application. As mentioned in previous section, thermoelectric materials with high value of Seebeck coefficient, low value of both electrical resistivity and thermal conductivity are essential for performance enhancement. Thermoelectric materials' candidates are summarized in Fig. 1.4 which classifies the materials according to ZT value [5].

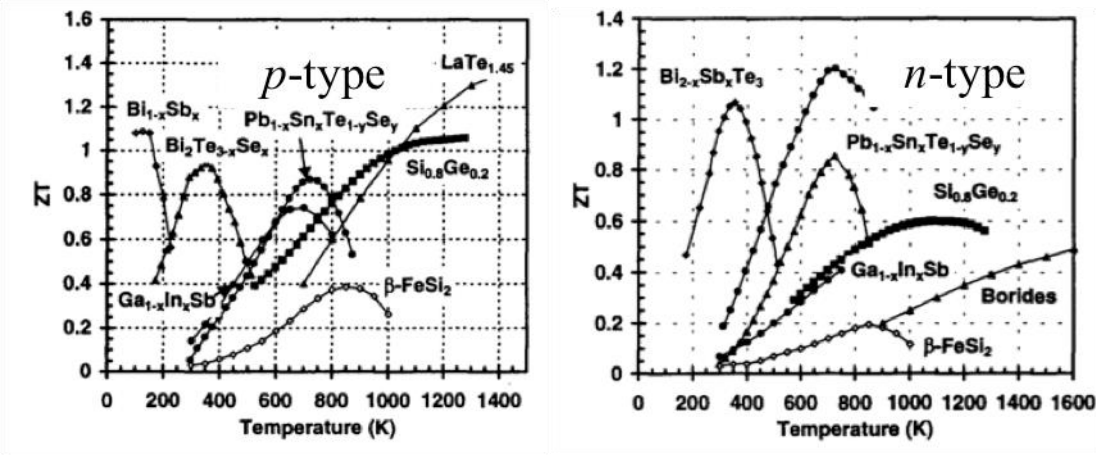

Figure 1.4 ZT value of thermoelectric materials' candidates.

Silicide is a group of thermoelectric materials consists of silicon (Si) as its main component of the alloys, which is abundant in resources on the earth, environmental friendly and cheap. This is essential towards realizing Japan's demand in energy. Example of thermoelectric materials from silicide group includes Mg_2Si, $MnSi_{1.73}$, β-$FeSi_2$ and so on. Among them, semiconducting β-$FeSi_2$ is one of the promising candidates for

thermoelectric materials. The precedence of semiconducting β-$FeSi_2$ includes;

I Available both in *p*-type and *n*-type.

II Exhibits high value of Seebeck coefficient.

III Exhibits high oxidation resistance.

On the other hand, the drawbacks of β-$FeSi_2$ include;

I Consumes a long time production process up to 3-5 days.

II Exhibits high value of electrical resistivity and thermal conductivity.

As a way to overcome the drawbacks above, a new heterogeneous phase of β-$FeSi_2$/Si composite has potentials to overcome these drawbacks because the production time of this phase is relatively short. Furthermore, the coexisting Si phase in this composite phase is likely able to help reduce both its electrical resistivity and thermal conductivity. This promising composite is introduced in detail in the following section.

1.4 New phase of β-$FeSi_2$/Si based composite

According to the binary phase diagram of the Fe-Si system [11], shown in Fig. 1.5, there are three main phases of FeSi compound ; metallic phases of (1) ε-FeSi and (2) α-Fe_2Si_5, followed by the (3) semiconducting phase of β-$FeSi_2$.

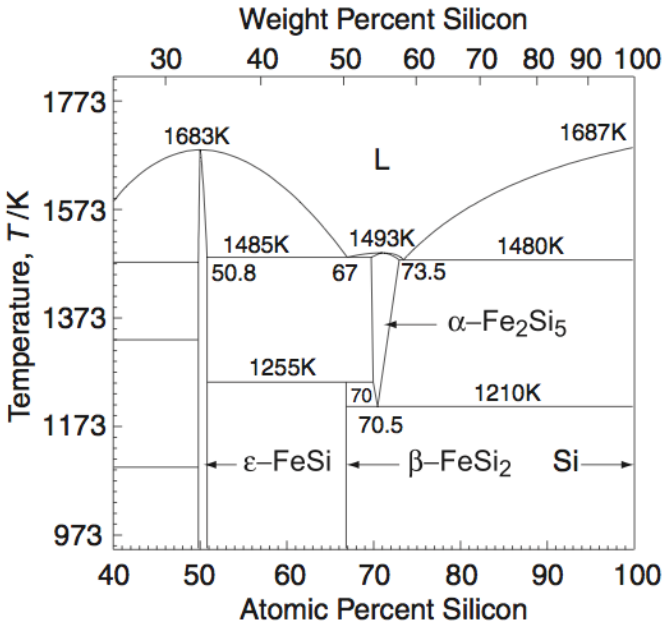

Figure 1.5 Binary phase diagram of the Fe-Si system [11].

This semiconducting phase of β-$FeSi_2$ mainly can be obtained by the following two reactions as shown in Table 1.1.

Table 1.1 Phase transformation reaction to obtain β-$FeSi_2$ phase.

Type of reaction	Phase transformation	Transition temperature (℃)
Peritectoid reaction	$\alpha + \varepsilon \rightarrow \beta$	980
Eutectoid decomposition	$\alpha \rightarrow \beta + Si$	900

Generally, these reactions engage through appropriate isothermal heat treatment at

certain temperature, known as annealing. In most studies, semiconducting phase of β-$FeSi_2$ is synthesized via peritectoid reaction. Peritectoid reaction involves the reaction of two solid phases of α-Fe_2Si_5 and ε-FeSi phase, yielding one new solid phase of β-$FeSi_2$. This reaction needs a long annealing time because the product phase will form at the boundary between the two reacting phases which is separating them, slowing down further reaction [24]. On the other hand, eutectoid decomposition involves the separation from one solid phase of α-Fe_2Si_5 phase to the two new solid phases of β-$FeSi_2$ and Si. Therefore, the annealing time needed for the formation of β-$FeSi_2$ can be largely reduced leaving no traces of other initial solid phases like ε-FeSi phase that usually requires a long time to be eliminated during peritectoid reaction [12]. The α-Fe_2Si_5 phase has a composition of Si more than two times higher than that of Fe, resulting to the final product of two-phase or composite structure. The composite structure consists of β-$FeSi_2$ as main matrix, followed by the Si secondary phase. The secondary phase was determined to exist in the form of fine precipitations. From here, we understand that the fine precipitations of Si helps increase the Seebeck coefficient, but increase electrical resistivity [1]. Nonetheless, it was expected that the fine Si precipitations helps contribute to the reduction of the thermal conductivity. This can be attributed to the increasing in phonon scattering [1]. Hence, the evaluation suggested that phonons with mean free path below 200 nm, which is the size of Si particles spacing, contributes to the reduction of lattice thermal conductivity [1].

1.5 Literature review - Strategies to enhance TE performance of β-$FeSi_2$/Si composite

In this section, we would like to elaborate on the strategies constructed in composing the aims and targets of this work towards enhancing the TE performance of β-$FeSi_2$/Si based composite. First, essential findings from previous works related to this work are discussed. As mentioned earlier in section 1.3, semiconducting β-$FeSi_2$ studied from the 1960's till present is still facing these two major issues:

I Exhibits a relatively low TE performance value due to the high value of electrical resistivity and thermal conductivity [1,10,15,25,27,32].

II Requires long processing time to obtain β-$FeSi_2$, reaching more than 4 days at 900℃ for complete transformation from the peritectoid reaction [14,23].

Previous efforts to encounter issue I mainly focus on introducing various doping elements that substitute Fe atoms in β-$FeSi_2$, to improve electrical conduction [4]. For example, doping of Mn, Cr, Al yields p-type conduction [23,28,29], while doping of Co and Ni that yields n-type conduction [3,27,29]. In addition, there were also attempts to substitute elements to the Si site with P producing n-type conduction [10]. However, the contradictory relation between electrical resistivity and thermal conductivity continue to cause insufficient enhancement of TE performance in β-$FeSi_2$ by only adding these dopants either to the Fe or Si site in β-$FeSi_2$.

Meanwhile, the attempts to solve issue II include by attempting improved synthesis methods like rapid solidification and hot pressing which helps accelerate the production of β-$FeSi_2$ [3]. Other than that, adding phase accelerating elements like Cu in order to increase phase transformation rate of β-$FeSi_2$ were also tried in these

previous works [20,31,32]. However, existence of Cu within β-$FeSi_2$ phase as a metallic element was found to cause deterioration in the thermopower or Seebeck coefficient of β-$FeSi_2$ leaving insufficient enhancement of TE performance for this material. Then, attempt on completely utilizing new composite phase of β-$FeSi_2$/Si with accelerated production process was also studied in previous works [11,12,16,21], leaving major drawback on the increase in electrical resistivity due to the precipitations of Si secondary phase. Nonetheless, the coexistence of Si precipitations may potentially be advantageous for reduction of thermal conductivity due to possible enhanced phonon scattering, which is not thoroughly studied and solidly proven from those previous works.

Complementing the idea on utilizing new composite phase of β-$FeSi_2$/Si with shorten processing time and possible reduction of thermal conductivity, we also expect that minimizing the size of Si precipitations in β-$FeSi_2$/Si may be valuable towards enhancing its TE properties, supported by the trending vast findings on bulk nanostructured TE material. This recent trend of studying bulk nanostructure materials with distinct enhancement of TE performance is further driven by the need to make nano-structured TE materials applicable because fabrication process to produce nano-structures like quantum dots are only available in thin films, which remains impractical for wide usage [19]. Furthermore, the recent progress of approaching nano-structuring in bulk TE material is found to be significant in reducing thermal conductivity with minimum degeneration in electrical properties thus increasing the ZT value efficiently [30].

Therefore, this thesis aimed to clarify the processes feasible to improve both electrical and thermal properties of the β-$FeSi_2$/Si based composite towards enhancing its TE

performance. We aimed that the newly introduced β-$FeSi_2$/Si based composite with a significantly accelerated time of synthesis, to be consisting of fine Si precipitations within the main β-$FeSi_2$ phase. Subsequently, the fine precipitations may help further reduce thermal conductivity. We initiated this work by attempting to synthesize β-$FeSi_2$/Si composite via the eutectoid decomposition of high temperature metallic α-Fe_2Si_5 phase, which can be obtained from annealing process. We then aimed to improve electrical properties of the β-$FeSi_2$/Si composite without deteriorating its thermal properties by adding n-type dopants. First, doping of Co is expected to cause substitution of Co atoms for Fe atoms within the main phase of β-$FeSi_2$. Then, jointly doping of P is expected to cause substitution of P atoms for Si atoms preferably in the Si secondary phase with high electrical resistivity, which is also expected to be beneficial for further improvement in TE properties. We also aimed to improve its thermal properties by controlling the microstructure of the composite from adding Cu to the β-$FeSi_2$/Si based composite because previous studies have proven the accelerated phase transformation in the peritectoid reaction yielding β-$FeSi_2$ phase mentioned earlier. Therefore, we can expect a further reduction in Si size within the β-$FeSi_2$/Si based composite after Cu is added. The reduced size of Si is expected to be achievable as the decomposition of α-Fe_2Si_5 phase is accelerated yielding the composite phase at a lower annealing temperature and shorter annealing time. Furthermore, we also tried tuning various annealing conditions in the effort to control the size of Si, and make the Si size small enough to help reduce thermal conductivity where phonon scattering is expected to be greatly enhanced. Hence, these concurrent efforts are expected to be conducive for providing guidance on the viable processes towards vast enhancement in TE properties of β-$FeSi_2$ based TE material.

1.6 Thesis Organization

The remainder of this work is organized as follows:

Chapter 2 initiates the discussion in the attempt of synthesizing β-$FeSi_2$/Si composite. This chapter focuses on the annealing conditions viable for decomposition of α-Fe_2Si_5 producing β-$FeSi_2$/Si composites. The electrical properties of β-$FeSi_2$/Si composite are also evaluated and discussed. **Chapter 3** discusses the attempt to improve the performance of β-$FeSi_2$/Si composite by introducing Co as doping element within the main phase of β-$FeSi_2$. This time we use sintered bodies in order to not only produce samples measureable for high temperature analysis toward defining its thermoelectric performance, but also with improved electrical properties as they are more densified. **Chapter 4** discusses the attempt to co-dope P in secondary phase Si towards enhancing its thermoelectric performance without eliminating the composite structure in Co doped β-$FeSi_2$/Si with fine precipitations of Si. **Chapter 5** discusses the attempt to further minimize the size of Si by adding Cu, which then proves that the minimized size of Si reaching less than 100 nm in size cause a great decrease in thermal conductivity. **Chapter 6** discusses the kinetics of decomposition of α-Fe_2Si_5 producing β-$FeSi_2$/Si composites. Here we compare phase transformation analysis of β-$FeSi_2$/Si composites with and without Cu. From this findings, they will be useful for future attempts in setting the best annealing conditions to obtain β-$FeSi_2$/Si with the most significant microstructure towards enhancing its thermoelectric performance. In **chapter 7**, we conclude our work by emphasizing the major novel findings of this work. Moreover, we also include the remaining issues that require future attention for the enhancement in thermoelectric material.

1.7 References

[1] U. Ail, S. Gorsse, S. Perumal, M. Prakasam, A. Umarji, S. Vivès, P. Bellanger, R. Decourt, *Thermal conductivity of β-$FeSi_2$/Si endogenous composites formed by the eutectoid decomposition of α-Fe_2Si_5*, J. Mater. Sci. 50 (2015) 6713–6718.

[2] I. BCS, *Waste Heat Recovery: Technology and Opportunities in U.S. Industry*, U. S. Department of Energy, 2008.

[3] H.Y. Chen, X.B. Zhao, C. Stiewe, D. Platzek, E. Mueller, *Microstructures and thermoelectric properties of Co-doped iron disilicides prepared by rapid solidification and hot pressing*, J. Alloys Compd. 433 (2007) 338–344.

[4] M.I. Fedorov, G.N. Isachenko, *Silicides: Materials for thermoelectric energy conversion*, Jpn. J. Appl. Phys. 54 (2015) 07JA05.

[5] J.-P. Fleurial, *Design and Discovery of Highly Efficient Thermoelectric Materials*, Int. Union Mater. Res. Soc. - Florence, Italy. (1998).

[6] P.D. Heinz, *First Principles Study of Thermoelectric Properties*, 2010.

[7] J.P. Holdren, *Population and the Energy Problem*, Popul. Environ. 12 (1991) 231–255.

[8] B. Ismail, W. Ahmed, *Thermoelectric Power Generation Using Waste-Heat Energy as an Alternative Green Technology*, Recent Patents Electr. Eng. 2 (2009) 27–39.

[9] B. Ismail, W. Ahmed, *Thermoelectric Power Generation Using Waste-Heat Energy as an Alternative Green Technology*, Recent Patents Electr. Eng. 2 (2009) 27–39.

[10] M. Ito, H. Nagai, E. Oda, S. Katsuyama, K. Majima, *Effects of P doping on the thermoelectric properties of β-$FeSi_2$*, J. Appl. Phys. 91 (2002) 2138–2142.

[11] J. Jiang, K. Matsugi, G. Sasaki, O. Yanagisawa, *Resistivity Study of Eutectoid Decomposition Kinetics of α-Fe_2Si_5 Alloy*, Mater. Trans. 46 (2005) 720–725.

[12] J.X. Jiang, T. Sasakawa, K. Matsugi, G. Sasaki, O. Yanagisawa, *Thermoelectric properties of β-$FeSi_2$ with Si dispersoids formed by decomposition of α-Fe_2Si_5 based alloys*, 391 (2005) 115–122.

[13] H. Jouhara, N. Khordehgah, S. Almahmoud, B. Delpech, A. Chauhan, S.A. Tassou, *Waste heat recovery technologies and applications*, Therm. Sci. Eng. Prog. 6 (2018) 268–289.

[14] S. Kiatgamolchai, J. Parinyataramas, S. Nilpairach, A. Thueploy, J. Wanichsampan, M. Gao, *Thermoelectric properties of β-$FeSi_2$ prepared by the mechanical alloying technique and pressureless sintering*, Acta Metallurgica Slovaca, 12 (2006) 119–127.

[15] N. Kiyoshi, K. Takuji, *Influence of Copper Addition on the Rapid Production of β-$FeSi_2$ by Spark-Plasma Sintering*, Materials Transaction 41 (2005) 815–821.

[16] T. Kojima, K. Masumoto, M.. Okamoto, I. Nishida, *Formation of β-$FeSi_2$ from the sintered eutectic alloy FeSi-Fe_2Si_5 doped with cobalt*, J. Less Common Met. 159 (1990) 299–305.

[17] P. Kolasiński, E. Kolasińska, *Direct waste heat recovery via thermoelectric materials - Chosen issues of the thermodynamic description*, IOP Conf. Ser. Mater. Sci. Eng. 113 (2016).

[18] C.E. Markets, K. Ito, Y. Morita, A. Yanagisawa, S. Suehiro, R. Komiyama, Z. Shen, *Japan Long-Term Energy Outlook*, (2006) 1–70.

[19] A.J. Minnich, M.S. Dresselhaus, Z.F. Ren, G. Chen, *Bulk nanostructured thermoelectric materials: current research and future prospects*, Energy Environ.

Sci. 2 (2009) 466.

[20] H. Nagai, H. Nakayama, S. Katsuyama, K. Majima, *Preparation and themoelectric properties of sintered β-$FeSi_2$ doped with Cu by MG*, Japan Society of Powder and Powder Metallurgy, 42 (1995) 151–155.

[21] T. Nagase, I. Yamauchi, I. Ohnaka, *Eutectoid decomposition in rapidly solidified α-Fe_2Si_5-based thermoelectric alloys*, J. Alloys Compd. 316 (2001) 212–219.

[22] S. Nakakuki, *Discussion Points in Japan's Renewable Energy Promotion Policy Effect* , Impact and Issues of the Japanese RPS, (2003) 1–13.

[23] I. Nishida, *Study of Semiconductor-to-Metal Transition in Mn-Doped $FeSi_2$*, Phys. Rev. B. 7 (1973) 2710.

[24] D.A. Porter, E.E. Kenneth, M.Y. Sherif, *Binary Phase Diagrams*, in : Phase Transform. Met. Alloy, 3 (2014) 31–40.

[25] F.L.B.M. Redzuan, I. Mikio, T. Masatoshi, *Synthesis of Co-doped β-$FeSi_2$/Si composites through eutectoid decomposition and its thermoelectric properties*, J. Mater. Sci. 53 (2018) 7683–7690.

[26] D.M. Rowe, *Thermoelectric Waste Heat Recovery as a Renewable Energy Source*, Int. J. Innov. Energy Syst. Power. 1 (2006) 13–23.

[27] J. Tani, H. Kido, *Electrical properties of Co-doped and Ni-doped β-$FeSi_2$*, J. Appl. Phys. 84 (1998) 1408–1411.

[28] J. Tani, H. Kido, *Electrical Properties of Cr-Doped β-$FeSi_2$*, Jpn. J. Appl. Phys. 38 (1999) 2717.

[29] U. Birkholz J. Schelm, *Mechanism of Electrical Conduction in β-$FeSi_2$*, Basic Solid State Phys. 27 (1968) 413–425.

[30] A. Usenko, D. Moskovskikh, A. Korotitskiy, M. Gorshenkov, A. Voronin, D.

Arkhipov, M. Lyange, G. Isachenko, V. Khovaylo, *Thermoelectric Properties of n-Type $Si_{0.8}Ge_{0.2}$-$FeSi_2$ Multiphase Nanostructures*, J. Electron. Mater. 45 (2016) 3427–3432.

[31] I. Yamauchi, T. Okarnoto, H. Ohata, I. Ohnaka, *3-phase transformation and thermoelectric power in $FeSi_2$ and Fe_2Si_5 based alloys containing small amounts of Cu*, J. Alloys Compd. 260 (1997) 162–171.

[32] I. Yamauchi, S. Ueyama, I. Ohnaka, *β-$FeSi_2$ Phase formation from a unidirectionally solidified rod-type eutectic structure composed of both α and ε phases*, Materials Science and Engineering A 208 (1996) 108–115.

[33] *Economic and Energy Outlook of Japan through FY2018 in Executive summary of outlook through FY2018*, Macro economy, (2017) 1–5.

Chapter 2

β-$FeSi_2$/Si composite as a promising candidate of thermoelectric material

2.1 Overview

This chapter discusses the attempt to synthesize the newly introduced heterogeneous phase of β-$FeSi_2$/Si composites by annealing samples with the initial phase of α-Fe_2Si_5. There were two methods tried to synthesize the α-Fe_2Si_5 phase; (1) the arc melting method, and (2) the spark plasma sintering (SPS) method. We then annealed these samples at 800℃ to obtain β-$FeSi_2$/Si phase. The annealing time varies from 4 h to 48 h for method (1). Then, the relation of 'annealing time-resistance' from phase transition analysis was done to determine the shortest annealing time needed at 800℃. From here, we chose 4 h as the annealing time to proceed from method (2). This is because phase transition analysis shows a constant value of resistance at approximately 4 h after annealing. TE performance analysis shows that β-$FeSi_2$/Si phase has a very high value of electrical resistivity at room temperature due to the precipitation of Si, expected to degenerate the TE performance. However, Seebeck coefficient of β-$FeSi_2$/Si was found to be higher than that of both single phase non-doped β-$FeSi_2$ and Co-doped β-$FeSi_2$ ones. On the other hand, the expected suppression of thermal conductivity due to the precipitations of Si could not be achieved. Nonetheless, the significant improvement in Seebeck coefficient leads to the vast increase in ZT value, enhancing performance β-$FeSi_2$ based TE material.

2.2 Introduction

As mentioned in section 1.3 of chapter 1, it is essential to expand the study on enhancing thermoelectric properties of β-$FeSi_2$ by focusing on the new potential composite phase of β-$FeSi_2$/Si. The co-existing Si in this composite phase has a very high value of thermal conductivity and electrical resistivity [11] despite the high value of thermopower it exhibits. We found various studies on nano-structuring of Si materials, which remains effective to improve electrical properties and decrease thermal conductivity in many silicide materials [2]. As the first step of this work in this chapter, we attempt to produce β-$FeSi_2$/Si composite by initially synthesizing high temperature metallic phase of α-Fe_2Si_5. We melt the Fe and Si pieces producing α-Fe_2Si_5 using arc melting method. Arc melted samples are expected to be small in size and brittle due to the existence of cracks, limiting its further evaluation in high temperature environment. Therefore, we consider another method of obtaining α-Fe_2Si_5 phase via SPS method after confirming the best annealing time at 800℃ from the phase transformation analysis. The phase transformation analysis is the evaluation at selected isothermal temperature of 800℃, where the relation of annealing time at that temperature and electrical resistance is determined. We finally determined the potential of these newly introduced phase by evaluating the TE properties and comparing them with previously studied singular phase of β-$FeSi_2$ and Co doped β-$FeSi_2$ up to higher temperature range.

2.3 Experimental procedures

This section divides the experimental procedures for the study on β-$FeSi_2$/Si composite to the synthesize process and properties analysis process as illustrated in Fig. 2.1.

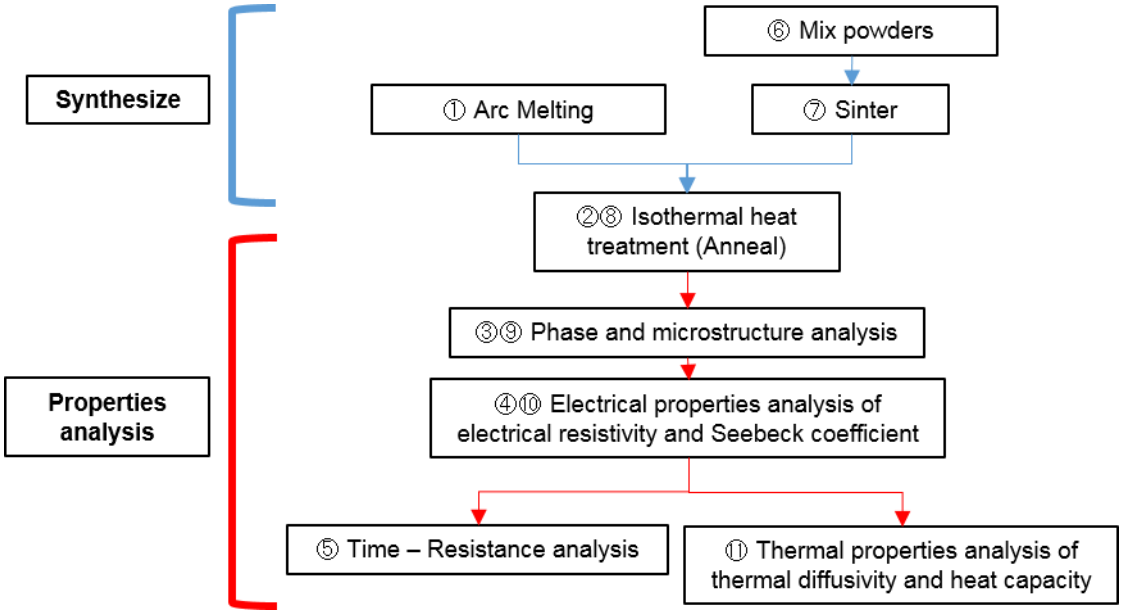

Figure 2.1 Graphical flow of experimental procedures.

There are 2 parts of procedures discussed in this chapter.

I Step ①-⑤; this part discusses the first-step method to obtain β-$FeSi_2$/Si composite in a smaller scale, followed by electrical properties analysis at room temperature. Analysis of 'Time-Resistance' to determine its kinetics in phase transformation was also done at the annealing temperature that is found conducive for complete decomposition of α-Fe_2Si_5 to β-$FeSi_2$/Si composite.

II Step ⑥-⑪; This part applies the annealing conditions revealed from the first part, for sintered bodies expected to be larger in size and more durable. The

processed sample was then evaluated until high temperature of 700℃ to determine its temperature dependence of thermoelectric performance value, from both electrical and thermal properties analysis.

The detailed description on sample's preparation, apparatus information and measurement conditions are described in the following sections.

2.3.1 Melting of samples via arc melting

Starting materials used are listed in Table 2.1. The materials were in bulk form (pieces/grains) to minimize the weight decrement during arc melting process to avoid error in composition of alloys produced.

Table 2.1 Description of powder types and amount used for arc melting process.

Material	Purity	Form
Si	99.9999%	Pieces (<20mm)
Fe	99.99%	Grains (5-15mm)

Weight of each material was calculated based on Eq. 2.1 to obtain a sample with a composition of $A_{xA}B_{xB}$ and weight of W_{total}.

$$W_i = \frac{M_i x_i}{M_A x_A + M_B x_B} W_{total} \quad \ldots \textbf{Equation 2.1}$$

where W_i is weight of material i (i=A, B), M_i is atomic weight of material i. Weighed sample was inserted into an arc furnace (ACM-C01 Diavac Limited) as illustrated in Fig. 2.2. Samples were melted by shooting arc towards starting materials from Tungsten (W) electrode producing ingot. The ingot was turned over and melted again. This process was repeated several times. Weight of ingot was then measured to calculate the weight

difference of before and after melting. From here, error in composition was considered to occur if the weight of decrement exceeds 2% of its original weight. Therefore, we did not utilize samples with reduced weight of more than 2%.

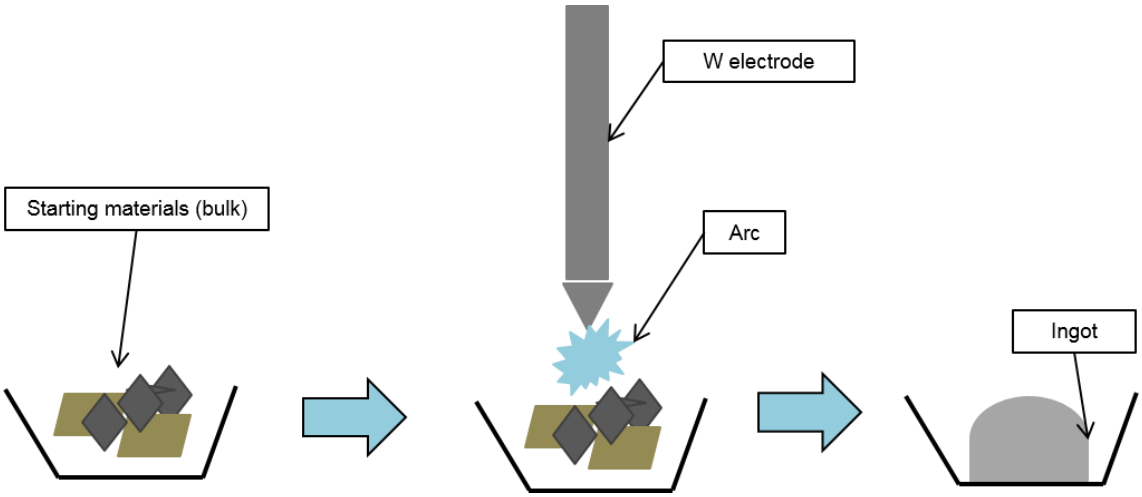

Figure 2.2 Schematic illustration of arc melting process.

2.3.2 Isothermal heat treatment (Annealing) of ingot

These ingots were set in a furnace for isothermal annealing process under argon (Ar) atmosphere. The annealing conditions are summarized in Table 2.2. This chapter focuses on the annealing temperature of 800℃ due to the previous findings by Jiang.X et al., where 800℃ is the essential annealing temperature for complete decomposition of α-Fe_2Si_5 phase yielding β-$FeSi_2$/Si heterogeneous phase at a faster rate [5].

Table 2.2 Annealing conditions for ingots.

Temperature (℃)	Time (h)
800	4
	24
	48

2.3.3 Phase and microstructure analysis I

The evaluation from X-ray Diffraction (XRD) equipment (PANanalatical X'PERT PRO) was done to determine the phase of annealed ingots. The detailed information of apparatus and measurement conditions are summarized in Table 2.3.

Table 2.3 Apparatus and measurement condition of phase analysis via XRD

Apparatus condition	
Scintillation counter	Kβ filter
Slit conditions	DS / SS = 0.5°, RS = 0.3 mm
Incident side and receiving side Soller slit	2°
Incident height limiting slit	5.5 mm
Tube current	40 mA
Tube voltage	45 kV
Measurement condition	
Scan range	2θ = 10 ~ 70°
Step width	0.02°
Scan speed	4° / min.

The Scanning Electron Microscope (SEM) and the energy dispersive X-ray spectroscopy (EDX) are used to observe microstructure and to determine the element and composition of annealed samples. SEM-EDS equipment during this process was JOEL JSM-6360A. Evaluation via Auger Electron Spectroscopy (AES) equipment (AES PHI685-8) was performed to determine elements that could not be detected by SEM-EDS system through mapping the scanned image. AES is an analytical technique that uses a primary electron beam to probe the surface of a solid material. Auger electrons that are emitted as a result of the Auger process are analyzed and their kinetic energy is

determined. Element and quantity of the elements are determined from the kinetic energy and intensity of the Auger peaks. A finely focused electron beam can be scanned to create Auger electron and Auger images, or the beam can be positioned to perform microanalysis of specific sample features. We polished the observed surface of sample until it turns to a mirror-like surface with series of abrasive papers.

2.3.4 Electrical properties analysis at room temperature

The electrical resistivity and Seebeck coefficient are measured at room temperature (RT), manually by the ordinary 4 probe direct current (DC) unit. As shown in Fig. 2.3, sample was sandwiched between 2 Copper (Cu) blocks. Two T-type thermocouple probes were contacted on the upper surface of the sample to measure the electrical potential ΔV between the probes. Hence electrical resistivity is determined, as simultaneous current is flown between 0 mA to 100 mA.

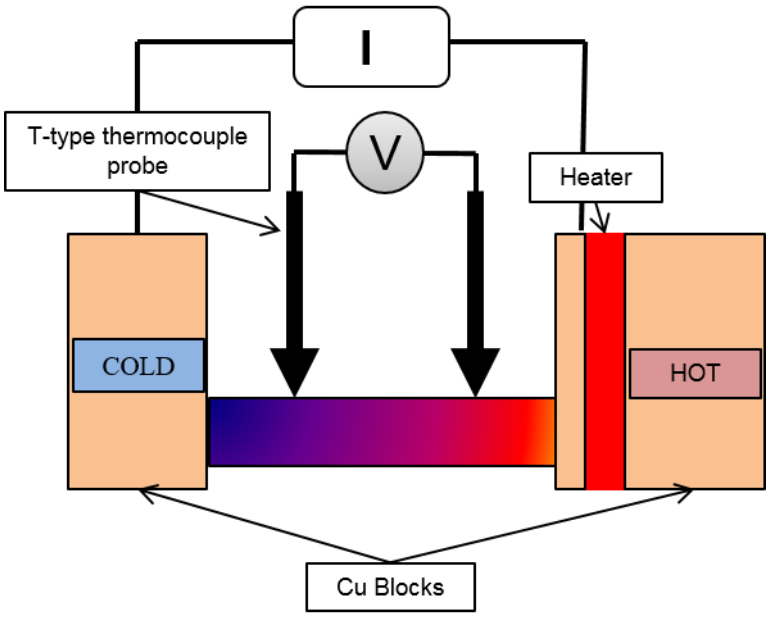

Figure 2.3 Schematic illustration of determining electrical resistivity at RT.

During the measurement of Seebeck coefficient, as illustrated in Fig. 2.4, a heater is set at one end to create a temperature difference of 5℃, creating electrical potential difference ΔV. Thus, Seebeck coefficient is calculated from the relation of $\Delta V = S\Delta T$.

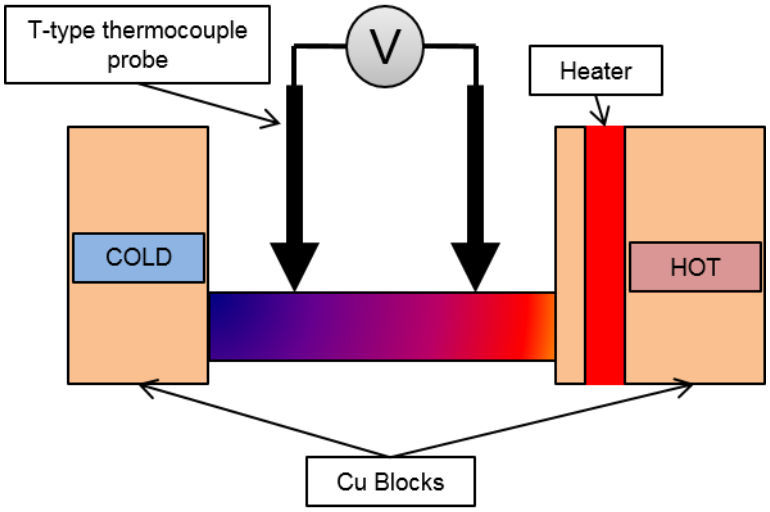

Figure 2.4 Schematic illustration of determining Seebeck coefficient at RT.

2.3.5 Phase transformation analysis

The relation of 'annealing time-electric resistance' was determined to analyze the occurrence point of complete phase transformation, in this case the decomposition of α-Fe_2Si_5 producing β-$FeSi_2$/Si composite phase. As illustrated in Fig. 2.5, a cut sample is placed in a lamp furnace, and the furnace temperature is set to 800℃. A source measure unit (YOKOGAWA GS610) provides electric current, measuring electrical resistance. From here, the relation of electrical resistance and annealing time is plotted.

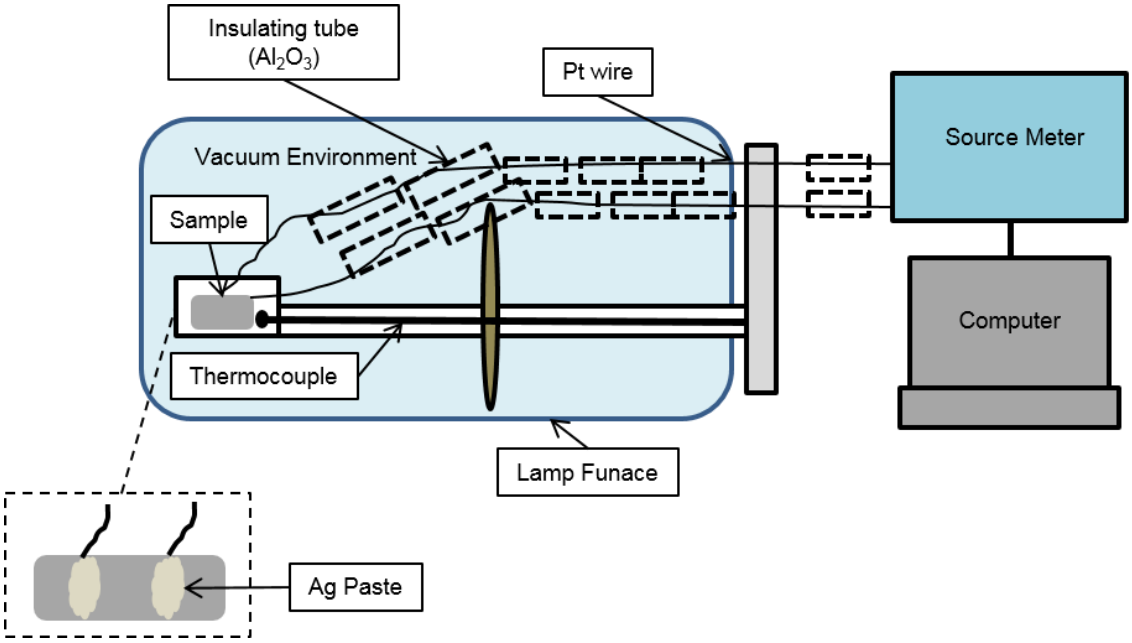

Figure 2.5 Schematic illustration for phase transition analysis.

2.3.6 Mixing of powders

Powders of Fe, Si and Co as described in Table 2.4 are mixed with a planetary ball mill in a stainless steel (SUS) pot under argon (Ar) atmosphere, together with SUS balls and Hexane. The powders were mixed at 300 rpm of speed for 5 h to obtain a homogeneous mixture of Fe, Si and Co powders. This will lead to the formation of single α-Fe_2Si_5 phase by the following sintering process, as described in the next section.

Table 2.4 Description of powder types and amount used during mixing process.

Element	Size (purity)	Manufacturer	Amount (atomic %)
Iron (Fe)	150 μm (99.9%)	Wako Pure Chemicals Industries, Ltd	29.5
Silicon (Si)	150 μm (99.9%)		70.5

2.3.7 Sintering process

The uniformed powder mixtures were then sintered with a Spark Plasma Sintering (SPS) machine (SPS – 511S SPS, Fuji Electronic Industrial Co., Ltd.) at 1000℃ for 10 minutes with the pressure of 50 MPa to form a pellet, in a vacuum condition (SPS – 511S SPS, Fuji Electronic Industrial Co., Ltd.). As shown in Fig. 2.6, mixed powders were sandwiched between 2 carbon punches in a dye, covered by carbon papers to avoid leakage of samples during the sintering process.

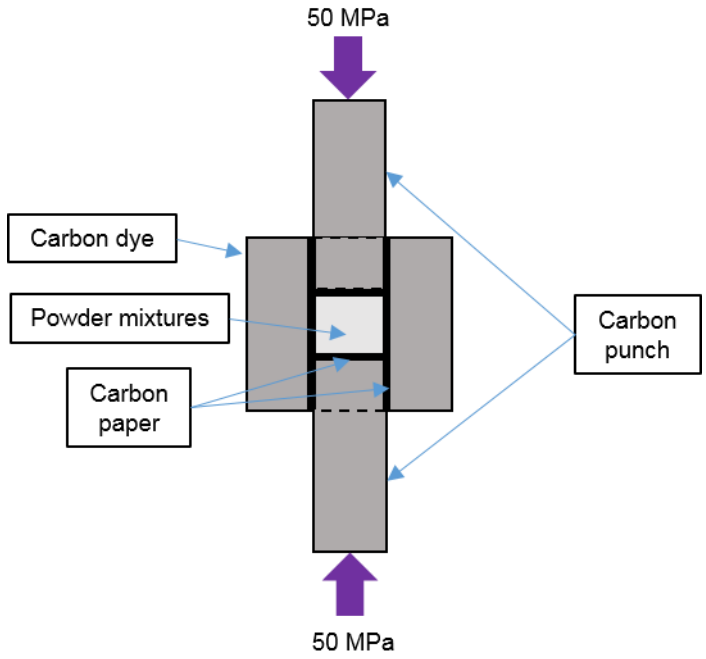

Figure 2.6 Setting of sample during sintering processes.

2.3.8 Isothermal heat treatment (annealing)

These pellets were set in a furnace for isothermal heat treatment (annealing) process under argon (Ar) atmosphere similar to section 2.3.2 in order to obtain β-$FeSi_2$/Si

composite bulks via the eutectoid decomposition of α-Fe_2Si_5 phase.

2.3.9 Phase and microstructure analysis II

The phases of the processed samples were characterized by X-Ray Diffraction (XRD, RIGAKU MINIFLEX60) analysis. These samples were polished first to remove contaminated areas from carbon paper formed during sintering process and annealing process using non-adhesive abrasive SiC papers with the granulometric value of P 240 and P 600 (PRESI France). The condition of apparatus and measurement are summarized in Table 2.5.

Table 2.5 Conditions of apparatus and measurement during XRD analysis.

Apparatus condition	
Scintillation counter	Kβ filter
Slit conditions	DS / SS = 1.25°, RS = 0.3 mm
Tube current	15 mA
Incident side and receiving side Soller slit	5°
Incident height limiting slit	10 mm
Tube current	15 mA
Tube voltage	40 kV
Measurement condition	
Scan range	2θ = 10 ~ 70°
Step width	0.02°
Scan speed	4° / min.

These samples were then polished with the same paper with granulometric value of P 1200 and P 2400. The finishing surface were polished to produce mirror-liked surface via 5 Mecrapex self-adhesive polishing cloths to be analyzed by Scanning Electron

Microscope (SEM, JEOL JSM-5600). This is to determine the microstructure of the annealed pellets. The SEM observation was carried out in the Secondary Electron Imaging (SEI) mode.

2.3.10 Electrical properties analysis (200℃ – 700℃)

The electrical resistivity, ρ and Seebeck coefficient, S were simultaneously measured from room temperature (RT) to 700℃ by the ordinary 4 probe direct current (DC) method in a flowing Ar gas atmosphere using computer-controlled equipment as illustrated in Fig. 2.7. The electrical resistivity is determined by measuring the voltage output drop, V between points AB of sample as 10 mA of electrical current is flown through it. The relation of these measured and set values is expressed in Eq. 2.2,

$$\rho = \frac{V}{I} \times \frac{Q}{L} \quad \ldots \textbf{Equation 2.2}$$

where L is the length between points AB and Q is the cross-sectional area of sample. Seebeck coefficient can be calculated from the relation of $S = \Delta V/\Delta T$, where ΔV and ΔT are voltage difference and temperature difference respectively. The value of ΔV is obtained when ΔT of 5℃ is set between points AB.

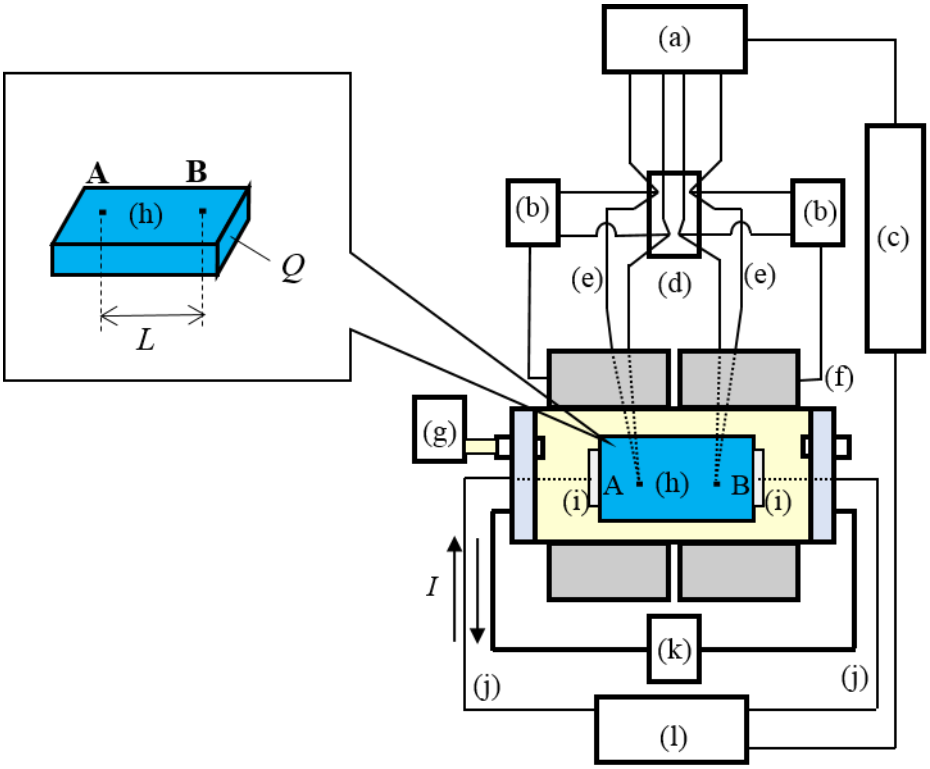

Figure 2.7 Schematic illustration of electrical properties analysis showing (a) Multimeter; (b) Digital program controller; (c) Computer; (d) 0℃ contact; (e) R-type thermocouple; (f) Furnace tube; (g) Ar gas tank; (h) Sample; (i) Pt sheet; (j) Pt electrode; (k) Coolant tank; (l) Programmable voltage-current supply.

2.3.11 Analysis of thermal properties (RT – 700℃)

The thermal conductivity, κ was calculated from the measurement values of thermal diffusivity and heat capacity of these samples obtained from laser flash (LF) machine (TC-7000, ULVAC RIKO) in vacuum condition. Eq. 2.3 is used to calculate the thermal conductivity, κ,

$$\kappa = C_T \times T_D \times \rho \quad \textbf{… Equation 2.3}$$

where, C_T, T_D and ρ are specific heat capacity, thermal diffusivity and sample's density respectively. The sample is polished to the size of ∅10 x 1 ~ 1.5 mm for this analysis.

The heat capacity, C_T at each measured temperature from RT to 700℃ is calculated from the measured values from the LF machine, expressed in Eq. 2.4,

$$C_T = C_{T0}\frac{\Delta T_{0m}}{\Delta T_m} \quad \textbf{... Equation 2.4}$$

where $C_{T0}, \Delta T_{0m}, \Delta T_m$ are heat capacity at room temperature, room temperature and measured temperature respectively. The setting of measurement is illustrated in Fig. 2.8.

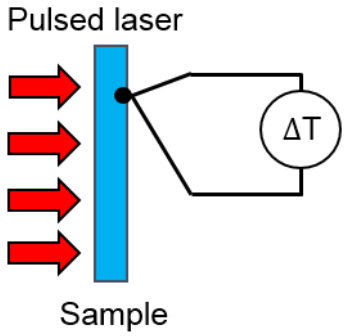

Figure 2.8 Schematic illustration on setting during measurement of heat capacity.

As for the measurement of thermal diffusivity, a laser pulse is radiated through the sample, causing the sample to heat up. As the sample is heated through its body, the temperature response pattern is detected via the pyrometer located behind the sample as illustrated in Fig. 2.9.

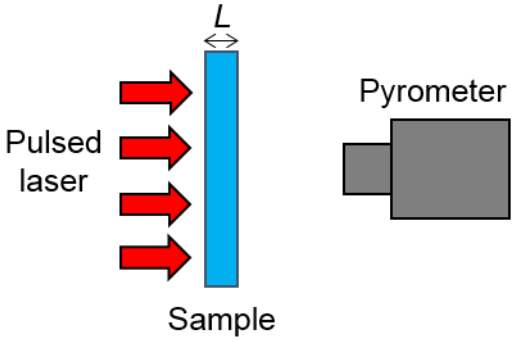

Figure 2.9 Schematic illustration on setting during measurement of thermal diffusivity.

When heat diffuses through the sample with the thickness of L, response of temperature pattern detected via the pyrometer is illustrated for example shown in Fig 2.10. All these values are then calculated in Eq. 2.5, obtaining thermal diffusivity at each measured temperature,

$$T_D = 0.1388 \times \frac{L^2}{t_{1/2}} \quad \cdots \quad \textbf{Equation 2.5}$$

where $t_{1/2}$ is the buffering time for detected temperature to reach its half value.

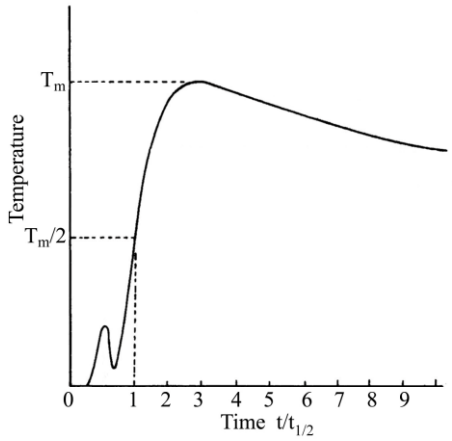

Figure 2.10 Example of temperature response pattern detected via pyrometer to obtain $t/t_{1/2}$.

2.4 Results and Discussion

2.4.1 Phase and microstructure evaluations for synthesized samples

Fig. 2.11 shows the phases determined by XRD for the melted ingots to obtain α-Fe_2Si_5 phase. Main peaks clearly exhibited by α-Fe_2Si_5 without any traces of either unwanted elements or compounds. Phase and microstructure observation is summarized in Fig. 2.12 after the ingots annealed at 800℃ for 4 h, 24 h and 48 h. Under the same held temperature, phase analysis shows a complete decomposition from α-Fe_2Si_5 to β-$FeSi_2$/Si composites. This is proven by the detection of main peaks showing β-$FeSi_2$ phase, while secondary peaks show Si phase.

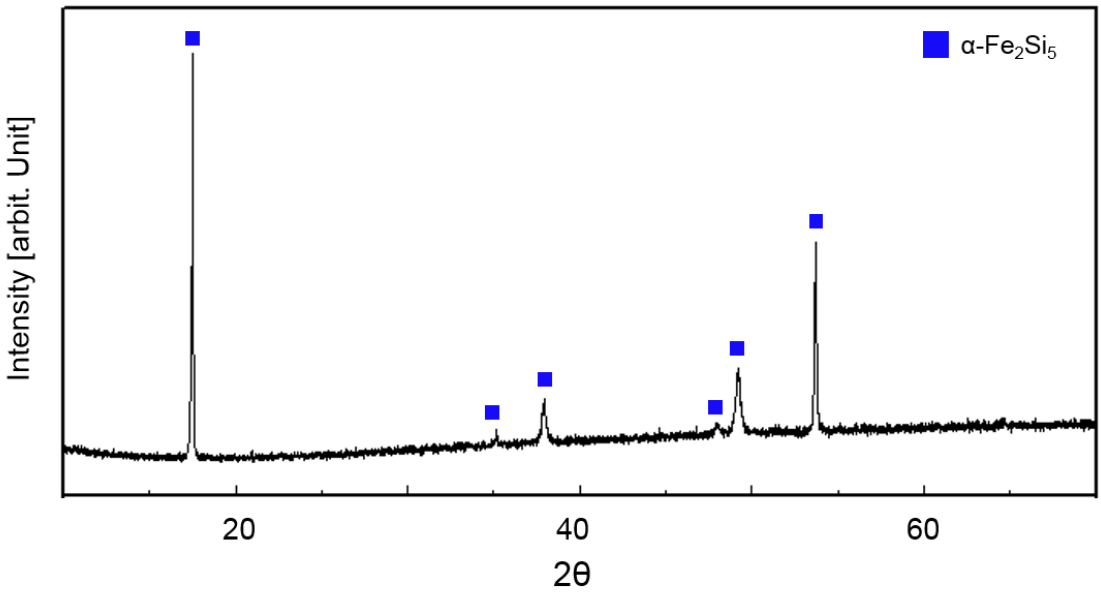

Figure 2.11 Phase analysis via XRD for ingots after arc melting process.

The microstructure observation in Fig. 2.12 shows a contrast of light grey as main

phase, followed by dark fine spots indicating the secondary phase.

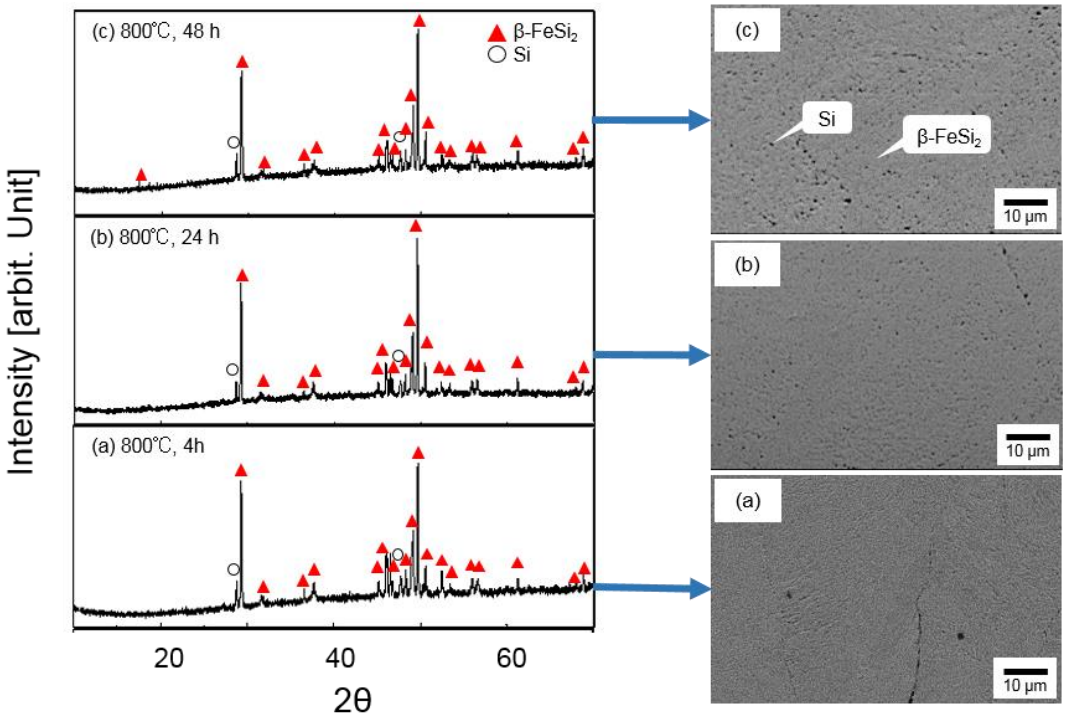

Figure 2.12 Phase analysis via XRD and the designated microstructure observation via SEM annealed at 800℃ 2 for (a) 4 h, (b) 24 h and (c) 48 h.

From here, we can expect the main phase is consisting of β-$FeSi_2$, while the secondary phase consists of Si, which could not be detected by EDS evaluation due to the fine size of Si. Elements of the light grey phase and dark fine spots were also confirmed via AES evaluation, which will be discussed later. We estimated the size of these darks spots were not larger than 500 nm. Among the annealing time of 4 h, 24 h and 48 h under 800℃, size of Si seems to show a gradual growth as the annealing time becomes longer. During the phase transformation of α-Fe_2Si_5 to β-$FeSi_2$/Si, also defined as eutectoid decomposition, the final product of β-$FeSi_2$ and Si has a different phase from the initial phase, and are divided into two phases [15]. Therefore, this reaction is generally diffusion-

dependent. During this diffusion-dependent process, two main processes related are described below [14].

I The nucleation of the new phase, where stable new particles are newly formed known as nuclei and;

II growth of the new phase, where the newly formed phase expand its size.

Hence, at 800℃, as annealing time prolongs, the newly formed Si precipitations grew in size.

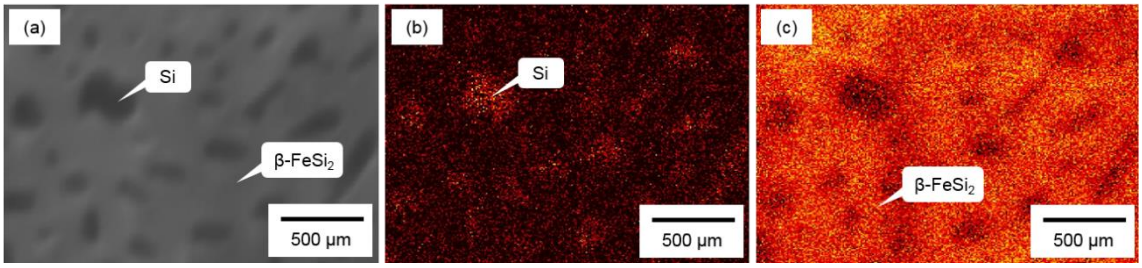

Figure 2.13 Determination of elements of microstructure observation via AES showing (a) SEM image, (b) Si mapping and (c)Fe mapping.

As mentioned previously, we determined the elements of the two distinct phases detected via SEM-EDS observation using AES equipment. It is clearly proven that the main matrix in light grey consists of β-$FeSi_2$ phase, while the darker spots consists of Si. Therefore, the hypothesis of α-Fe_2Si_5 phase completely transformed to β-$FeSi_2$/Si composite is confirmed, as can be seen in Fig. 2.13.

Next, the same phase and microstructure analysis for samples initially went through process II mentioned in section 2.3.6-2.3.7 of powder mixing via ball milling and sintering using SPS to obtain α-Fe_2Si_5 phase are discussed. Fig. 2.14 summarizes the phase analysis of sample after (a) mixing, (b) sintering and (c) annealing. As shown in Fig. 2.14 (a), mixed powders via ball milling show main peaks of Si and Fe only, suggesting that the powders are mixed homogeneously without producing any unwanted

compounds and elements. Insertion of Fe can possible occur from the SUS pot and/or balls during mixing. This is then confirmed by the minor existence of ε-FeSi phase peaks after the sample was sintered as shown in Fig. 2.14 (b). The excessive Fe from the SUS pot is expected to react with Si powders during sintering process yielding the mentioned high temperature metallic ε-FeSi phase. However, phase analysis on annealed sample signifies β-$FeSi_2$ as main peaks, followed by Si as secondary peaks as shown in Fig. 2.14 (c). Agreeing to the phase analysis of annealed ingots discussed previously, annealing at 800℃ for 4 h allows the complete decomposition of α-Fe_2Si_5 phase yielding β-$FeSi_2$/Si duplex phase/composite.

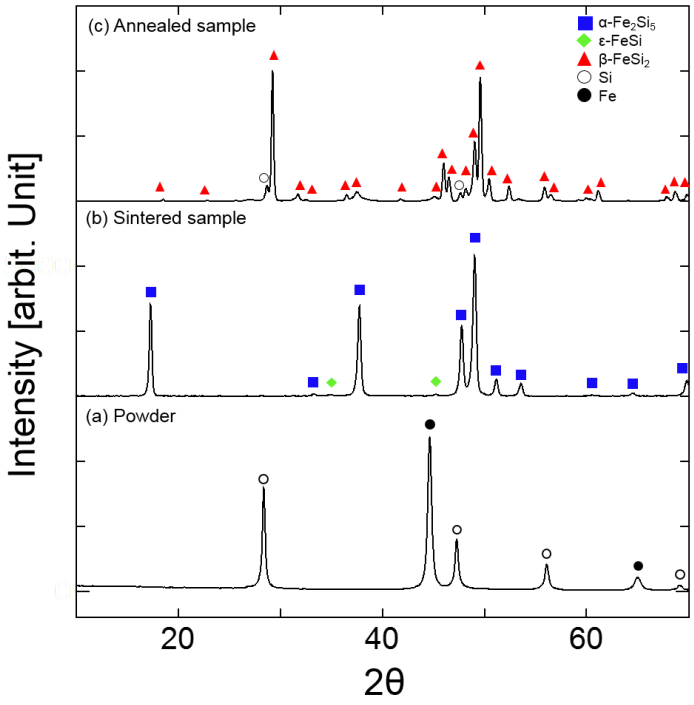

Figure 2.14 Phase analysis of (a) mixed powders via ball mill at 300 rpm for 5 h, (b) sintered sample at 1000℃ for 10 min under 50 MPa and (c) annealed sample at 800℃ for 4 h.

Fig. 2.15 shows the microstructure images analyzed by SEM for sample annealed at

800℃ for 4h in two resolutions. The element analysis via EDS signifies that the light grey matrix is exhibited by the composition of β-$FeSi_2$. On the other hand, the darker, precipitated spots are exhibited by Si element. From this observation, there were also no other detection of unwanted element on compounds. These results are consistent with the microstructure analysis of annealed ingots under the same annealing condition of 800℃-4h, conveying that the sintered sample also transformed completely to β-$FeSi_2$/Si duplex phase from high temperature α-Fe_2Si_5 phase.

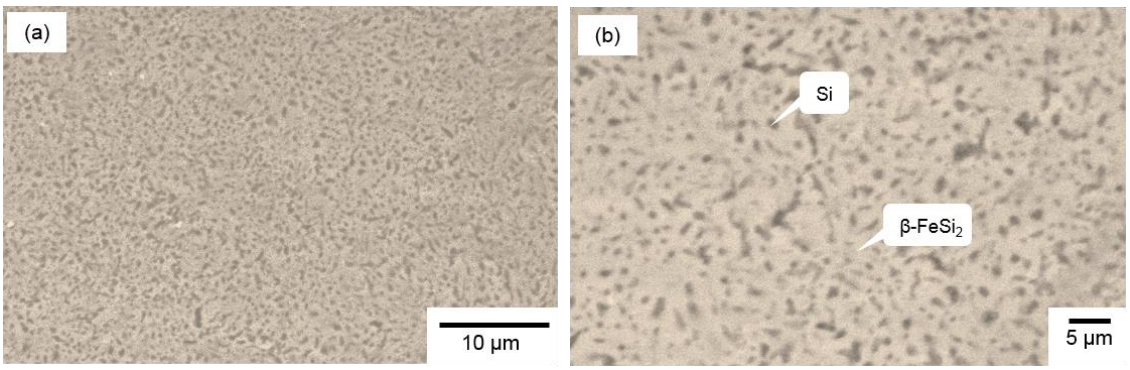

Figure 2.15 Microstructure analysis of annealed samples at 800℃-4h with different resolutions of (a) 5,000 times and (b)10,000 times.

2.4.2 Phase transformation analysis at 800℃

This section discusses the phase transformation analysis executed to evaluate the kinetics of the decomposition of α-Fe_2Si_5 phase. Study on kinetics of phase transformation is generally a method to determine the time dependence of a specific phase transformation, in this case the eutectoid decomposition of α-Fe_2Si_5 phase yielding β-$FeSi_2$/Si heterogeneous phase. In this evaluation, we continue to focus on the annealing temperature of 800℃. The evaluation is carried out by measuring the electrical resistance value as time goes on at 800℃. Fig. 2.16 shows the relation of electrical resistance plotted along the y-axis, and annealing time plotted along the x-axis. As shown in Fig. 2.16,

during the first 10 ks of annealing time shown by the red line in this figure, a lower consistent resistance value can be observed. This indicates that almost no phase transformation occurred from α-Fe_2Si_5 phase. However, as the annealing time increases to approximately 100 ks, a steep rise of electrical resistance value can be observed. This suggests the decomposition from the metallic phase of α-Fe_2Si_5 to the semiconducting phase of β-$FeSi_2$/Si composite is actively progressing. Finally, the resistance value became consistent starting at approximately 200 ks of annealing time, indicating the completion for eutectoid decomposition of α-Fe_2Si_5 phase yielding the heterogeneous phase of β-$FeSi_2$/Si.

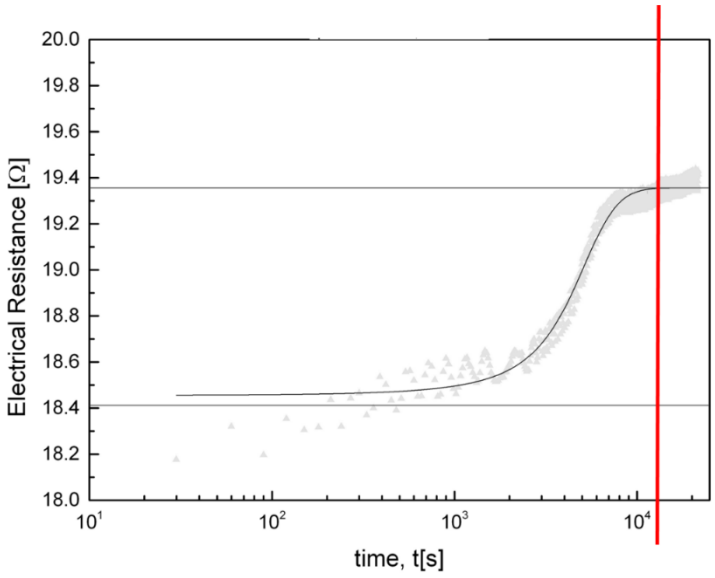

Figure 2.16 Relation of 'electrical resistance-annealing time' during phase transformation analysis.

The point of annealing time where the electrical resistance value started to remain constant is quite close to the annealing time that we have chosen to discuss in this chapter, indicating that there is a wide possibility for the complete transformation to occur at less

than 4 h of annealing time. Furthermore, smaller size of Si or finer precipitations of Si can be expected at this condition. We will discuss further on the phase transformation analysis to determine the Temperature-Time-Transformation diagram (TTT diagram) for isothermally formed phase in chapter 6 with evidence of other examined samples under different annealing conditions and sample composition.

2.4.3 Electrical properties analysis of annealed ingots at RT

Fig. 2.17 shows the (a) electrical resistivity, (b) Seebeck coefficient and, (c) the calculated value of PF from the relation of $PF = S^2/\rho$ indicating the electrical property of evaluated samples. The electrical resistivity value of β-$FeSi_2$/Si composite for all annealing conditions ranged between 100 to 1000 mΩ, least of 100 times larger than that of the typical singular phase β-$FeSi_2$ [1,3,4]. The high value of electrical resistivity in these ingots are mainly caused by the large amount of cracks. The existence of cracks is usually common in ingots because arc melted samples went through a sudden temperature drop during the rapid cooling process after being shot by the initiated arc throughout the melting process at a very high temperature. Meanwhile, among the different annealing time, sample with the shortest annealing time of 4 h has the highest value of electrical resistivity, followed by annealing time of 24 h and 48 h with gradual decrease of the resistivity value. This can be explained by the finer precipitates of Si in samples at shorter annealing time. The fine precipitates of Si are responsible in hindering the mobility and conduction of carriers throughout the composite. Therefore, these high value of electrical resistivity in composite synthesized in this section opposed the need to overcome the issues mentioned in section 1.3 of chapter 1, where singular phase β-$FeSi_2$ originally has relatively high value of electrical resistivity that needs to be countered.

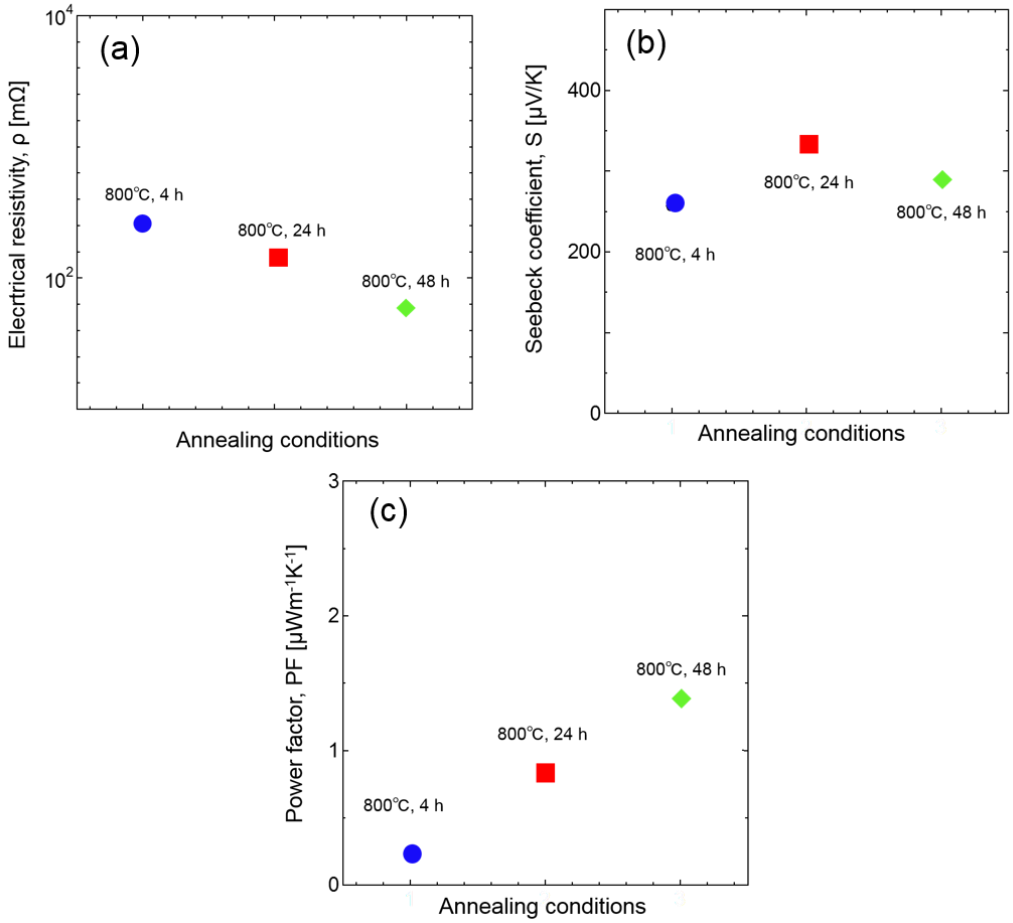

Figure 2.17 Electrical properties analysis for ingots annealed at 800℃-4h under RT.

On the other hand, the absolute values of Seebeck coefficient for β-$FeSi_2$/Si composite overall is significantly high for all conditions ranging from 200 – 350 μV/K. These values are comparatively high compared to not only the single phase of β-$FeSi_2$ but also other highly performed silicide thermoelectric materials like $MgSi_2$, $CrSi_2$ and many more [8–10]. When we calculated the PF value indicating the electrical property, ingot annealed at 800℃ for 48 h has the highest value followed by ingots annealed at the same temperature for 24 h and 4 h. The PF value as a whole for this composite is relatively low when compared to the single phase of β-$FeSi_2$, where the dominant cause of this is from the steeply high value of electrical resistivity. Hence, it is essential to apply a synthesize

method that is crack-free and well-dense, like from the SPS method, which will be discussed in the following sections, expecting to exhibit improved properties. Meanwhile, from the evaluation of Seebeck coefficient or the thermopower of this composite, it can be concluded that β-$FeSi_2$/Si composite delivers a potential prospect to be studied in detail towards enhancing performance of β-$FeSi_2$ based TE materials. We can also expect the fine precipitations of Si to cause a significant suppression of thermal conductivity.

2.4.4 Thermoelectric properties of β-$FeSi_2$/Si composite (200℃ to 700℃)

Next, we evaluate the thermoelectric properties of the sintered bodies annealed at 800℃ for 4 h within the temperature range of 200℃ to 700℃ for both of its electrical and thermal properties, followed by calculating the ZT value.

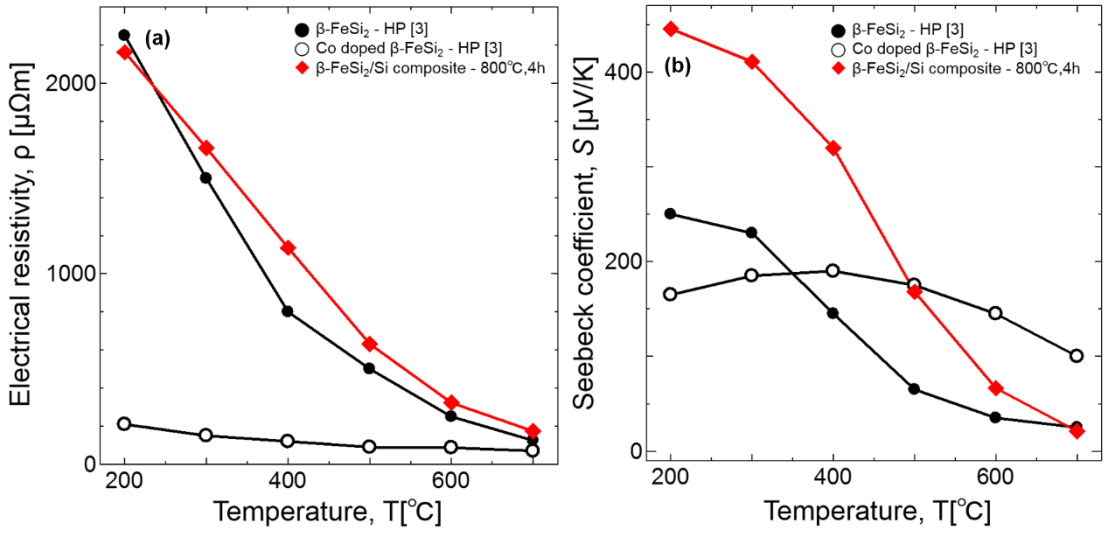

Figure 2.18 The temperature dependence of (a) electrical resistivity and (b) Seebeck coefficient of sintered samples annealed at 800℃ for 4h compared with previous works.

Fig. 2.18 (a) shows the temperature dependence of electrical resistivity for β-$FeSi_2$/Si

produced in current work, followed by singular phase from previous work of β-$FeSi_2$ and Co doped β-$FeSi_2$. As temperature increases from 200℃, electrical resistivity of all samples decrease exponentially, agreeing to the general character of a semiconductor [12]. This proves that the mobility of charged carriers and increase in carrier concentration causing electrical conduction is enhanced by the increase in temperature [6]. As discussed previously, the fine precipitations of Si may cause limitations in the mobility of charge carriers. Therefore, β-$FeSi_2$/Si was found to exhibit the highest value of electrical resistivity within the whole temperature range compared to single phase β-$FeSi_2$, both non-doped and doped ones. Co doped β-$FeSi_2$ shows a significant and distinct decrease in electrical resistivity value within the whole temperature range. This proves the n-type conduction caused by the doping of Co contributes to the increase in carrier concentration, thus decreasing its electrical resistivity over the whole temperature range.

On the contrary, a significant and distinct enhancement of Seebeck coefficient's absolute value can be found in β-$FeSi_2$/Si composite, indicating a vast improvement in thermopower of this material. There are two possible hypotheses of this enhancement of Seebeck coefficient value.

I Si phase itself has a significantly high value of Seebeck coefficient [7,11].

II Fine precipitations of Si results to increase in scattering parameter, thus increasing its Seebeck coefficient value [13].

Therefore, fine precipitations of Si are proven effective to help increase the Seebeck coefficient value of β-$FeSi_2$ based TE material.

Fig. 2.19 (a) shows the temperature dependence of thermal conductivity β-$FeSi_2$/Si produced in current work, followed by singular phases from previous work of β-$FeSi_2$ and Co doped β-$FeSi_2$. We expected that the fine precipitations of Si might show

significant decrease in thermal conductivity, lower than that of the singular phase of both non-doped and doped β-$FeSi_2$. Contrarily, it exhibits the highest value of thermal conductivity value. This indicates that the size of Si is not small enough to interfere the conduction of heat through possible phonon scattering. Furthermore, Si phase itself exhibits a very high value of thermal conductivity, possibly contributing to the increase in thermal conductivity value [7,11]. Hence, it is essential to tune the size of Si to small enough to suppress the transport of heat, in order to enhance its thermoelectric properties as whole.

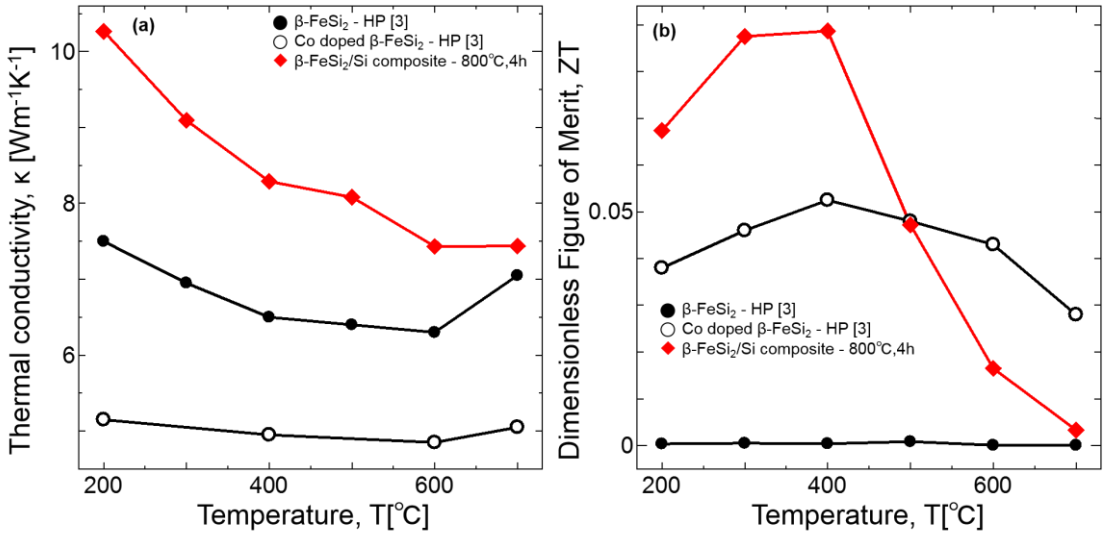

Figure 2.19 The temperature dependence of (a) thermal conductivity and (b) ZT value of sintered samples annealed at 800℃ for 4h compared with previous works.

As shown in Fig. 2.19 (b), β-$FeSi_2$/Si reaches its highest ZT value at approximately 400℃, surpassing those values of all previous works on single phase β-$FeSi_2$. This significant enhancement is primarily influenced by the distinct increase in Seebeck coefficient value despite the detrimental increase of both electrical resistivity and thermal conductivity that might deteriorate its TE performance. Then, we are expecting for the enhancement of TE properties for β-$FeSi_2$/Si composite by attempting to dope Co in it, in

order to help reduce the high value of electrical resistivity observed in this chapter. So, the effects on doping of Co in β-$FeSi_2$/Si composite will be discussed in chapter 3.

2.5 Conclusion

We summarize the findings in chapter 2 as follows:

I β-$FeSi_2$/Si composite is successfully synthesized by the annealing of high temperature metallic α-Fe_2Si_5 phase, both from the arc melting method and SPS method to initially produce α-Fe_2Si_5 phase.

II β-$FeSi_2$/Si composite from the annealing of sintered bodies is proven to be viable for further evaluation in high temperature environment, with easier handling and improved electrical characteristic.

III The existence of Si precipitations within β-$FeSi_2$ phase greatly enhances the thermopower. The Seebeck coefficient value, indicating its thermopower significantly surpasses those values on single phase β-$FeSi_2$ and even Co doped β-$FeSi_2$ below 500℃.

IV The doping of Co is proven effective to help reduce electrical resistivity in single phase β-$FeSi_2$, expected to potentially improve further on the TE performance of β-$FeSi_2$/Si composite.

2.6 References

[1] H.K. Akemoto, Y.M. Akita, S.S. Akuragi, T.T. Sukamoto, *Synthesis and Properties of Semiconducting Iron Disilicide β-$FeSi_2$,* 38 (1999) 5192–5199.

[2] S.K. Bux, R.G. Blair, P.K. Gogna, H. Lee, G. Chen, M.S. Dresselhaus, R.B. Kaner, J.-P. Fleurial, *Nanostructured Bulk Silicon as an Effective Thermoelectric Material*, Adv. Funct. Mater. 19 (2009) 2445–2452.

[3] M. Ito, H. Nagai, E. Oda, S. Katsuyama, K. Majima, *Effects of P doping on the thermoelectric properties of β-$FeSi_2$,* J. Appl. Phys. 91 (2002) 2138–2142.

[4] M. Ito, H. Nagai, E. Oda, S. Katsuyama, K. Majima, *Thermoelectric properties of β-$FeSi_2$ with B_4C and BN dispersion by mechanical alloying*, J. Mater. Sci. 37 (2002) 2609–2614.

[5] J. Jiang, K. Matsugi, G. Sasaki, O. Yanagisawa, *Resistivity Study of Eutectoid Decomposition Kinetics of α-Fe_2Si_5 Alloy*, Mater. Trans. 46 (2005) 720–725.

[6] D.G. Rethwisch, Jr. William, D. Callister, *Electrical properties*, Book section of Mater. Sci. and Eng. An Introduction, 2006.

[7] K. Kurosaki, A. Yusufu, Y. Miyazaki, Y. Ohishi, H. Muta, S. Yamanaka, *Enhanced Thermoelectric Properties of Silicon via Nanostructuring*, Mater. Trans. 57 (2016) 1018–1021.

[8] W. Liu, K. Yin, Q. Zhang, C. Uher, X. Tang, *Eco-friendly high-performance silicide thermoelectric materials*, Natl. Sci. Rev. 4 (2017) 611–626.

[9] T. Nonomura, C. Wen, A. Kato, K. Isobe, Y. Kubota, T. Nakamura, *Thermoelectric properties of group VI metal silicide semiconductors,* Phys. Procedia. 11 (2011) 110–113.

[10] Y. Ohishi, Y. Miyazaki, H. Muta, K. Kurosaki, S. Yamanaka, *Thermoelectric*

properties of $Cr_{1-x}Mo_xSi_2$, Journal of Physics and Chemistry of Solids 87 (2015) 153–157.

[11] Y. Ohishi, J. Xie, Y. Miyazaki, Y. Aikebaier, H. Muta, K. Kurosaki, S. Yamanaka, N. Uchida, T. Tada, *Thermoelectric properties of heavily boron and phosphoru-doped silicon*, Jpn. J. Appl. Phys. 54 (2015) 1–6.

[12] K. Safa, K. Cyril, E.R. Harry, *Electrical conduction in metals and semiconductors*, in : Springer Handb. Electron. Photonic Mater., (2017) 19–45.

[13] M. Yoshinao, K. Yoshisato, K. Sung Wng, *Enhancement of Thermoelectric Figure of Merit through Nanostructural Control on Intermetallic Semiconductors toward High-Temperature Applications*, in : Nanomater. From Res. to Appl., (2006) 383–418.

[14] *Introduction to Materials Science : Phase Transformations* in : Metals, Univ. Tennessee, Dept. Mater. Sci. Eng.

[15] *Solid-State Phase Transformations and Reactions*, in : Ceram. Mater., Springer, New York, NY, 2007: pp. 444–462.

Chapter 3

Doping Co in β-$FeSi_2$/Si Composites towards enhancing TE properties

3.1 Overview

This chapter discusses the attempt to enhance thermoelectric performance by doping of Co in the Fe site of β-$FeSi_2$/Si composites, maintaining the fine precipitations of Si. The synthesize process starts from the sintering process of α-Fe_2Si_5 phase. Annealing process follows after sintering through eutectoid decomposition of high temperature α-Fe_2Si_5 phase to low temperature semiconducting β-$FeSi_2$/Si phase in Fe-Si system. Differences in Si size were obtained, which is caused by the different annealing time and temperature. The Si size ranged between 100 – 300 nm. Seebeck coefficient of Co doped β-$FeSi_2$/Si composite is higher than that of the conventional singular phase Co doped β-$FeSi_2$, overpowering the increase in electrical resistivity and thermal conductivity. This caused improvement of the ZT value from approximately 0.05 to 0.09. On the other hand, lowest thermal conductivity value of Co-doped β-$FeSi_2$/Si composite annealed at 700℃ for 4h was lower than calculated value from the rule of mixture. In this calculation, structure of precipitated secondary phase was not considered in the calculation, proving that Si dispersions help reduce thermal conductivity.

3.2 Introduction

Previous studies have proven that the substitution of Co for Fe contributes to the release of free electron resulting in n-type semiconducting β-$FeSi_2$ thermoelectric material, thus decreasing the value of electrical resistivity [7,15,18]. Although we succeeded to produce β-$FeSi_2$/Si composite in a short time by utilizing eutectoid decomposition mentioned in previous chapter, the fine precipitations of Si have caused a great increase in electrical resistivity compared to the singular phase Co doped β-$FeSi_2$, deteriorating the thermoelectric performance despite the distinct increase of Seebeck coefficient value. Therefore, we choose to dope Co in the β-$FeSi_2$/Si based composite expected to help enhance its thermoelectric performance. Using the same method of mixing and sintering introduced in chapter 2, Co doped β-$FeSi_2$/Si was prepared through eutectoid decomposition from α phase to the heterogeneous phase of β-$FeSi_2$ and Si via annealing. Then, we investigate the effects of annealing condition on microstructure and thermoelectric properties. Here, we apply the rule of mixture to further discuss the role of fine precipitations in β-$FeSi_2$ expected to contribute in the suppression of thermal conductivity. The rule of mixture is generally used to predict properties in composite materials theoretically, in this case thermal conductivity of composites. We applied the idea derived by Maxwell-Eucken [10,14,21] to discuss the effects of Si dispersion this section.

3.3 Experimental Procedures

This part divides the experimental procedures of this work to the synthesize process and properties analysis process as illustrated in Fig. 3.1. The detailed description on sample's preparation, apparatus information and measurement conditions are described in the next section.

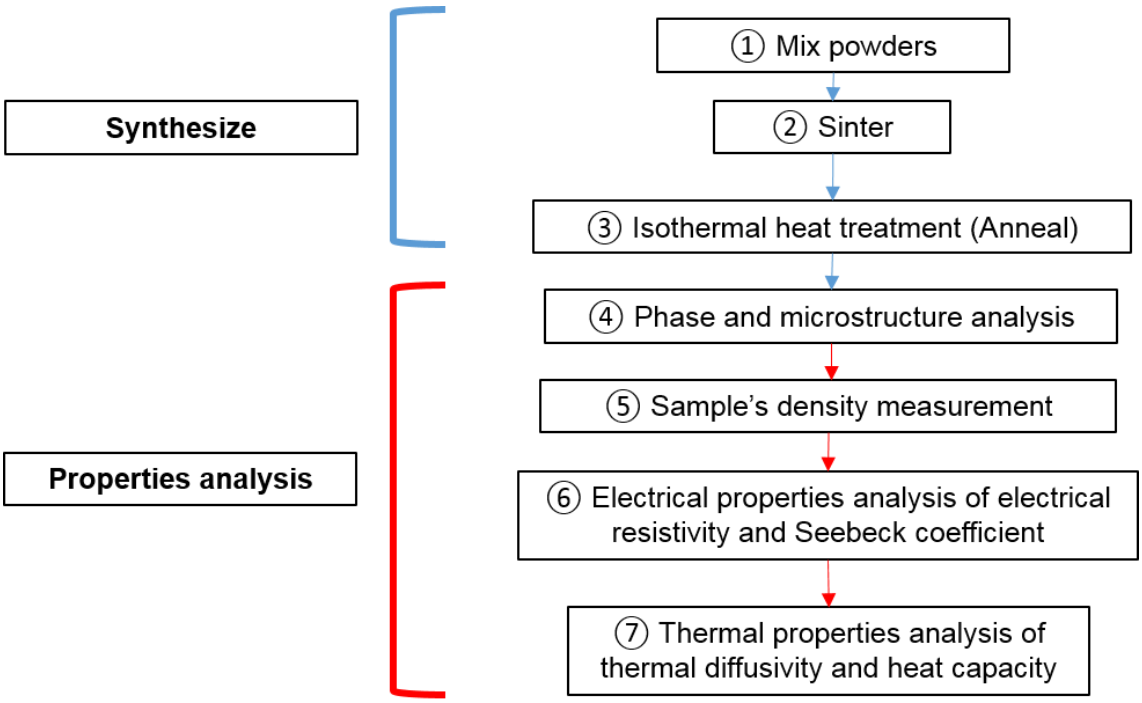

Figure 3.1 Graphical flow of experimental procedures.

3.3.1 Synthesis process (mixing, sintering and annealing)

Powders of Fe, Si and Co as described in Table 3.1 are mixed using the same method described in section 2.3.6. They are also sintered and annealed using the same method as described in section 2.3.7 and 2.3.8. The annealing conditions examines this time is summarized in Table 3.2.

Table 3.1 Description of powder types and amount used during mixing process.

Element	Size (purity)	Manufacturer	Amount (atomic %)
Iron (Fe)	150 μm (99.9%)	Wako Pure Chemicals Industries, Ltd	28.49
Silicon (Si)	150 μm (99.9%)		70.5
Cobalt (Co)	5 μm (99.99%)	Kojundo Chemical Laboratory Co.	0.51

Table 3.2 Sample's name and its annealing condition (temperature and time).

Sample name	Annealing temperature (℃)	Annealing time (h)
AN700T3	700	3
AN700T4	700	4
AN700T5	700	5
AN700T10	700	10
AN800T4	800	4

3.3.2 Properties analysis (phase, microstructure, density, electrical properties and thermal properties)

The detailed explanation of phase analysis via XRD and microstructure observation using SEM-EDS is the same as described in section 2.3.9. Then, The density, ρ_s of processed samples were measured by Archimedes method using a density measuring equipment (SHIMADZU, AUX120). The equation used in this method is shown in Eq. 3.1 below,

$$\rho_s = \frac{W_a}{W_a - W_w}\rho_w \quad \textbf{... Equation 3.1}$$

where W_a, W_w, ρ_w are sample weight in air, sample weight in water and density of water respectively. The electrical properties and thermal properties were simultaneously measured from room 200℃ to 700℃ by the same methods described in section 2.3.10 and 2.3.11 respectively.

3.4 Results and Discussion

3.4.1 Determination of α-Fe_2Si_5 phase decomposition via phase and microstructure analysis

Fig. 3.2 (a) shows the phase determination by XRD of powders after ball milling process, while Fig. 3.2 (b) shows the phase determination by XRD after sintering process. From Fig. 3.2 (a), main peaks of Fe and Si indicated that the powders were homogenously mixed without creating unfavorable compounds. The milled powder was composed of typically agglomerated particles with several micrometers in size. Furthermore, its crystalline size was calculated to be about 200 nm from the Scherrer's method using the XRD data. From Fig. 3.2 (b), high temperature metallic α-Fe_2Si_5 was also obtained after sintering at 1000℃ for 10 min under 50 MPa.

Fig. 3.3 shows the phases of all samples after annealed at conditions summarized previously in Table 3.2. From here, main peaks are composed of β-$FeSi_2$, followed by the secondary peak of Si. This indicates that all annealed samples successfully transformed to the heterogeneous phase of β-$FeSi_2$ and Si from high temperature metallic α-Fe_2Si_5 phase. However, small peak at $2\theta = 16°$, which corresponds to α-Fe_2Si_5 phase was detected for sample AN700T3 (annealed at 700℃ for 3h). Moreover, the peak from Si at $2\theta = 48°$ was not clearly identified, indicating that the decomposition of α-Fe_2Si_5 phase did not finish completely. The incomplete reaction is possibly due to the annealing temperature of 700℃, which is found to be not high enough to allow the decomposition completion of α-Fe_2Si_5. The annealing time of 3 h at this annealing temperature is also inadequate to help progress the phase transformation of α-Fe_2Si_5 yielding β-$FeSi_2$/Si

heterogeneous phase. Meanwhile, wide and low intensity of Si peaks in all samples indicated the small size of Si particles was formed.

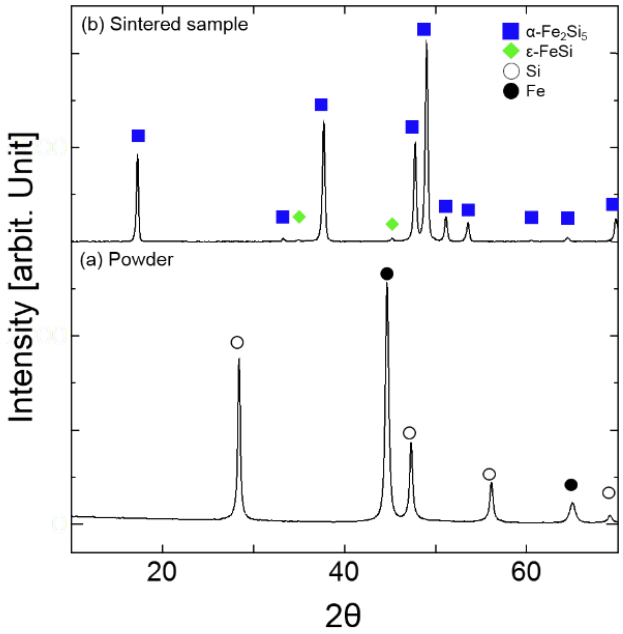

Figure 3.2 XRD patterns of $Fe_{28.49}Co_{0.59}Si_{70.5}$ (a) before sintered, (b) after sintered at 1000℃ for 10 min under 50 MPa.

Fig. 3.4 shows the SEM photographs of the annealed samples. From here, main matrix shown in light grey is composed of β-$FeSi_2$, while the darker precipitated spots are composed of Si. This microstructure observation agrees to the XRD analysis indicating main phase showed β-$FeSi_2$, followed by the dispersion of fine Si as secondary phase. Co based compound or Co single element was also not detected, indicating the complete substitution of Fe with Co. There are three types of observations can be made through these results as annealing conditions vary; (1) size of Si phase, (2) uniformity of its distribution, and (3) shape of Si particles. Sample AN700T4 not only exhibits the finest Si dispersion, but also a uniformed precipitation, mostly rounded in shape. Meanwhile, sample AN700T3, AN700T5 and AN700T10 had less uniformly dispersed Si,

combination of large and small rounded Si. The size of Si also increased as the annealing time increases under the same annealing temperature of 700℃. Si in sample AN800T4 scattered evenly with larger, oblong shaped Si. Comparing annealing temperature of 700℃ and 800℃, lower annealing temperature caused finer and even Si dispersion, while longer annealing time at 700℃ shows increase in size of some Si precipitates.

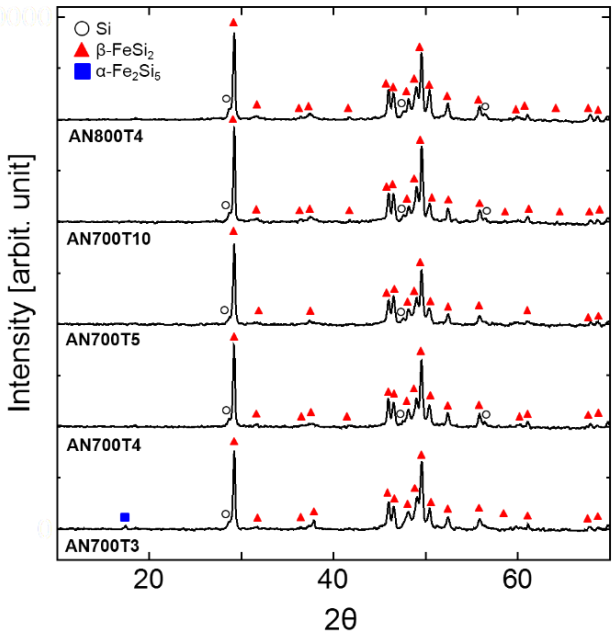

Figure 3.3 XRD patterns of $Fe_{28.49}Co_{0.59}Si_{70.5}$ after annealed at 700℃ for 3h (AN700T3), 700℃ for 4h (AN700T4), 700℃ for 5h (AN700T5), 700℃ for 10h (AN700T10) and 800℃ for 4h (AN800T4).

As discussed in section 2.4.1 of chapter 2, main factors affecting phase transformation for the decomposition of α-Fe_2Si_5 phase yielding heterogeneous phase are nucleation and growth rate [23,24]. In this case we discuss further on the factors affecting phase transformation rate of α-Fe_2Si_5 phase, where we evaluated the influence of

annealing time and temperature towards the microstructure of β-$FeSi_2$/Si composite.

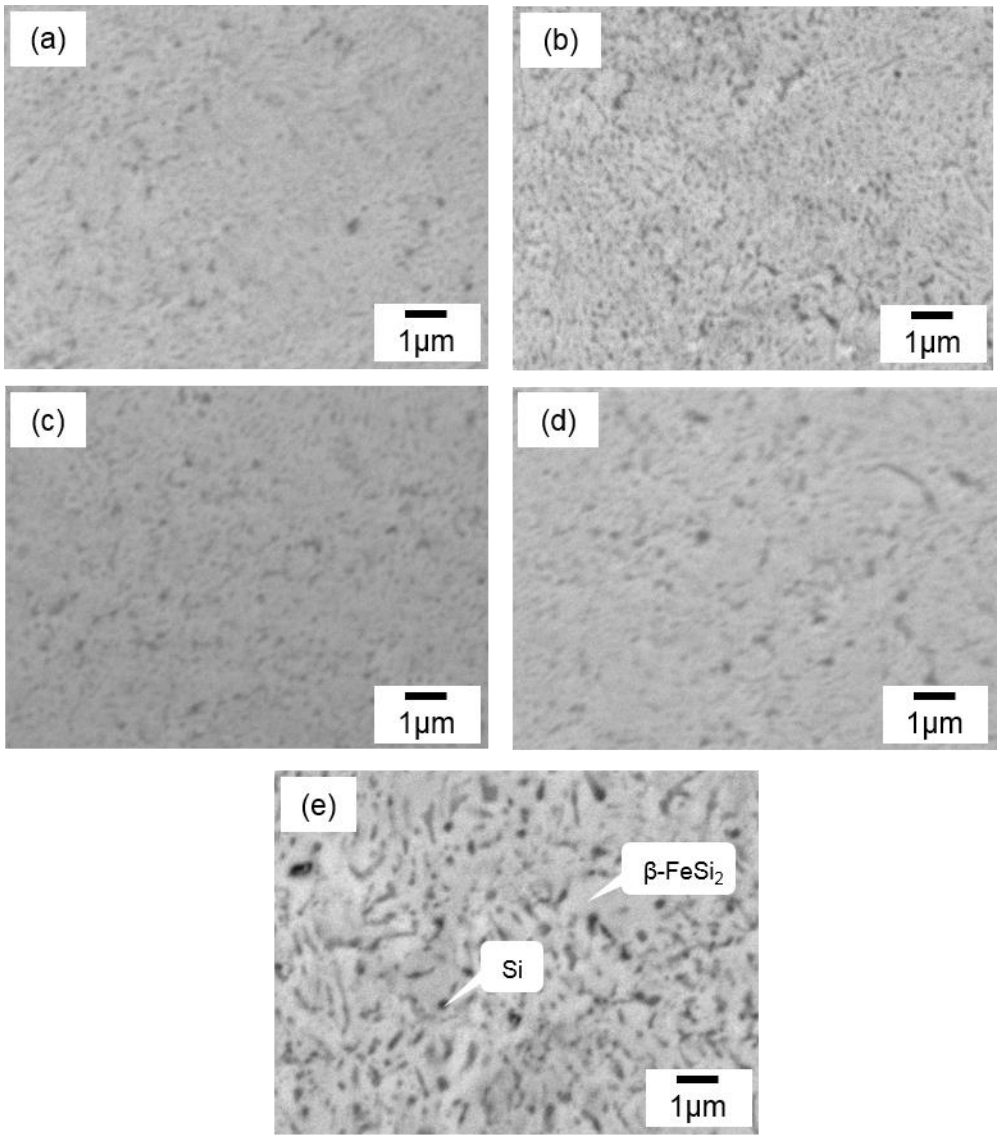

Figure 3.4 SEM photogtaphs of $Fe_{28.49}Co_{0.59}Si_{70.5}$ after annealed at (a) 700℃ for 3h (AN700T3), (b) 700℃ for 4h (AN700T4), (c) 700℃ for 5h (AN700T5), (d) 700℃ for 10h (AN700T10) and (e) 800℃ for 4h (AN800T4).

As annealing temperature increases nearing the material's melting point, grain growth occurs faster than the nucleation of new phase. On the other hand, at lower annealing temperature, nucleation occurs faster than the growth rate resulting in the domination of

fine Si phase formation rather than its growth [22]. Therefore, finer Si precipitations is observed in samples with lower annealing temperature, in this case 700℃.

3.4.2 Electrical properties of Co-doped β-$FeSi_2$/Si composite.

Fig. 3.5 shows the temperature dependence of (a) electrical resistivity and, (b) Seebeck coefficient for all annealed samples and previous data of Co-doped β-$FeSi_2$ singular phase [5]. From fig 3.5 (a), electrical resistivity for all samples decreases as temperature increases indicating a general semiconducting properties. Generally, this is due to the increase in temperature which enhances thermal excitation of carrier, decreasing electrical resistivity as discussed in chapter 2 [16]. Singular Co-doped β-$FeSi_2$ from previous study [5] exhibited the lowest electrical resistivity value over the entire temperature range because there is no existence of singular secondary phase Si. Furthermore, Si phase itself is known to have high value of electrical resistivity between the range of 0.1 – 60 Ωm [2], contributing to the high values of electrical resistivity for all Co-doped β-$FeSi_2$/Si composites compared to the singular phase ones. On the other hand, our data also address that there are no significant differences in electrical resistivity among the β-$FeSi_2$/Si composite samples. The lower electrical resistivity value of the sample AN700T3 may be associated with the residual metallic α-Fe_2Si_5 phase from the incomplete decomposition as described in the evaluation of phase via XRD analysis.

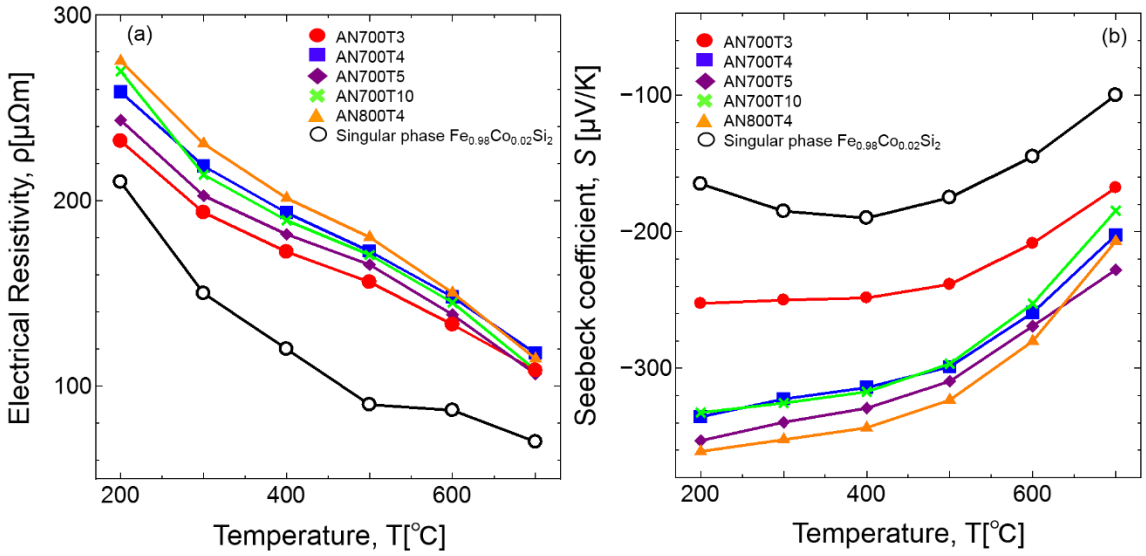

Figure 3.5 Temperature dependence of (a) electrical resistivity for $Fe_{28.49}Co_{0.59}Si_{70.5}$ after annealed at 700℃-3h (AN700T3), 700℃−4h (AN700T4), 700℃-5h (AN700T5), 700℃ -10h (AN700T10) and 800℃- 4h (AN800T4).

Fig. 3.5 (b) shows the Seebeck coefficient values, which are negative over the entire temperature range. This signifies that doping of Co in β-$FeSi_2$/Si composite results to the substitution of Co atoms for Fe atoms. Hence, Co which worked as donor in Co doped β-$FeSi_2$/Si composite yields an n-type composite semiconductor. Among composite samples, sample AN700T3 has the lowest absolute value of Seebeck coefficient because the transformation from α-Fe_2Si_5 to β-$FeSi_2$/Si phase was not complete leaving a scarce existence of metallic α-Fe_2Si_5 phase as detected in XRD shown in Fig. 3.3. The incompletion of this transformation was due to the low temperature and short time of annealing. In this condition, the nucleation of new phase assumed to be more dominant than the growth of the newly formed phase could not finish completely as the annealing time ends. No existence of Si as secondary phase in reference value of Co-doped β-$FeSi_2$ causes its lowest Seebeck coefficient value compared to the composites ones done in this

work. High Seebeck coefficient value of singular Si phase and its' scattering character within β-$FeSi_2$ phase are possible factors affecting Seebeck coefficient trend for these composites. It can be assumed that carriers within β-$FeSi_2$/Si composite is scattered due to the fine precipitations of Si. This is because, the dominant type of electron-impurity scattering most likely to occur. Hence, the increased scattered in carriers contributes to the increase in Seebeck coefficient [3,17,20]. On the other hand, multiple factors of Si size and uniformity of its precipitations for other samples of AN700T4, AN700T5, AN700T10 and AN800T4 cause the insignificant differences between them. However, which factor is more dominant remains unclear so far. Thus, the Si particle dispersion found to be quite effective for improving the Seebeck coefficient.

3.4.3 Thermal conductivity of Co-doped β-$FeSi_2$/Si composite

Fig. 3.6 shows the temperature dependence of (a) thermal conductivity for Co-doped β-$FeSi_2$/Si composite annealed at various conditions and (b) evaluation by rules of mixture. As shown in Fig. 3.6 (a), sample AN700T3 showed the highest thermal conductivity within all temperature range due to the existence of metallic α-Fe_2Si_5 phase as it is not completely transformed to β-$FeSi_2$/Si phase. The sample AN700T4 showed the smaller thermal conductivity than any other samples which is due to its fine and uniform distribution of Si precipitates within the β-$FeSi_2$ phase matrix. Then, the effect of this Si dispersion on the thermal conductivity of β-$FeSi_2$ was evaluated by the rule of mixture.

The rule of mixture (methods used for predicting properties theoretically) were used by applying simplified Maxwell-Eucken equation (Eq.2) to evaluate thermal conductivity [11,14],

$$k = k_\beta \left[\frac{2\left(\frac{k_{Si}}{k_\beta}-1\right)V_{Si}+\frac{k_{Si}}{k_\beta}+2}{\left(1-\frac{k_{Si}}{k_\beta}\right)V_{Si}+\frac{k_{Si}}{k_\beta}+2} \right] \text{ ...Equation 3.2}$$

where k, k_{Si}, and k_β are thermal conductivities of Co doped β-$FeSi_2$/Si composite, Si dispersion and β-$FeSi_2$ phase matrix, respectively, while V_{Si} is the volume fraction of Si dispersion. Thermal conductivity of single Si were extracted from a previous work [4]. In this equation, perfect bonding between dispersions and matrix were assumed [14]. We considered complete decomposition of β-$FeSi_2$ phase and Si phase from α-Fe_2Si_5 phase resulting in the ratio of β phase to Si as 2 : 1.

$$V_{Si} = \frac{W_{Si}/d_{Si}}{W_\beta/d_\beta + W_{Si}/d_{Si}} \quad \text{...Equation 3.3}$$

As shown in Eq. 3.3, each volume, *V* were then calculated by dividing its weight, *W* to theoretical density, *d*. Here, weight of β-$FeSi_2$ phase and Si phase were calculated by multiplying the decomposed ratio to their atomic weight. Therefore, volume fraction of Si was calculated as 0.217. As indicated in Fig. 3.6 (b), thermal conductivities of sample AN800T4, AN700T4 were compared with calculated values from Eq. 3.2 and reference value from previous research [5]. Only experimental values of AN800T4 and AN700T4 were evaluated because these two samples have even distribution of Si. The reference data of single Co doped β-$FeSi_2$ indicated the lowest thermal conductivity value. The composite samples of AN800T4 and AN700T4 showed thermal conductivity values higher than that of the singular β-$FeSi_2$ phase because of the large thermal conductivity value of Si phase [1,9,13]. The calculated value has the highest thermal conductivity generally because dispersed structure was not considered in calculation. In nano-

structured bulk material similar to our synthesized β-$FeSi_2$/Si composite, we expect that the reduced thermal conductivity is due to the enhanced phonon scattering at the grain boundaries between main phase β-$FeSi_2$ and the precipitated phase of fine Si [9]. This justifies that fine dispersion of Si effectively suppressed thermal conduction due to enhanced phonon scattering and interfacial thermal resistance between constituents within β-$FeSi_2$ phase and Si [8]

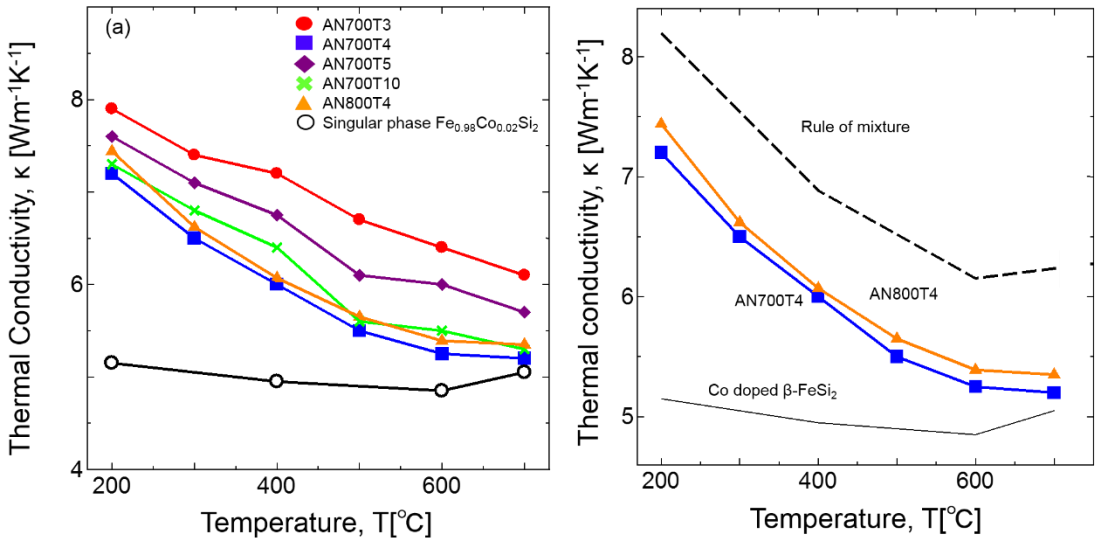

Figure 3.6 Temperature dependence of (a) thermal conductivity for $Fe_{28.49}Co_{0.59}Si_{70.5}$ after annealed at 700℃-3h (AN700T3), 700℃-4h (AN700T4), 700℃-5h (AN700T5), 700℃-10h (AN700T10) and 800℃-4h (AN800T4), and (b) evaluation from rule of mixture.

3.4.4 Enhanced TE performance of Co doped β-$FeSi_2$/Si composite

Concluding all the performance value in this work, as shown in Fig. 3.7, sample AN800T4 showed the highest ZT value of 0.09 at approximately 600℃, exceeding the maximum ZT value of conventional singular phase Co-doped β-$FeSi_2$ approximately 0.05

at 400℃ [5,7]. This is because, a significant increase of Seebeck Coefficient in the entire analysis temperature range from previous work on singular phase [5,7] was successfully obtained, overcoming the opposing factor of thermal conductivity and electrical resistivity increment, thus enhancing the ZT value.

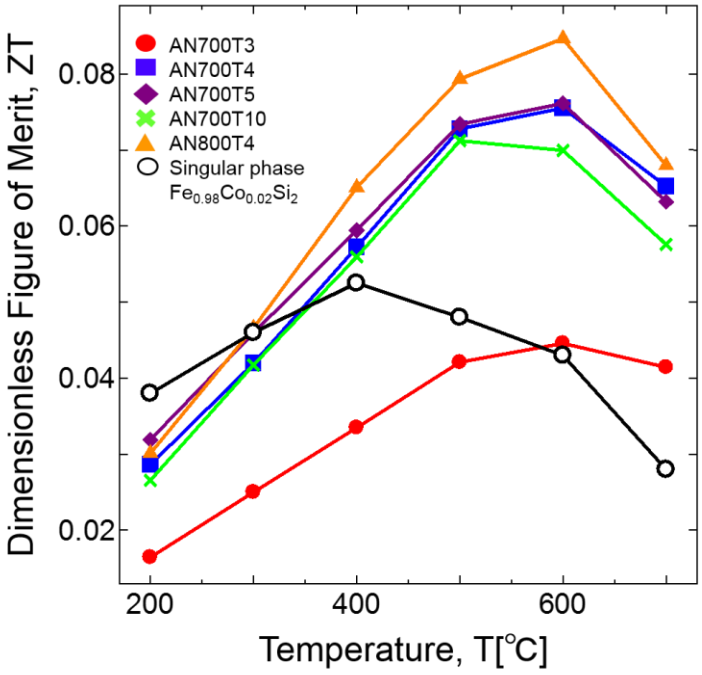

Figure 3.7 Temperature dependence of ZT value for $Fe_{28.49}Co_{0.59}Si_{70.5}$ after annealed at 700 ℃ -3h (AN700T3), 700 ℃ -4h (AN700T4), 700 ℃ -5h (AN700T5), 700 ℃ -10h (AN700T10) and 800 ℃ - 4h (AN800T4), showing a significant improvement in TE performance compared to the singular phase of Co doped β-$FeSi_2$.

From these results, we found that the doping of Co in β-$FeSi_2$/Si significantly reduce the electrical resistivity value of this composite. However, the value is still large than those of the Co-doped β-$FeSi_2$ single phase. The reduction of electrical resistivity towards the TE performance enhancement of β-$FeSi_2$ single phase has been tried by doping of various elements like Co [6,18], Cr [19], P [5], Ni [18], Mn [6], Al and Cu [12] into Fe and/or Si sites [15]. Among them, P is expected to easily dissolve into Si phase, also well

known as an n-type dopant for semiconducting Si. Therefore, introducing P to the Si phase is likely to help reduce the electrical resistivity of β-$FeSi_2$/Si composite significantly. Furthermore, it may be possible for the thermal conductivity of Si phase to be reduced as P is dissolved in Si phase. So, the effects of P doping towards Co doped β-$FeSi_2$/Si composite is discussed in the next chapter.

3.5 Conclusion

We summarize the findings in chapter 3 as follows:

I Co doped β-$FeSi_2$/Si composite is successfully synthesized by the annealing of high temperature metallic α-Fe_2Si_5 phase via SPS method to initially produce α-Fe_2Si_5 phase, without deteriorating the structure of fine Si precipitations.

II Annealing temperature of 700℃ and time of 3 h - the shortest annealing time and lowest annealing temperature in this work was found to be not conducive for complete decomposition from α-Fe_2Si_5 phase.

III The composites with fine Si dispersions showed clear increase in Seebeck coefficient, electrical resistivity and thermal conductivity when compared to the singular phase of Co doped β-$FeSi_2$.

IV Effects of Si dispersion within β-$FeSi_2$ phase matrix were then evaluated by the rule of mixture, indicating that the finely distributed secondary phase of Si helps suppress thermal conductivity, leading to the potential application for the future on enhancing thermoelectric performance of β-$FeSi_2$ system.

V The balance of electrical properties and thermal properties in β-$FeSi_2$/Si composite annealed at 800℃ for 4 h causes it to exhibit the highest TE performance value, higher than that of the Co doped β-$FeSi_2$ TE material.

3.6 References

[1] T. Chen, P. Yu, R. Chou, C. Pan, *Phonon thermal conductivity suppression of bulk silicon nanowire composites for efficient thermoelectric conversion*, Opt. Express. 18 (2010) 304–313.

[2] Douglas C. Giancoli, *Physics : Principle with Application*, Pearson, 2013.

[3] V.F. Gantmakher, Y.B. Levinson, *Carrier Scattering in Metals and Semiconductors*, Volume 19, Elsevier, 1987.

[4] C.J. Glassbrenner, G.A. Slack, *Thermal conductivity of silicon and germanium from 300K to the melting point*, Phys. Rev. 134 (1964).

[5] M. Ito, H. Nagai, E. Oda, S. Katsuyama, K. Majima, *Effects of P doping on the thermoelectric properties of β-$FeSi_2$*, J. Appl. Phys. 91 (2002) 2138–2142.

[6] M. Ito, H. Nagai, T. Tanaka, S. Katsuyama, K. Majima, *Thermoelectric performance of n-type and p-type β-$FeSi_2$ prepared by pressureless sintering with Cu addition*, J. Alloys Compd. 319 (2001) 303–311.

[7] M. Ito, K. Takemoto, *Synthesis of thermoelectric $Fe_{0.98}Co_{0.02}Si_2$ with fine Ag dispersion by mechanical milling with AgO powder*, Mater. Trans. 49 (2008) 1714–1719.

[8] J. Jiang, K. Matsugi, G. Sasaki, O. Yanagisawa, *Resistivity Study of Eutectoid Decomposition Kinetics of α-Fe_2Si_5 Alloy*, Mater. Trans. 46 (2005) 720–725.

[9] K. Kurosaki, A. Yusufu, Y. Miyazaki, Y. Ohishi, H. Muta, S. Yamanaka, *Enhanced Thermoelectric Properties of Silicon via Nanostructuring*, Mater. Trans. 57 (2016) 1018–1021.

[10] F.L. Levy, *A modified Maxwell-Eucken equation for calculating the thermal conductivity of two-component solutions or mixtures,* Int. J. Refrig. 4 (1981) 223–

225.

[11] K. Mizuuchi, K. Inoue, Y. Agari, M. Sugioka, M. Tanaka, T. Takeuchi, J. Tani, M. Kawahara, Y. Makino, M. Ito, *Bimodal and Monomodal Diamond Particle Effect on the Thermal Conductivity of Diamond Particle Dispersed Al Matrix Composite Produced by SPS*, Mater. Sci. Forum. 783–786 (2014) 2462–2467.

[12] N. Niizeki, M. Kato, I.J. Ohsugi, Y. Isoda, H. Kohri, I. Shiota, *Effect of Aluminum and Copper Addition to the Thermoelectric Properties of $FeSi_2$ Sintered in the Atmosphere*, Mater. Trans. 50 (2009) 1586–1591.

[13] Y. Ohishi, J. Xie, Y. Miyazaki, Y. Aikebaier, H. Muta, K. Kurosaki, S. Yamanaka, N. Uchida, T. Tada, *Thermoelectric properties of heavily boron- and phosphorus-doped silicon*, Jpn. J. Appl. Phys. 54 (2015) 1–6.

[14] K. Pietrak, T.S. Winiewski, *A review of models for effective thermal conductivity of composite materials,* Open Access J. J. Power Technol. 95 (2015) 14–24.

[15] D.M. Rowe, *CRC Handbook of Thermoelectrics*, 290, CRC Press, 1995.

[16] K. Safa, K. Cyril, E.R. Harry, *Electrical conduction in metals and semiconductors*, in : Springer Handb. Electron. Photonic Mater., (2017) 19–45.

[17] W.H. Shah, A. Khan, M. Waqas, W.A. Syed, *Effects of Pb doping on the Seebeck coefficient and ekectrical properties of $Tl_{8.67}Pb_xSb_{1.33-x}Te_6$ chalcogenide system*, Chalcogenide Lett. 14 (2017) 61–68.

[18] J. Tani, H. Kido, *Electrical properties of Co-doped and Ni-doped β-$FeSi_2$*, J. Appl. Phys. 84 (1998) 1408–1411.

[19] J. Tani, H. Kido, *Electrical Properties of Cr-Doped β-$FeSi_2$*, Jpn. J. Appl. Phys. 38 (1999) 2717.

[20] I. Terasaki, *Introduction to Thermoelectricity*, 1998.

[21] X.Shi, *Role of structures on thermal conductivity in thermoelectric materials*, Prop. Appl. Thermoelectr. Mater. Search New Mater. Thermoelectr. Devices. (2009) 19–49.

[22] L. V. Zhigilei, *Introduction to the Science and Engineering : Phase Transformation* in : http://people.virginia.edu/~lz2n/mse209/index.html (Online lecture notes), MSE 2090. (2010) 16.

[23] *Introduction to Materials Science : Phase Transformations in Metals*, Univ. Tennessee, Dept. Mater. Sci. Eng. (n.d.).

[24] *Solid-State Phase Transformations and Reactions*, in : Ceram. Mater., Springer, New York, NY, 2007: pp. 444–462.

Chapter 4

Doping of P to the Si phase in Co doped β-$FeSi_2$/Si composite towards enhancing its TE properties

4.1 Overview

This chapter discusses the influence of jointly doping phosphorus (P) to the Co-doped β-$FeSi_2$/Si composite. It is expected that the doping of P results in the substitution of P atoms within the Si phase of β-$FeSi_2$/Si composite without interfering the fine precipitations of Si. The electrical resistivity of $Fe_{28.49}Co_{0.59}Si_{70.5-x}P_x$ after annealed at 800℃ for 4h was reduced at x = 2.82 at%, but increased at x = 4.23 at%. The Seebeck coefficient of $Fe_{28.49}Co_{0.59}Si_{70.5-x}P_x$ after annealed at 800℃ for 4 h was negative, indicating that P atoms as *n*-type dopant in the Si phase. The thermal conductivity of the P-doped at 2.82 at% sample was smaller than singular phase of β-$FeSi_2$. ZT value was significantly enhanced by P doping as compared with that of the non-doped n-type Co doped β-$FeSi_2$/Si composites.

4.2 Introduction

In chapter 3, we highlighted the successful attempt to dope Co into β-$FeSi_2$/Si composite without deteriorating its composite structure with fine precipitations of Si. Moreover, the properties of TE were significantly enhanced even compared to the single phase Co doped β-$FeSi_2$. However, the TE properties are still relatively low compared to other silicide TE material. The secondary phase of Si exhibits a large value of electrical resistivity and thermal conductivity [13]. Hence, attempt to tune the secondary phase of precipitated Si is considered. Previous studies have proven that the substitution of P for Si in contributes to the production of n-type β-$FeSi_2$ [4]. Based on these results, it is expected that P doping at suitable amount contributes to the reduction in both electrical resistivity and thermal conductivity, and Seebeck coefficient is also not badly degenerated when P is added to Si phase, although its electrical resistivity is improved. We also gathered some findings on doping of P in the single element of Si or in other Si based alloys which contributes to the enhancement of its TE properties [2,6–8,12]. As a result, we may be able to achieve significant enhancement of TE properties compared to the β-$FeSi_2$ without P in it.. Therefore, in this chapter, we focused on the attempt to jointly dope P in Co-doped β-$FeSi_2$/Si composite, where P atoms are expected to be substituted with Si atoms in the secondary phase of precipitated Si. The composite material preparation of the *n*-type β-$FeSi_2$/Si with P substituted for the precipitated secondary phase of Si was tried using the same method presented in chapter 3. The effects of doping P in this work is then studied on its phase, microstructure, electrical and thermal properties.

4.3 Experimental Procedures

4.3.1 Synthesis process (mixing, sintering and annealing)

Powders of Fe, Si, Co and P as described in Table 4.1 are mixed using the same method described in section 2.3.6 at atomic percent of $Fe_{28.49}Co_{0.59}Si_{70.5-x}P_x$. The value of x with its simplified name of sample is summarized Table 4.2. They are also sintered and annealed using the same method as described in section 2.3.7 and 2.3.8. This time, the annealing temperature is set to 800℃, while the annealing time is set to 4 h because Co-doped β-$FeSi_2$/Si composite discussed in chapter 3 exhibits the highest ZT value at this annealing condition.

Table 4.1 Description of powder types and amount used during mixing process.

Element	Size (purity)	Manufacturer	Amount (atomic %)
Iron (Fe)	150 μm (99.9%)	Wako Pure Chemicals Industries, Ltd	28.49
Silicon (Si)	150 μm (99.9%)		70.5 - x
Phosphorus (P)	- (98%)		x
Cobalt (Co)	5 μm (99.99%)	Kojundo Chemical Laboratory Co.	0.51

Table 4.2 Composition of mixed powders in atomic % and its simplified name of sample

Sample name (simplified)	X value at atomic %
P0	0
P2	1.41
P4	2.82
P6	4.23

4.3.2 Properties analysis (phase, microstructure, density and electrical properties)

The phase determination from XRD patterns and microstructure observation from SEM photographs were done using the same method as described in section 2.3.9. We performed further evaluation on microstructure, elements and composition for composite with most P in it for for this work (P at 4.23 at%) using Auger Electron Spectroscopy (AES) equipment (AES PHI685-8). The method used for evaluation via AES is the same as described in section 2.3.3

Then, The density, ρ_s of annealed samples were measured by Archimedes method as described in section 3.3.1. The analysis for electrical properties of electrical resistivity and Seebeck coefficient from 200℃ to 700℃ were simultaneously measured using the same method as described in section 2.3.10.

4.3.3 Analysis of thermal properties

This time, similar to the method described in section 2.3.11, the thermal conductivity (κ) was calculated from the measurement values of thermal diffusivity and heat capacity shown in Eq. 4.1.

$$\kappa = C_T \times T_D \times \rho \ldots \textbf{Equation 4.1}$$

where, C_T, T_D and ρ are specific heat capacity, thermal diffusivity and sample's density respectively. The measurement method for thermal diffusivity remains unchanged as described in section 2.4.4. However, the heat capacity of processed samples was measured using a differential scanning calorimetry (DSC) machine (DSC-60 Plus 100 V, SHIMADZU). The annealed samples are crushed into fine powders using an Al_2O_3 mortar

and pestle. As shown in Fig. 4.1, there are two spaces utilized for each measurement with 3 scanning sets as summarized in Table 4.3.

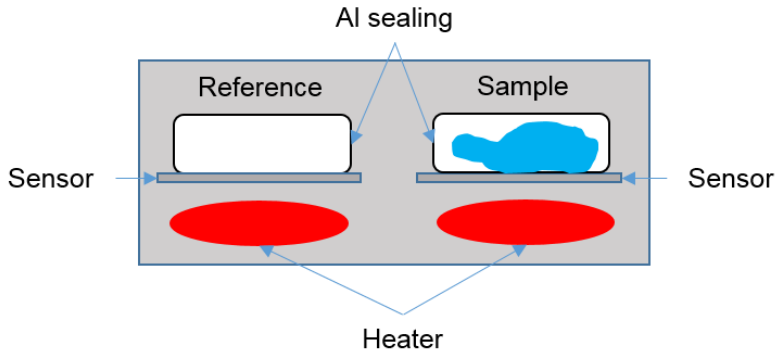

Figure 4.1 Schematic illustration for specific heat capacity measurement by DSC.

Table 4.3 Measurement (scanning) sets for evaluation of specific heat capacity

Scanning set	Reference side	Sample side
1	Empty	Empty
2	Empty	Standard sample (Al_2O_3) at m_0 [g]
3	Empty	Sample to be measured at m [g]

The detailed principle of this measurement is discussed as follows. The measurement is performed in the mode of 'isothermal retention – temperature increment at constant speed – isothermal retention' in each set of temperature point. From Eq. 4.2,

$$C_s - C_r = -\frac{T_s^{st} - T_r^{st}}{\alpha R} \quad \textbf{... Equation 4.2}$$

the values of C_s C_r, α and R are defined as heat capacity of the sample's side, heat capacity of reference side, speed of temperature increment, and constant value derived from the heat resistance within the equipment, respectively. $T_s^{st} - T_r^{st}$ is the output value from DSC, defined as the temperature difference between both sides when at stationary mode. From here, we can say the output value from DSC, S is proportionate to the

difference of heat capacity between sample's side and reference's side, expressed in Eq. 4.3.

$$C_s - C_r = \kappa S \quad \textbf{... Equation 4.3}$$

Therefore, from the scanning conditions summarized in Table 4.3, we obtained specific heat capacity by these three equations,

(1) $\kappa S_1 = C_s^h - C_r^h$ ... **Equation 4.4**

(2) $\kappa S_2 = (C_s^h + m_0 c_0) - C_r^h$ ... **Equation 4.5**

(3) $\kappa S_3 = (C_s^h + mc) - C_r^h$ ... **Equation 4.6**

where S_1, S_2, and S_3 are signals from DSC during stationary mode. From $\frac{(3)-(1)}{(2)-(1)}$, Eq. 4.7 is obtained.

$$\frac{mc}{m_0 c_0} = \frac{S_3 - S_1}{S_2 - S_1} \quad \textbf{... Equation 4.7}$$

Finally leading to the specific heat capacity of our sample, *c* is expressed in Eq. 4.8.

$$\mathbf{c} = \frac{m_0 c_0}{m} \times \frac{S_3 - S_1}{S_2 - S_1} \quad \textbf{...Equation 4.8}$$

Schematic illustration of DSC curves example utilized from all the equations are shown in Fig. 4.2.

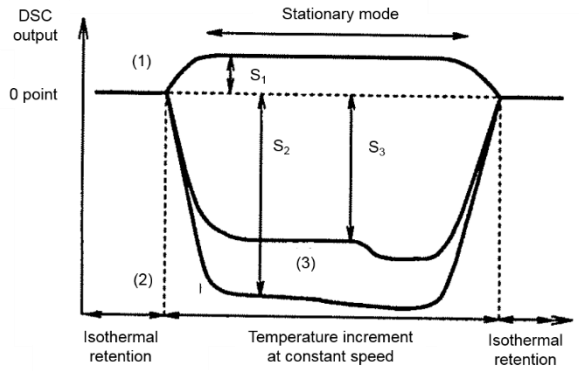

Figure 4.2 Example of DSC curves at one point of temperature to be evaluated to obtain specific heat capacity of sample.

4.4 Results and Discussion

4.4.1 Determination of α-Fe_2Si_5 phase decomposition via phase and microstructure analysis

Fig. 4.3 shows the phase determination by XRD of powders after ball milling process. Main peaks of Fe and Si indicated that the powders were homogenously mixed without creating unfavorable compounds. The milled powder was composed of typically agglomerated particles with several micrometers in size. As shown in Fig. 4.3, there are no peaks of P and Co detected due to their relatively small amount compared to Si and Fe powders. Furthermore, unwanted elements or compounds were also not detected from the XRD patterns of these powders mixture.

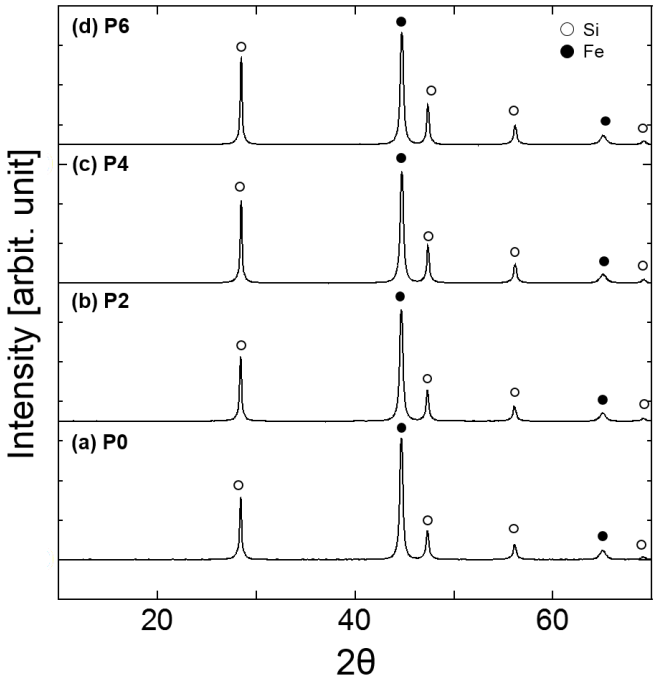

Figure 4.3 XRD patterns of $Fe_{28.49}Co_{0.59}Si_{70.5-x}P_x$ for x values at (a) 0, (b) 1.21, (c) 2.82, (d) 4.23 after mixed in a ball mill for 5h at 300 rpm.

Fig. 4.4 shows X-ray patterns of the sintered samples with compositions listed in Table 4.2. All samples after sintering were formed to be mostly composed of α-Fe_2Si_5 phase only, followed by the Fe-rich ε-FeSi phase. There are two possible factors contributing to the formation of these ε-FeSi phase. Firstly, as discussed in section 2.4.1, Fe element from the SUS pots and balls may intervene during the mixing process. The excessive Fe from the SUS pot is expected to react with Si powders during sintering process yielding the mentioned metallic ε-FeSi phase. The second possible factor contributing to the formation of ε-FeSi during sintering is the reduced amount of Si especially in P doped ones, thus making the starting powder mixture composition suitable for yielding the metallic ε-FeSi phase.

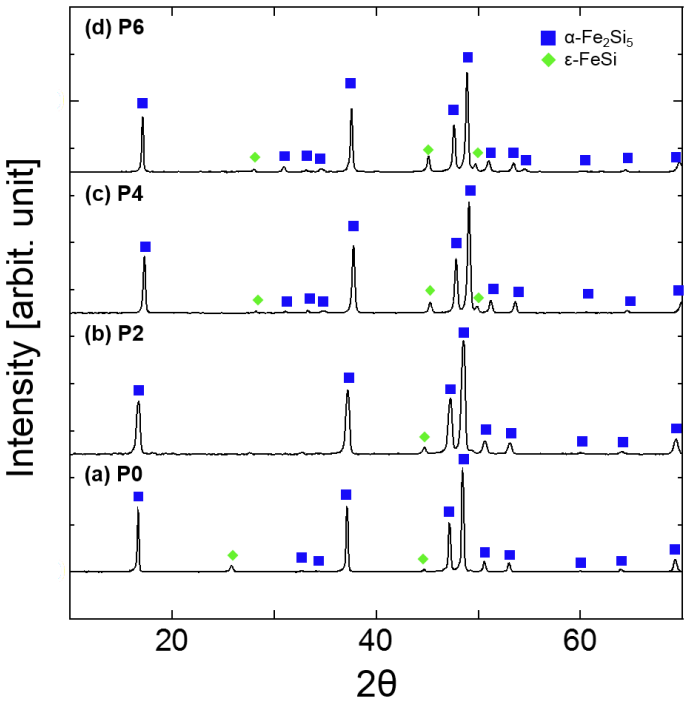

Figure 4.4 XRD patterns of $Fe_{28.49}Co_{0.59}Si_{70.5-x}P_x$ for x values at (a) 0, (b) 1.21, (c) 2.82, (d) 4.23 after sintered at 1000℃ for 10 min under 50 MPa.

As shown in Fig. 4.4 (c) and 4.4 (d), the peaks of ε-FeSi phase show an increase in

intensity, indicating that when the amount of P is increased, the formation of ε-FeSi phase is promoted. This is also possibly caused by the decreased amount of Si enhancing the feasibility of ε-FeSi phase production when P amount is increased.

The XRD patterns of these samples after annealing are then shown in Fig. 4.5. From here, it is indicated that all samples are composed of β-$FeSi_2$ peaks and secondary Si peaks. Hence, this proves that α-Fe_2Si_5 is decomposed to β-$FeSi_2$/Si completely despite the existence of metallic Fe-rich ε-FeSi phase after sintering. Annealed samples show that no peaks of ε-FeSi existed, expected to be due to the simultaneous reaction of excessive Si reacting with ε-FeSi phase producing β-$FeSi_2$ phase.

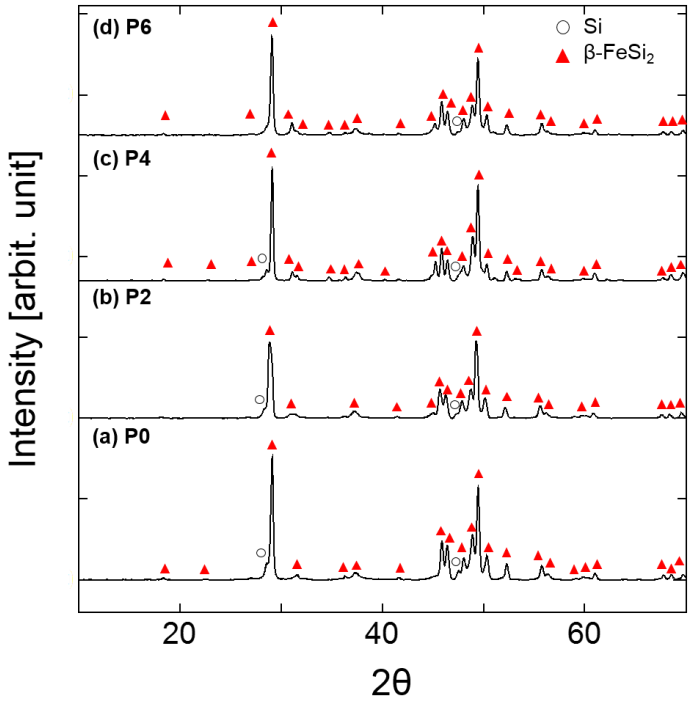

Figure 4.5 XRD patterns of $Fe_{28.49}Co_{0.59}Si_{70.5-x}P_x$ for x values at (a) 0, (b) 1.21, (c) 2.82, (d) 4.23 after annealed at 800℃ for 4h.

Fig. 4.6 shows the results of microstructure analysis by SEM of the annealed samples, indicating the main phase of β-$FeSi_2$ in lighter grey, followed by the dispersion of fine Si

in darker grey. Si size in sample P0 were approximately 100-200 nm. On the other hand, other samples of P2 to P6 indicated an increase in Si size possibly due to the P existence in Si. Therefore, it is essential to discuss about the change in Si size as amount of P is increased even at the same annealing condition.

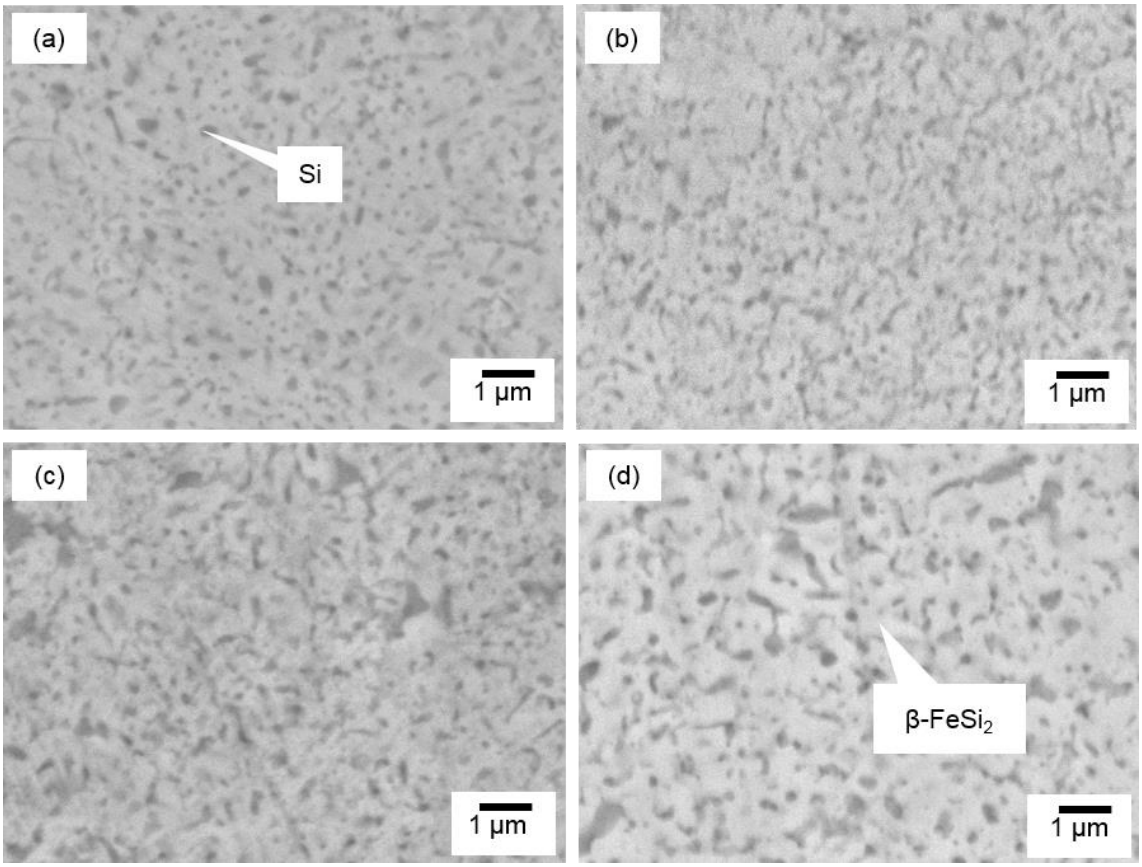

Figure 4.6 Microstructure observation of $Fe_{28.49}Co_{0.59}Si_{70.5-x}P_x$ for x values at (a) 0, (b) 1.21, (c) 2.82, (d) 4.23 after annealed at 800℃ for 4h.

We first confirmed the existence of P in Si via AES evaluation for sample P6 with the most amount of P in this work as shown in Fig. 4.7. From here, P was detected in large Si and not in small Si showing that the distribution of P is not uniform even within the secondary Si phase. Therefore, we can relate some grain coarsening of Si that occurs in sample to P in it.

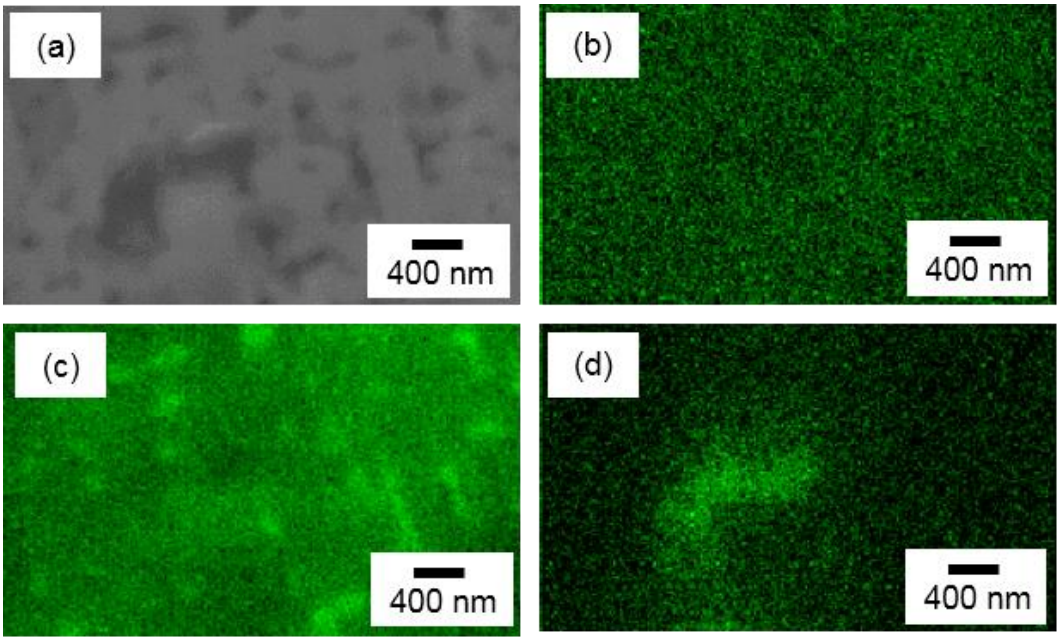

Figure 4.7 Determination of P in Si particles for sample P6 via AES equipment showing (a) SEM image, mappings for (b) Fe element, (c) Si element and (d) P element.

The main principle focused on to discuss on the grain coarsening of Si is recrystallization. Recrystallization in solids can be observed in cold working process including annealing, with its annealing temperature relatively low enough compared to its melting temperature. On the other hand, the doping of P resulting in possible substitutes of P atoms for Si atoms triggers more deformations in Si because P exists as an impurity element to Si. Thus, recrystallization process in Si-P compound may be further enhanced during annealing. The presence of P as impurity element towards Si affects significantly the process kinetics in Si-P compound. Principle studies have proven that influence of the impurity element on the recrystallization process may cause increase in stored energy and driving force to recrystallize the compound [1,3,5,11]. Therefore, we can expect the driving force of Si-P compound is larger than the driving force of Si without P in it during annealing. The driving force of Si-P compound is enhanced by the

weaken interphase energy released between Si atoms and P atoms as annealing process continues. Hence, this enhanced driving force allows the growth of Si with P in it (Si-P compound) compared to the Si without P in it. In other words, due to the possible increase in driving force of primary recrystallization from the decrease in interphase energy between Si and P cause the significant growth of Si-P compound, in β-$FeSi_2$/Si composite, which is also found in previous work on P doped Si related study [10].

4.4.2 Electrical properties

Fig. 4.8 shows the temperature dependence of (a) electrical resistivity and (b) Seebeck coefficient in the temperature range between 200℃ to 700℃ for all samples. As shown in Fig. 4.8 (a), electrical resistivity decreases as the temperature increases. This agrees to the general characteristic of semiconductor, as discussed in detailed in the section 2.4.4 [9]. The electrical resistivity is clearly reduced in Co-doped composites with P in it, as compared to the composites without P doping. This is possibly due to the increase in carrier concentration as P with 5 electron valence, leaving behind 1 free electron that moves freely enhancing the conduction by these carriers. On the other hand, the increase in P amount does not further reduce the electrical resistivity value of the composites. Even in the case of sample P6, the electrical resistivity value is slightly larger than those of samples P2 and P4. The increase in electrical resistivity values within the P doped samples are possibly due to the decrease in density values of a sintered body as shown in Table 4.4. Grain coarsening of Si may result in the poorer densification of the sintered body, suppressing electrical conduction thus increasing the electrical resistivity values.

As shown in Fig. 4.8 (b), Seebeck coefficient of all the composites over the entire temperature range shows a negative value, indicating they are n-type semiconductors.

This shows that P is substituted for Si acting as donors. As P is added to the composites, the absolute values of Seebeck coefficient decreases over the entire temperature range due to the increase in carrier density. Sample P6 exhibits the lowest absolute value of Seebeck coefficient due to the largest amount of carriers compared to samples P0, P2 and P4. However, the values of Seebeck coefficient for samples with P doping can be considered in an acceptable range of value as it is not poorly deteriorated because the evaluated electrical property as a whole is still enhanced compared to the samples without P as discussed in the next paragraph.

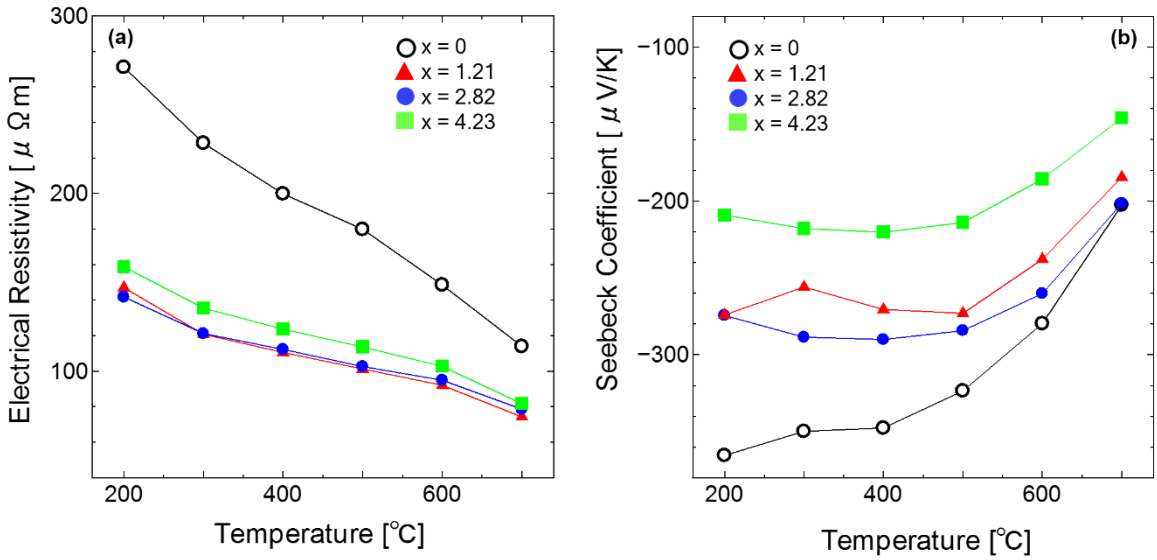

Figure 4.8 Temperature dependence of (a) electrical resistivity and (b) Seebeck coefficient for $Fe_{28.49}Co_{0.59}Si_{70.5-x}P_x$ at x = 0, 1.21, 2.82, 4.23.

Table 4.4 : Density of samples after annealed at 800℃ for 4h.

Sample	Composition [atm%]	Density [gcm^{-3}]
P0	$Fe_{28.91}Co_{0.59}Si_{70.5}$	4.4865
P2	$Fe_{28.91}Co_{0.59}Si_{69.09}P_{1.41}$	4.5143
P4	$Fe_{28.91}Co_{0.59}Si_{69.09}P_{2.82}$	4.4543
P6	$Fe_{28.91}Co_{0.59}Si_{69.09}P_{4.23}$	4.3824

The power factor (PF) indicating the electrical property of samples is calculated from the equation of $PF = S^2/\rho$, where S and ρ are Seebeck coefficient and electrical resistivity respectively. Fig. 4.9 shows the temperature dependence of power factor values in the temperature range between 200℃ to 700℃. As the temperature increases, PF for all samples increases until reaching a peak value at approximately 500℃, then continues to decrease up to 800℃, with the maximum value of 787 μW/mK. Sample P4 showed the highest value compared to other samples despite the decrement of Seebeck coefficient in sample P4 because of its small values of electrical resistivity. Hence, adding a suitable amount of P (in this case of 2.82 at%) to Co-doped β-$FeSi_2$/Si composite is an effective way to help improve its electrical properties.

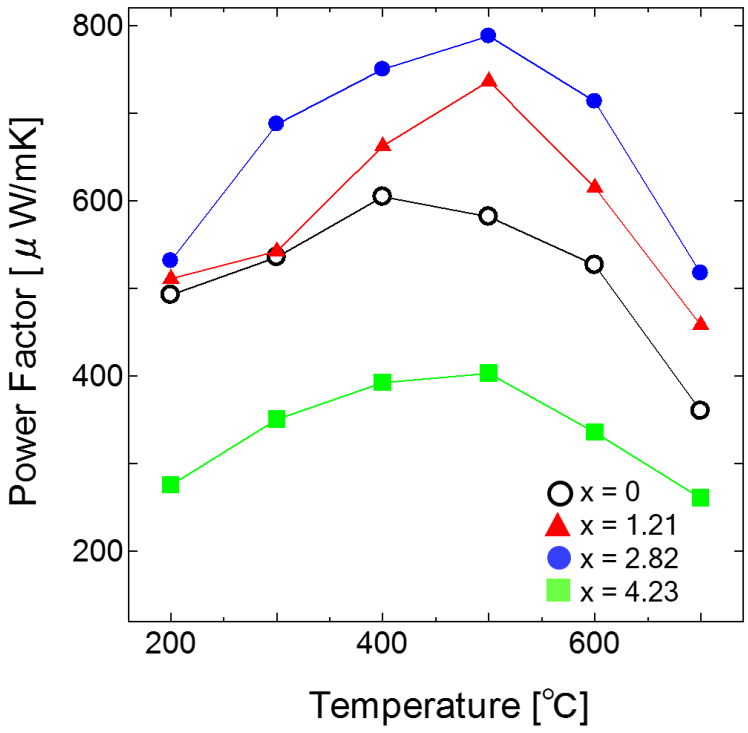

Figure 4.9 Temperature dependence of power factor for for $Fe_{28.49}Co_{0.59}Si_{70.5-x}P_x$ at x = 0, 1.21, 2.82, 4.23.

4.4.3 Thermal properties and the enhanced performance of TE properties in P doped n-type β-$FeSi_2$ composite

Fig. 4.10 (a) shows the temperature dependence of thermal conductivity for all samples annealed at 800℃ for 4h within the temperature range of 200℃ to 700℃. Thermal conductivity in semiconductors is the sum of lattice contribution influenced by phonons and electronic contribution influenced by carriers [14]. As P is added and its amount continues to increase, electronic contribution to the thermal conductivity is expected to increase. However, the thermal conductivity of the sample P4 exhibits the lowest value over the entire temperature range. This is possibly attributable to significant reduction in thermal conductivity from lattice contribution due to enhancement of phonon scattering, which is caused by P solution in the Si secondary phase. On the other hand, when P was further doped, the thermal conductivity of the sample P6 increased as compared to the sample P4. This result implies that carrier contribution to the thermal conductivity is significantly enhanced by the further P doping. Thus, P doping can affect both the electrical and lattice contributions to the thermal conductivity, so it is considered to be important to optimize the amount of doped P to obtain smaller thermal conductivity of the β-$FeSi_2$/Si composite, as our future work. Fig. 4.10 (b) shows the dimensionless figure of merit, ZT value calculated from Eq. 1.2, where these values for all samples increase to a peak point of 600℃, then continue to decrease until measurement finished at 700℃. From here, sample P4 shows the highest value of ZT more than 0.1, followed by samples P2, P0 and P6. When we compare the ZT values of P doped and non-doped ones, despite the decrease in Seebeck coefficient, the decrease in thermal conductivity and electrical resistivity helps increase the ZT value indicating the success in improving

its TE performance. From these results obtained, it was found that P doping is a promising candidate in improving the thermoelectric performance of n-type β-$FeSi_2$ composites. However, P was revealed to be not uniformly distributed in Si phase of this composite. Hence, if P can be uniformly doped in Si phase, thermoelectric properties may be further improved. So, more precise and focused control of size and P uniformity in Si phase are essential towards improving the TE performance. For example, longer mixing time of ball milling towards more uniformed distribution of P in Si should be tried as our future work.

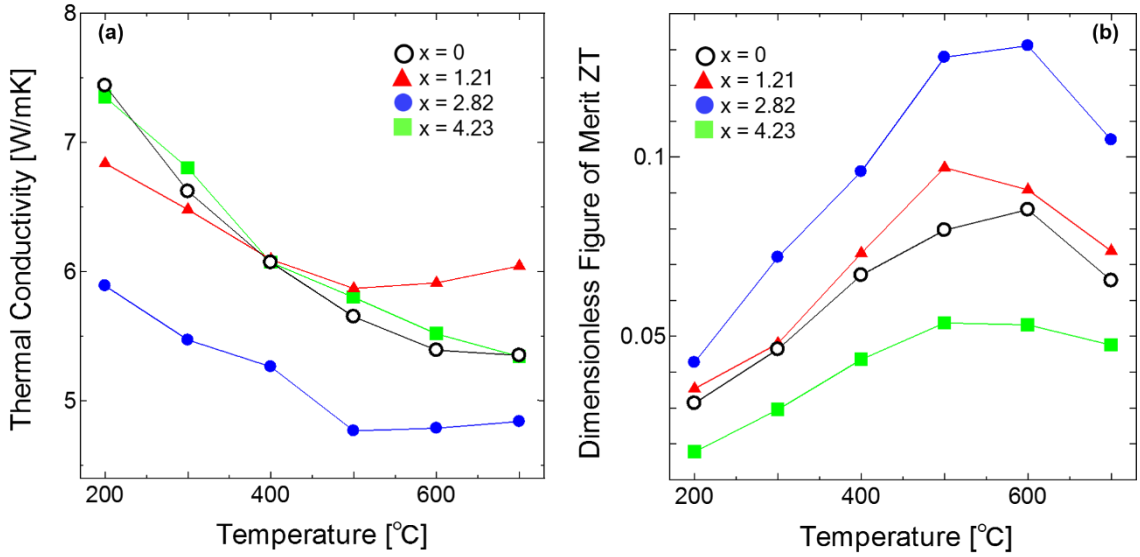

Figure 4.10 Temperature dependence of (a) thermal conductivity and (b) ZT value for $Fe_{28.49}Co_{0.59}Si_{70.5-x}P_x$ at x = 0, 1.21, 2.82, 4.23.

4.5 Conclusion

We summarize the findings in chapter 4 as follows:

I The attempt on jointly doping of P to the Co doped β-$FeSi_2$/Si composites was conducted by annealing the initially sintered samples with α-Fe_2Si_5 phase, at 800℃ for 4h. The attempt was found successful as the evaluation from the phase and microstructure analysis shows a complete decomposition from α-Fe_2Si_5 phase to β-$FeSi_2$/Si heterogeneous phase. It is expected for the P atoms to be substituted with Si atoms in the secondary phase of precipitated Si.

II The evaluation from microstructure observation also indicated that P was not distributed uniformly within the secondary phase of Si. In addition, large amount of P within the secondary phase of Si caused its grain coarsening.

III Doping of P to Co doped β-$FeSi_2$/Si composite contributes to the further decrease in electrical resistivity. However, excessive amount of P showed an increase in the electrical resistivity due to the decrease in the composite's density.

IV The composite with the composition of $Fe_{28.49}Co_{0.59}Si_{70.5-x}P_x$ at x = 2.82 at% exhibits the lowest value of thermal conductivity due to the expected essential balance of lattice contribution and electronic contribution of thermal conductivity.

V Therefore, the highest ZT value was obtained by the composite with the composition of $Fe_{28.49}Co_{0.59}Si_{70.5-x}P_x$ at x = 2.82 at%, surpassing 0.1, indicating a distinct improvement compared to the Co doped β-$FeSi_2$/Si composites without P doping.

4.6 References

[1] R. Abbaschian, A. Abaschian, R.E. Reed-Hill, *Annealing*, in : Phys. Metall. Princ., 8(1)-8 (17).

[2] J.P. Fleurial, C.B. Vining, A. Borshchevsky, *Multiple doping of Si-Ge alloys for thermoelectric applications*, Proc. 24th Intersoc. Energy Convers. Eng. Conf. 2 (1989) 701–705.

[3] F.J. Humphreys, M. Hatherly, *Recrystallization Of Two-Phase Alloys*, in: Recryst. Relat. Annealing Phenom., (2004) 285–286.

[4] M. Ito, H. Nagai, E. Oda, S. Katsuyama, K. Majima, *Effects of P doping on the thermoelectric properties of β-FeSi$_2$*, J. Appl. Phys. 91 (2002) 2138–2142.

[5] P. Matusiewicz, W. Ratuszek, A. Zielińska-Lipiec, *Recrystallization of ferrite in spheroidite of Fe-0.67%C steel*, Arch. Metall. Mater. 56 (2011) 63–69.

[6] R. Murugasami, P. Vivekanandhan, S. Kumaran, R.S. Kumar, T.J. Tharakan, *Thermoelectric power factor performance of silicon-germanium alloy doped with phosphorus prepared by spark plasma assisted transient liquid phase sintering*, Scr. Mater. 143 (2018) 35–39.

[7] Y. Ohishi, J. Xie, Y. Miyazaki, Y. Aikebaier, H. Muta, K. Kurosaki, S. Yamanaka, N. Uchida, T. Tada, *Thermoelectric properties of heavily boron and phosphorus doped silicon*, Jpn. J. Appl. Phys. 54 (2015) 1–6.

[8] X. Pi, *Doping silicon nanocrystals with boron and phosphorus*, J. Nanomater. 2012 (2012) 1–9.

[9] K. Safa, K. Cyril, E.R. Harry, *Electrical conduction in metals and semiconductors*, in : Springer Handb. Electron. Photonic Mater., (2017) 19–45.

[10] Y. Wada, S. Nishimatsu, *Grain Growth Mechanism of Heavily Phosphorus-*

Implanted Polycrystalline Silicon, J. Electrochem. Soc. 125 (1978) 1499.

[11] K. Wierzbanowski, J. Tarasiuk, B. Bacroix, K. Sztwiertnia, *Stored energy and its role in recrystallization process*, J. Neutron Res. 9 (2001) 61–64.

[12] D.L. Young, H.M. Branz, F. Liu, R. Reedy, B. To, Q. Wang, *Electron transport and band structure in phosphorus-doped polycrystalline silicon films*, J. Appl. Phys. 105 (2009) 033715.

[13] A. Yusufu, K. Kurosaki, Y. Miyazaki, M. Ishimaru, A. Kosuga, Y. Ohishi, H. Muta, S. Yamanaka, *Bottom-up nanostructured bulk silicon : a practical high-efficiency thermoelectric material*, Nanoscale. 6 (2014) 13921–13927.

[14] X. Zhang, L.-D. Zhao, *Thermoelectric materials : Energy conversion between heat and electricity*, J. Mater. 1 (2015) 92–105.

Chapter 5

Adding Cu to n-type β-$FeSi_2$/Si Composite in the attempt to minimize Si size towards enhancing TE properties

5.1 Overview

This chapter discusses the attempt to add Cu in Co-doped β-$FeSi_2$/Si composite. It is expected that the addition of Cu contributes to the increase in phase transformation rate from α-Fe_2Si_5 phase to β-$FeSi_2$/Si phase, hence minimizing the size of Si precipitates. In other words, Cu is expected to help accelerate the eutectoid decomposition of α-Fe_2Si_5 phase. We examined samples with 1 mass% and 2 mass% of Cu amount with various annealing conditions. A significant decrease in Si size, reaching less than 100 nm for composites with 2 mass% Cu annealed at 650℃ for 2h was obtained. Within the same amount of Cu, Si size was clearly increased after annealed at 800℃ for 4h. These results suggest the phase transition is accelerated with the existence of Cu. The thermal conductivity value was greatly reduced for sample with 2 mass% Cu, compared to the experimental value of single β-$FeSi_2$ and calculated value from the rule of mixture from previous works. This proves that the fine distribution of Si help suppresses thermal conductivity despite the high value of Si phase itself. However, the excessive amount of Cu (2 mass%) degenerated the electrical properties of Co doped β-$FeSi_2$/Si. Nonetheless, sample with 1 mass% Cu showed the highest value of ZT, indicating that it is essential to keep the balance of Cu amount and annealing conditions.

5.2 Introduction

In chapter 4, we highlighted the successful attempt to simultaneously dope P in the Si phase of Co doped β-$FeSi_2$/Si composite with significant enhancement of TE properties. The TE properties were enhanced due to the significant decrease of electrical resistivity and thermal conductivity without affecting badly its Seebeck coefficient. However, the size of Si still remains in the range of 200 – 300 nm in size. Therefore, we would like to focus on developing methods to minimize effectively the size of Si precipitations in β-$FeSi_2$/Si composite. Yamauchi and Ito et al. revealed that the addition of Cu was quite effective in increasing the phase transformation rate of singular β-$FeSi_2$ phase initially formed from metallic phases of α-Fe_2Si_5 and ε-FeSi [3,16]. However, studies on the effects of Cu towards the phase transformation rate of β-$FeSi_2$/Si and its thermoelectric properties has not been done. Hence, in this chapter we focused on the attempt to accelerate the decomposition rate in α-Fe_2Si_5 by adding Cu. Furthermore, the accelerated phase transformation is expected to contribute to the reduction of Si size, thus suppressing thermal conductivity. Therefore, we added Cu in various amounts and tried to clarify the effects of Cu addition and annealing condition on the microstructure and TE properties.

5.3 Experimental procedure

5.3.1 Synthesis process (mixing, sintering and annealing)

Powders of Fe, Si, Co and Cu as described in Table 5.1 are mixed using the same method described in section 2.3.6 at atomic percent of $Fe_{28.49}Co_{0.59}Si_{70.5}$ with addition of Cu in various amount at mass%. The amount of Cu with its simplified name of sample is summarized in Table 5.2, together with its annealing conditions.

Table 5.1 Description of powder types and amount used during mixing process

Element	Size (purity)	Manufacturer	Amount (atomic %)
Iron (Fe)	150 μm (99.9%)	Wako Pure Chemicals Industries, Ltd	28.49
Silicon (Si)	150 μm (99.9%)		70.5
Cobalt (Co)	5 μm (99.99%)	Kojundo Chemical Laboratory Co., Ltd	0.51
Copper (Cu)	1 μm (99.99%)		x (mass%)

Table 5.2 Composition of mixed powders in atomic % and its simplified name of sample and annealing conditions

Sample	Cu content	Annealing temperature	Annealing time
CU0A800T4	0 mass%	800℃	4 h
CU1A650T2	1 mass%	650℃	2 h
CU1A800T4	1 mass%	800℃	4 h
CU2A650T2	2 mass%	650℃	2 h
CU2A800T4	2 mass%	800℃	4 h

The mixed powders were then sintered via the same method and equipment as described in section 2.3.6, followed by the same annealing process as described in section and 2.3.7. However, the sintering conditions differ for Cu added samples. The uniformed

powder mixtures were sintered at 1000℃ for samples without Cu and 1100℃ for samples with Cu in them. Sintering temperature for Cu added samples was set to 1100℃ because Cu existence caused partial formation of β-$FeSi_2$ at 1000℃. For example, as shown in Fig. 5.1 (a), sintered body with Cu in it revealed some existence of β-$FeSi_2$ and Si peaks when sintered at 1000℃, while these peaks disappeared as sintered at 1100℃ shown in Fig. 5.1 (b). This indicates an initial hint where Cu contributes to the accelerated decomposition of α-Fe_2Si_5 yielding β-$FeSi_2$/Si heterogeneous phase. Sintering time for all compositions is 10 min under the pressure of 50 MPa in a vacuum condition.

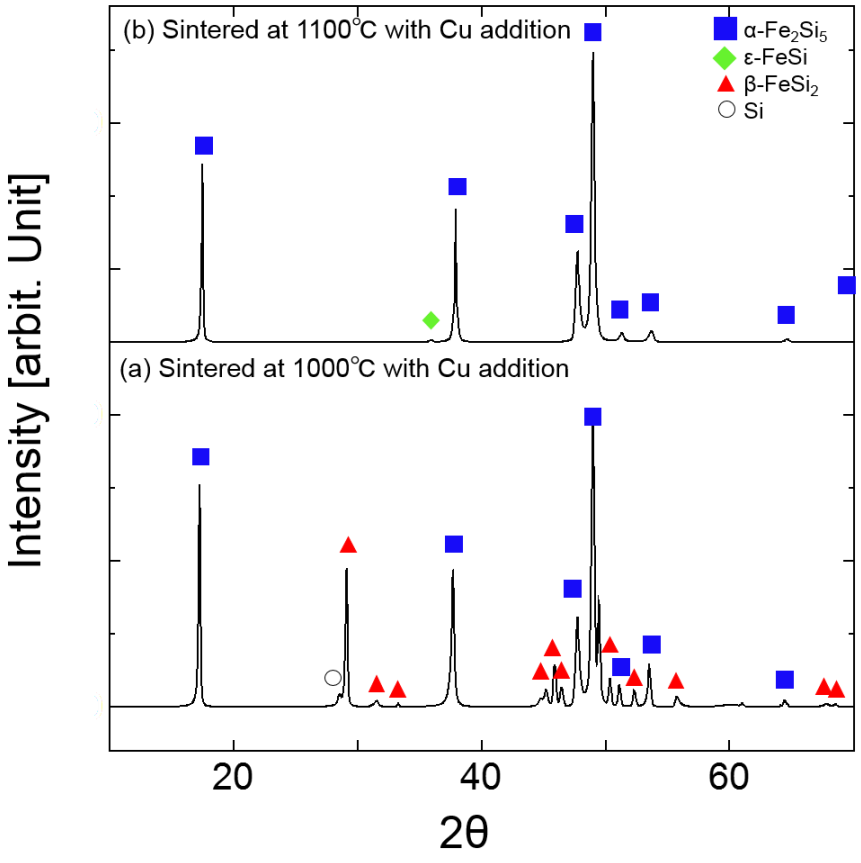

Figure 5.1 XRD patterns for samples with Cu at 2 mass% sintered at (a) 1000℃ and (b) 1100℃

5.3.2 Properties analysis (phase, microstructure, density, electrical properties and thermal properties)

The phase determination from XRD patterns and microstructure observation from SEM imaging were done using the same method as described in section 2.3.9. Then, The density of annealed samples were measured by Archimedes method as described in section 3.3.1. The analysis for electrical properties of electrical resistivity and Seebeck coefficient from 200℃ to 700℃ were simultaneously measured using the same method as described in section 2.3.10. The thermal properties consists of both thermal diffusivity and specific heat capacity were measured from 200℃ to 700℃ by the same process described in section 4.4.3.

5.4 Results and Discussion

5.4.1 Determination of α-Fe_2Si_5 phase decomposition to β-$FeSi_2$/Si heterogeneous phase.

Fig. 5.2 shows the phase analysis by XRD for mixed powders with Cu amount at (a) 0 mass%, (b) 1 mass% and (c) 2 mass%. Main peaks of Fe and Si from XRD patterns shown in Fig. 5.2 for all compositions indicated that the powders were successfully mixed without creating unwanted element or compounds. Moreover, peaks of Cu and Co was not detected due to its relatively small amount compared to more dominant components of Si and Fe.

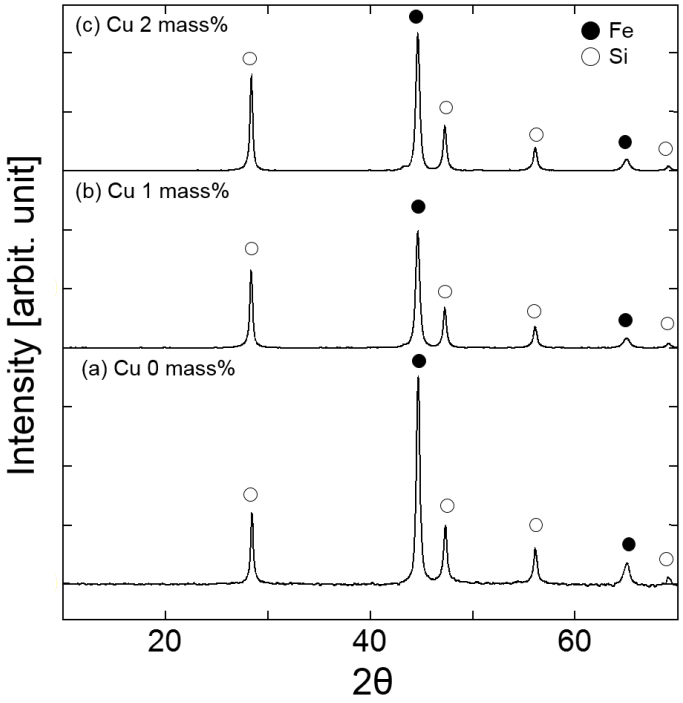

Figure 5.2 XRD patterns of $Fe_{28.49}Co_{0.59}Si_{70.5}$ + Cu at x mass% (a) x = 0, (b) x = 1, (c) x = 2 after mixed in a ball mill for 5h at 300 rpm.

Fig. 5.3 shows the XRD patterns of the sintered samples with Cu amount at (a) 0 mass%, (b) 1 mass%, and (c) 2 mass%. From here, high temperature metallic α-Fe_2Si_5 phase is mainly obtained, followed by scarce amount of ε-FeSi phase after being sintered in their respective conditions mentioned earlier. As discussed in section 2.4.1, the excessive Fe amount during ball milling process results to the existence of these ε-FeSi peaks.

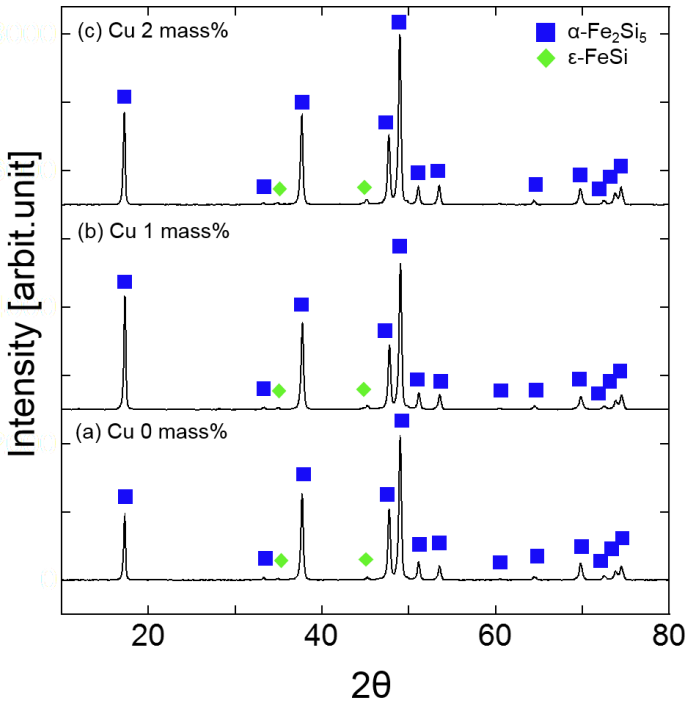

Figure 5.3 XRD patterns of $Fe_{28.49}Co_{0.59}Si_{70.5}$ + Cu at x mass% (a) x = 0, (b) x = 1, (c) x = 2 after sintered under 50 MPa for 10 mins at 1000℃ for x = 0 and 1100℃ for x = 1, 2.

XRD patterns of all samples after annealed at conditions listed in Table 5.2 are shown in Fig. 5.4. From here, main peaks are composed of β-$FeSi_2$, while the secondary peaks are composed of Si. This indicates that all annealed samples with various Cu quantity were successfully decomposed to the heterogeneous phase of β-$FeSi_2$/Si from the high temperature metallic α-Fe_2Si_5 phase. No ε-FeSi after annealing was detected despite the

formation of it during sintering process. This is possibly due to the simultaneous reaction that occur where the excessive Si reacted with ε-FeSi phase producing β-$FeSi_2$ phase. We also confirmed the incomplete phase transformation in Co doped β-$FeSi_2$/Si composite without Cu addition annealed at 700℃ for 3 h from XRD patterns discussed in section 3.4.1, where peak of α-Fe_2Si_5 still existed. Meanwhile, the Co doped β-$FeSi_2$/Si composite with Cu in it were completely decomposed from the initial α-Fe_2Si_5 phase at lower annealing temperature of 650℃. This justifies the contribution of Cu to help accelerate the decomposition of α-Fe_2Si_5 phase to the β-$FeSi_2$/Si heterogenous phase.

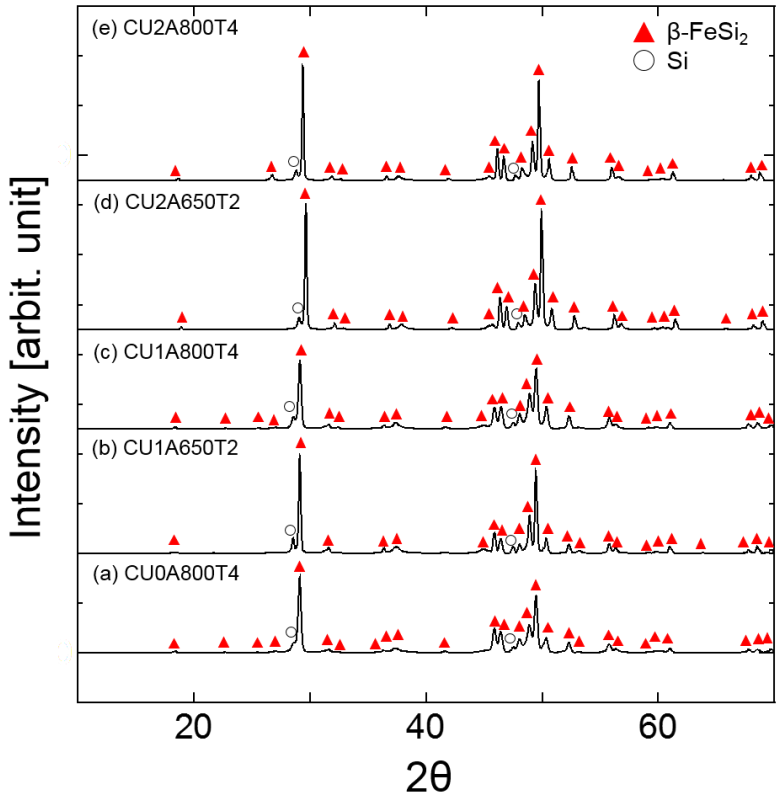

Figure 5.4 XRD patterns of $Fe_{28.49}Co_{0.59}Si_{70.5}$ + Cu at x mass% with various annealing conditions; (a) x = 0, annealed at 800℃ for 4h; (b) x = 1, annealed at 650℃ for 2h; (c) x = 1, annealed at 800℃ for 4h; (d) x = 2, annealed at 650℃ for 2h, (e) x = 2, annealed 800℃ for 4h in Ar environment.

Fig. 5.5 shows the microstructure analysis by SEM imaging for all samples after annealing process. This analysis indicates a general observation of main matrix in light grey is composed of β-$FeSi_2$, with darker precipitated spots composed of Si. The microstructure analysis agrees to the results from XRD patterns shown in Fig. 5.4, indicating β-$FeSi_2$ as main phase, followed by the precipitations of Si as secondary phase. However, Cu shown in white spots were viable in samples with 2 mass% of added Cu only as shown in Fig. 5.5 (d) and (e), although not detected from the XRD patterns.

Furthermore, both XRD patterns and SEM photographs of Co-doped β-$FeSi_2$/Si composites with Cu in them reveal no existence of unwanted element and compounds that may deteriorate further both the targeted microstructure with fine Si and their TE properties. Meanwhile, there is a significant difference in Si size depending on the various content of Cu and annealing conditions of holding temperature and time. Sample that has the maximum Cu content in this work (2 mass%) annealed at 650℃for 2 h shown in Fig. 5.5 (d) has the finest precipitations of Si. The size of Si of this sample is found to be far less than 100 nm. On the contrary, sample CU2A800T4 with the same Cu amount, but with longer annealing time and higher annealing temperature, has the largest size of Si as shown in Fig. 5.5 (e).

From this analysis, it was confirmed that Cu contributes in accelerating the decomposition of α-Fe_2Si_5 producing β-$FeSi_2$/Si composites. Furthermore, Si grain coarsening was also detected in the samples CU1A800T4 and CU2A800T4 as compared with sample at the same composition in samples CU1A650T2 and CU2A650T2, respectively. Both samples CU1A800T4 and CU2A800T4 were annealed at higher temperature of 800℃ and for longer time of 4h. In chapter 3, we have discussed on the factors affecting phase transformation rate of α-Fe_2Si_5 phase, where we evaluated the

influence of annealing time and temperature towards the microstructure of β-$FeSi_2$/Si composite. As annealing temperature increases nearing the material's melting point, grain growth occurs faster than the nucleation of new phase.

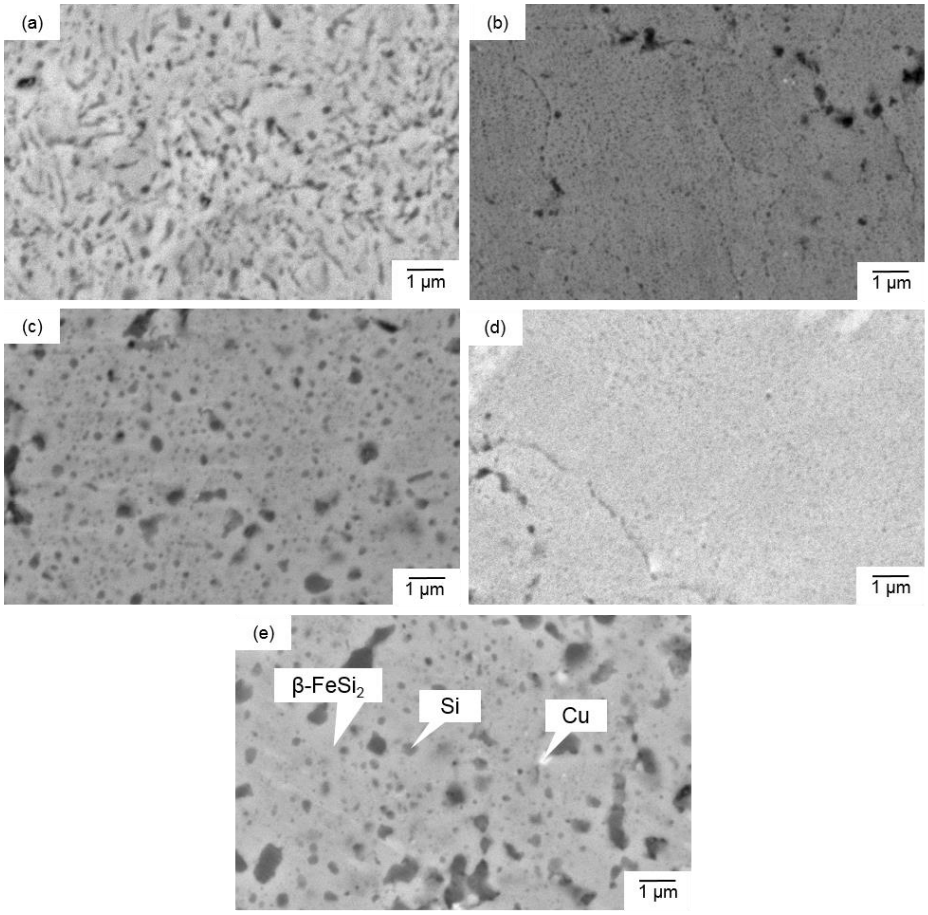

Figure 5.5 SEM images of samples (a) CU0A800T4, (b) CU1A650T2 (c) CU1A800T4 (d) CU2A650T2 (e) CU2A800T4 with various Cu amount and annealing conditions previously summarised in Table 5.2.

On the other hand, at lower annealing temperature, nucleation occurs faster than the growth rate resulting to the domination of fine Si phase formation rather than its growth [18]. Therefore, grain growth of Si in samples annealed at higher temperature and longer time is enhanced in both samples CU1A800T4 and CU2A800T4 when compared to their same compositions respectively annealed at lower temperature and time.

Meanwhile, Si size in sample CU2A800T4 is larger than that of sample CU1A800T4, indicating that the addition of Cu help accelerates the growth of Si. This can be discussed from the kinetics during phase transformation occurred in the decomposition of α-Fe_2Si_5. In the case of the β-$FeSi_2$ single phase, it was discovered that the existence of Cu attributes to the shift of endothermic peak towards a lower temperature in a thermal analysis done by Yamauchi et al. [16,17]. This means that eutectoid decomposition from α-Fe_2Si_5 to the composites phase reach its equilibrium at a lower temperature when Cu is added. Cu is reported to have a high thermal conductivity value [9] which eventually speeds up the heat energy absorption during the phase transformation [16]. Since the decomposition of α-Fe_2Si_5 reaches its equilibrium at a lower temperature when Cu is added, the co-existing Si in the β-$FeSi_2$/Si continues to grow in size during annealing at higher temperature, for longer time.

5.4.2 Electrical properties

Fig. 5.6 shows the temperature dependence of (a) electrical resistivity and (b) Seebeck coefficient within the temperature range from 200℃ to 700℃ for all samples. From Fig. 5.6 (a), electrical resistivity for all samples decreases as temperature increases indicating a general semiconducting properties similar to the findings regarding this property as discussed in detailed in section 2.4.4 . The analysis also revealed that factors affecting the trend of thermoelectric properties' parameters for β-$FeSi_2$/Si composites remain difficult to be emphasized as they have different dominant factors respectively. For example, sample CU2A800T4 exhibits the lowest value of electrical resistivity, which is consistent with the fact that it has the maximum amount of highly electrical conductive Cu. On the other hand, sample CU2A650T2 with the same amount of Cu exhibits a higher value of

electrical resistivity, as compared to the samples with lower amount of Cu possibly due to the fine precipitations of Si. From our observation, sample CU2A650T2 with the maximum amount of Cu, lowest annealing temperature and shortest annealing time exhibits the highest value of electrical resistivity due to its finest precipitations of Si (smallest Si size) which contributes to the increased resistance of electric conduction. As shown in Fig. 5.5 and Fig. 5.6, there is a significant trend of decreased size of Si results in increased value of electrical resistivity attributed to the increase in interfacial carrier scattering [8,13]. However, the electrical resistivity values between sample CU1A650T2 and CU1A800T4 with the same amount of Cu proves contrarily. Here, sample CU1A650T2 is expected to have higher value of electrical resistivity due to the finer precipitations of Si compared to sample CU1A800T4.

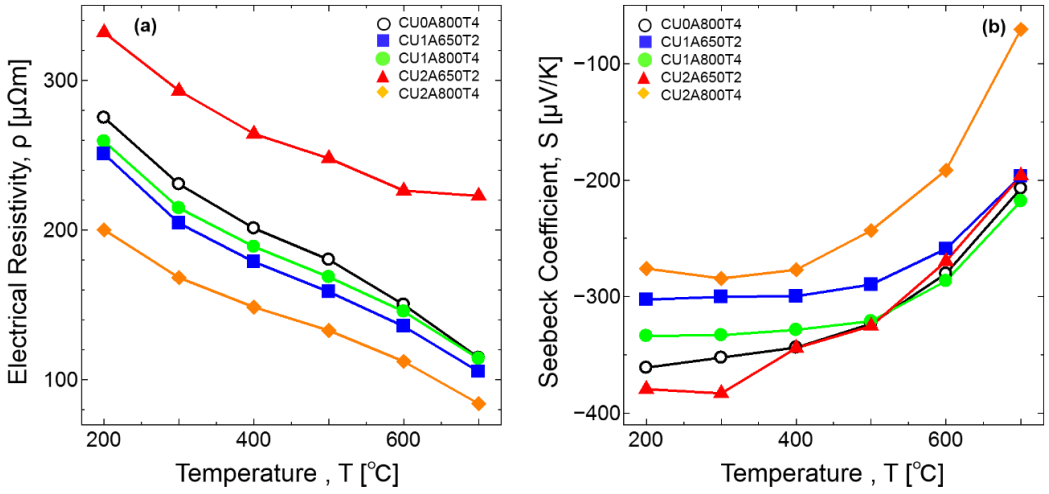

Figure 5.6 Temperature dependence of (a) electrical resistivity and (b) Seebeck coefficient for samples CU0A800T4, CU1A650T2, CU1A800T4, CU2A650T2 and CU2A800T4 with various Cu amount and annealing conditions as summarised in Table 5.2**.**

Table 5.3 Sample's density after annealed at various conditions for different amount of Cu addition.

Sample name	Density (gcm^{-3})
CU0A800T4	4.49
CU1A650T2	4.46
CU1A800T4	4.45
CU2A650T2	4.43
CU2A800T4	4.42

However, density of samples is also anticipated to be one of the factors affecting the trend of electrical resistivity values too. Therefore, the slightly higher density value of sample CU1A650T2 shown in Table 5.3 may cause the reduction in electrical resistivity values within the entire temperature range compared to sample CU1A800T4.

As shown in Fig. 5.6 (b), Seebeck coefficient values for all samples are negative, signifying n-type semiconductor as Co substituted for Fe worked as donor, which seems not to be affected by the addition of Cu at any amount. In most cases, the increase in electrical resistivity corresponds to the increase in Seebeck coefficient due to the mutual relationship between electrical resistivity and Seebeck coefficient [8]. However, a steep decrease in absolute value of Seebeck Coefficient for sample CU2A650T2 and sample CU2A800T4 from 500℃ is observed due to the existence of excessive metallic component (Cu). This proves that the excessive amount of Cu, in this case 2 mass%, contributes to the deterioration of thermoelectric power in thermoelectric materials as temperature is further increased. Nevertheless, sample CU2A650T2 exhibits highest absolute value of Seebeck coefficient before it deteriorates at a higher temperature range. This is possibly due to the scattering factor from fine precipitations of Si that remains dominant before reaching 500℃, where Seebeck coefficient is expected to increase as

scattering parameter increases [6]. Thus, it can be concluded that the addition of Cu which contributes to a finer dispersion of Si helps enhance the Seebeck coefficient.

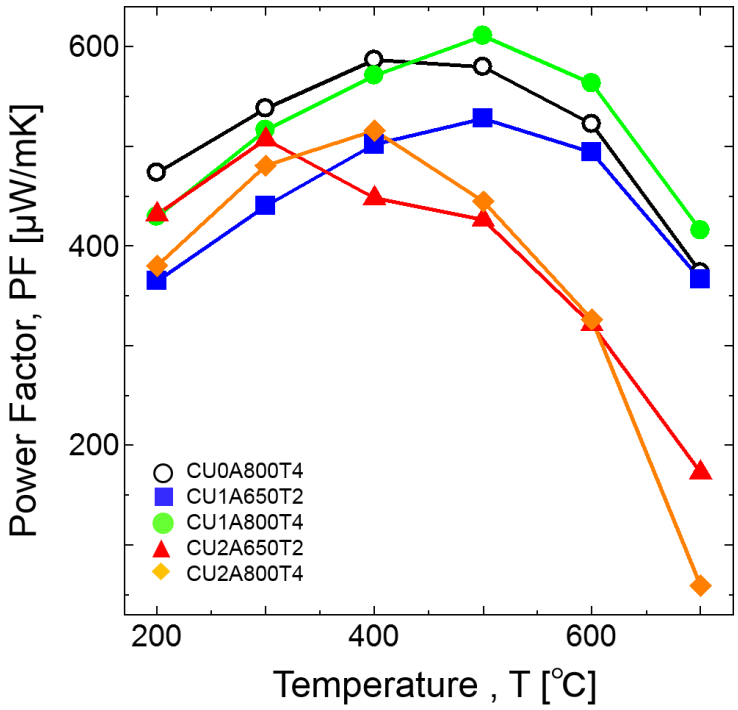

Figure 5.7 Temperature dependence of Power Factor for samples CU0A800T4, CU1A650T2, CU1A800T4, CU2A650T2 and CU2A800T4 with various Cu amount and annealing conditions as summarised in Table 5.2.

The electrical properties is then evaluated from the value of PF expressed in the relation of $PF = S^2/\rho$. The temperature dependence of PF values within the temperature range from 200℃ to 700℃ is expressed in Fig. 5.7. As temperature increases, PF for all samples increases until reaching a peak value at various temperature point for each sample, then continues to decrease up to 700℃. Sample CU1A800T4 with 1 mass% amount of Cu shows the largest PF value compared to other samples, indicating that excess amount of Cu addition degenerates the electrical properties of β-$FeSi_2$/Si based composites for samples with 2 mass% Cu. This is due to the increase in carrier concentration from the

increased amount of metallic Cu, thus deteriorating the thermoelectric power or Seebeck coefficient values [19]. Therefore, adding a suitable amount of Cu to n-type β-$FeSi_2$/Si composite is an effective way to help suppress the deterioration of Seebeck coefficient despite the initial target to minimize the size of Si by increasing the amount of Cu.

5.4.3 Thermal properties

Fig. 5.8 shows the temperature dependence of (a) total thermal conductivity and (b) its component within entire temperature range from 200℃ to 700℃ elaborated as follows. The components of total thermal conductivity can be evaluated from Eq. 5.1 shown below,

$$\kappa_{To} = \kappa_{La} + \kappa_{El} \quad \textbf{... Equation 5.1}$$

where, $\kappa_{To}, \kappa_{La}$and κ_{El} are the total thermal conductivity, lattice component of thermal conductivity and electronic/carrier component of thermal conductivity, respectively [15]. κ_{El} is expressed in the Wiedemann-Franz Law of $\kappa_{El} = LT/\rho$, where L is the Lorentz number [10]. From here, L can be expressed in the equation below,

$$L = \frac{\pi^2}{3}\left(\frac{k_B}{q}\right)^2 \quad \textbf{... Equation 5.2}$$

where k_B and q are the Boltzmann constant and charge of electron, respectively [14]. From this equation, Lorentz number is generally estimated as 2.45×10^{-8} W Ω/K^2, known as the degenerate limit. However, it is arguable to determine the Lorentz number at a constant value for semiconductors because the degenerate limit is found to be applicable for metals and heavily doped semiconductors mostly, where their charge carriers move like a free electron. On the other hand, semiconducting thermoelectric materials including β-$FeSi_2$ has a more complex Fermi surfaces, thus affecting the transport of charge carriers dissimilar to the metal ones [7,11]. Therefore, we approach the method introduced by

Kim et al. to determine the approximation of Lorentz number as shown below [7],

$$L = 1.5 + exp\left[\frac{|-S|}{116}\right] \quad \textbf{... Equation 5.3}$$

This simplified equation was proved to be accurate within 5% for semiconductors with acoustic phonon scattering, exhibiting absolute Seebeck Coefficient value higher than 10 $\mu V/K$, which includes semiconducting β-$FeSi_2$ based materials [1,2,7,14]. The temperature dependence of thermal conductivity components is illustrated in Fig. 5.8 (b). As shown in Fig. 5.8 (b), values of κ_{El} slightly increased as temperature increased due to the increase in metallic component of Cu in Cu added samples. On the other hand, lattice contribution of κ_{La} remains dominant which explains the main cause of suppression in total thermal conductivity is affected by the scattering of phonon due to the fine precipitations of Si. As a whole, sample CU2A650T2 showed the lowest value of total thermal conductivity within all temperature range due to the dominant factor from the minimized Si size of lesser than 100 nm, enhancing phonon scattering, while CU2A800T4 with largest size of Si exhibits highest value of thermal conductivity. This proves that the decreased size of Si successfully helps suppress thermal conduction through the enhanced phonon scattering despite the high thermal conductivity value of Si phase itself.

We then try to evaluate the total thermal conductivity value of sample CU2A650T2 by comparing with results from previous works including the calculated value from rule of mixture as shown in Fig. 5.9. Fig. 5.9 gathers the total thermal conductivity values from calculation of rule of mixture [12], experimental results of Co doped β-$FeSi_2$/Si without Cu after annealed at 800℃ and 700℃ for 4h from our previous work [12], followed by the experimental value of singular-phased Co doped β-$FeSi_2$ [4,5] and values from current work of sample CU2A650T2. In this study, we managed to obtain minimum value of total

thermal conductivity from sample CU2A650T2 even compared to the value from singular-phased Co doped β-$FeSi_2$ without Si precipitations. Furthermore, thermal conductivity of Co doped β-$FeSi_2$/Si composite without Cu was not successfully decreased previously when compared to the single Co doped β-$FeSi_2$ by just introducing composite structure from the decomposition of α-Fe_2Si_5. This again justifies that finer dispersion of Si obtained by adding Cu effectively suppressed thermal conduction due to enhanced phonon scattering and interfacial thermal resistance between constituents within β-$FeSi_2$/Si composites [6,12].

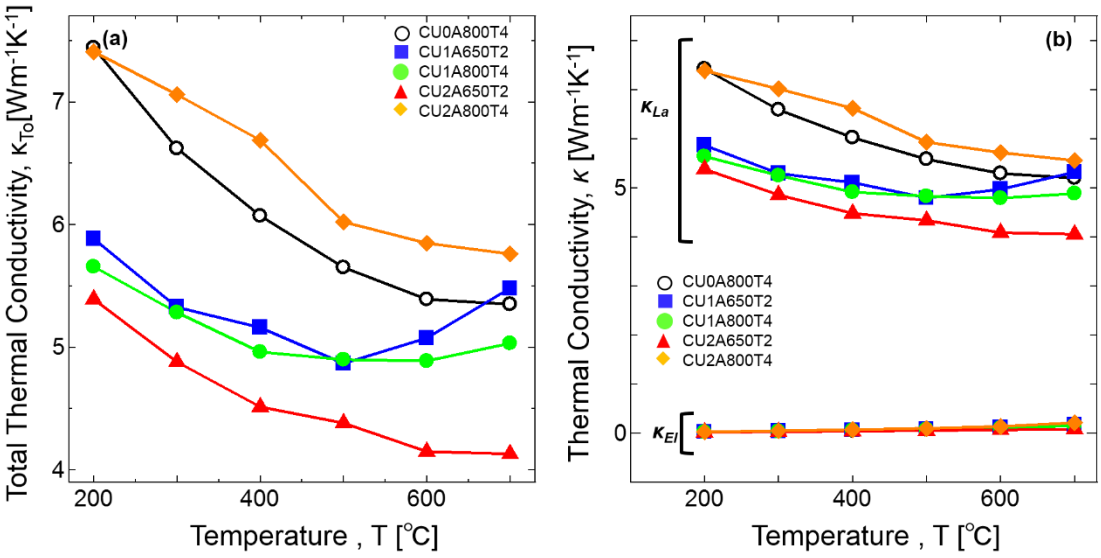

Figure 5.8 Temperature dependence of (a) total thermal conductivity and (b) its components for samples CU0A800T4, CU1A650T2, CU1A800T4, CU2A650T2 and CU2A800T4 with various Cu amount and annealing conditions previously summarised in Table 5.2.

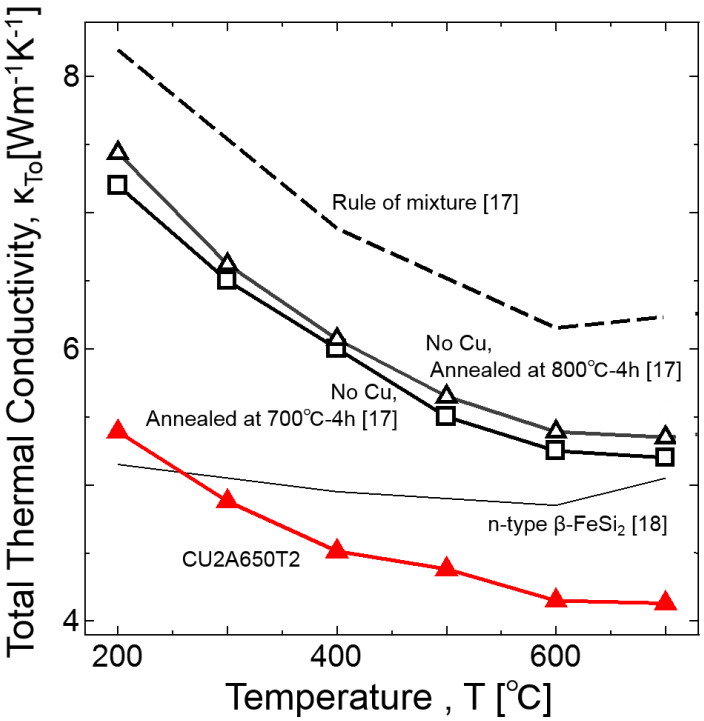

Figure 5.9 Temperature dependence of total thermal conductivity for sample CU2A650T2 with lowest value of thermal conductivity done in this work and previous work by Farah et al. [12] to evaluate the suppression of thermal conductivity from rule of mixture.

5.4.4 Enhanced TE properties by adding Cu in Co-doped β-$FeSi_2$/Si composite

The temperature dependence of ZT value for all samples calculated from Eq. 1 within the temperature range from 200℃ to 700℃ are expressed in Fig. 5.10. As can be seen, we found that sample CU1A800T4 exhibits the highest ZT value of 0.1 at approximately 600℃, exceeding the ZT value of Co doped β-$FeSi_2$/Si composite without addition of Cu. We initially hypothesized the sample with lowest value of thermal conductivity in sample CU2A650T2 to have the highest performance due to the Si size that have been greatly reduced. But it was found that, due to the balance of relatively high value of power factor

and second lowest value of thermal conductivity in sample CU1A800T4, this sample possess the highest ZT value surpassing the value of sample CU2A650T2. Significantly, we found that the addition of Cu helps accelerate the phase transformation of β-$FeSi_2$/Si composites even at a lower annealing temperature and shorter annealing time.

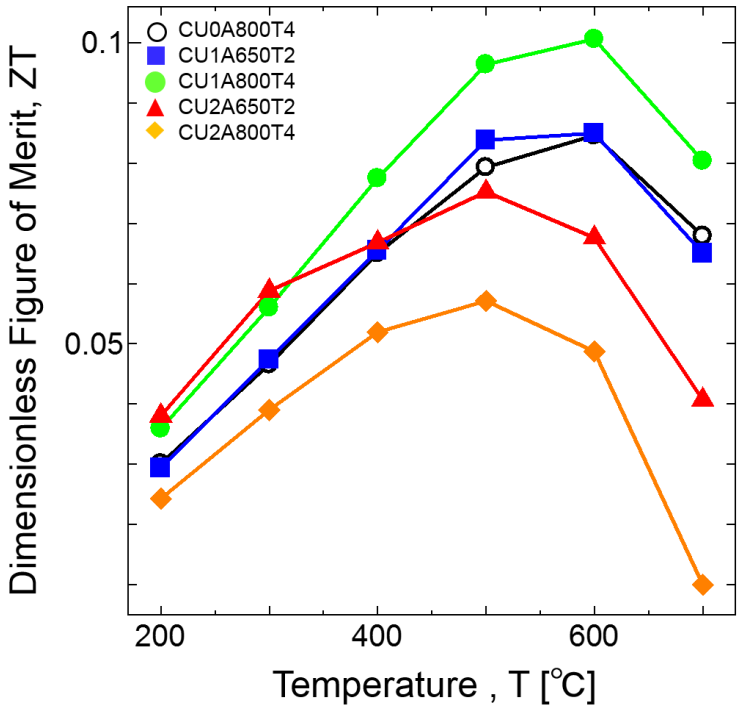

Figure 5.10 Temperature dependence of ZT values for samples CU0A800T4, CU1A650T2, CU1A800T4, CU2A650T2 and CU2A800T4 with various Cu amount and annealing conditions previously summarised in Table 5.2

Furthermore, the accelerated transformation is also clearly proved by the increase in size of Si at higher amount of Cu, even at the same annealing time and annealing temperature between samples CU0A800T4, CU1A800T4 and CU2A800T4. We plan to study on the possibility of compensating the degeneration of electrical properties with the existence of Cu by doping another carrier component in the precipitated Si phase, preserving the nano-scale size of Si as our future work. One example of carrier component that can be considered to be doped in the Si phase is P because it was proven in chapter 4

of this work that silmutaneous doping of P in Co doped β-$FeSi_2$/Si composites caused an enhancement of TE properties due to the significant decrease in both electrical resistivity and thermal conductivity.

5.5 Conclusion

We summarize the findings in chapter 5 as follows

I Addition of Cu helps accelerate the phase decomposition of α-Fe_2Si_5 phase producing β-$FeSi_2$/Si phase.

II The accelerated phase decomposition of α-Fe_2Si_5 phase by adding Cu showed a complete decomposition yielding β-$FeSi_2$/Si composite phase at a lower temperature and shorter annealing time of 650℃ and 2 h respectively. The β-$FeSi_2$/Si composite without Cu in it was unable to be completely transformed even at a higher annealing temperature and longer annealing time of 700℃ and 3 h, respectively, discussed in chapter 3.

III We obtained smallest size of Si phase within β-$FeSi_2$ phase (or finest Si precipitations) in the composite with the maximum amount of Cu, lowest annealing temperature and shortest annealing time examined in this work.

IV The reduced size of Si secondary phase contributes to the significant suppression of thermal conductivity. As a result, the ZT values of β-$FeSi_2$/Si based composites were significantly enhanced.

5.6 References

[1] E. Arushanov, K.G. Lisunov, *Transport properties of β-$FeSi_2$*, Jpn. J. Appl. Phys. 54 (2015) 07JA02.

[2] P. Golinelli, L. Varani, L. Reggiani, *Generalization of thermal conductivity and lorenz number to hot-carrier conditions in nondegenerate semiconductors*, Phys. Rev. Lett. 77 (1996) 1115–1118.

[3] M. Ito, H. Nagai, D. Harimoto, S. Katsuyama, K. Majima, *Effects of Cu addition on the thermoelectric properties of hot-pressed β-$FeSi_2$ with SiC dispersion*, J. Alloys Compd. 322 (2001) 226–232.

[4] M. Ito, H. Nagai, E. Oda, S. Katsuyama, K. Majima, *Effects of P doping on the thermoelectric properties of β-$FeSi_2$*, J. Appl. Phys. 91 (2002) 2138–2142.

[5] M. Ito, K. Takemoto, *Synthesis of thermoelectric $Fe_{0.98}Co_{0.02}Si_2$ with fine Ag dispersion by mechanical milling with AgO powder*, Mater. Trans. 49 (2008) 1714–1719.

[6] J.X. Jiang, T. Sasakawa, K. Matsugi, G. Sasaki, O. Yanagisawa, *Thermoelectric properties of β-$FeSi_2$ with Si dispersoids formed by decomposition of α-Fe_2Si_5 based alloys*, 391 (2005) 115–122.

[7] H. Kim, Z.M. Gibbs, Y. Tang, H. Wang, G.J. Snyder, H. Kim, Z.M. Gibbs, Y. Tang, H. Wang, G.J. Snyder, *Characterization of Lorenz number with Seebeck coefficient measurement*, Appl. Phys. Lett. Mater. 041506 (2016) 1–6.

[8] M.H. Lee, J. Rhyee, *Thermoelectric properties of p-type PbTe/Ag_2Te bulk composites by extrinsic phase mixing*, Am. Instittute Phys. Adv. 127223 (2016) 1–7.

[9] M. Li, S.J. Zinkle, *Physical and mechanical properties of copper and copper alloys*,

Compr. Nucl. Mater. 4 (2012) 667–690.

[10] Y. Noda, H. Kon, Y. Furukawa, N. Otsuka, I.A. Nishida, K. Masumoto, *Preparation and thermoelectric properties of $Mg_2Si_{1-x}Ge_x$ (x=0.0~0.4) Solid Solution Semiconductors*, Mater. Trans. 33 (1992) 845.

[11] M. Otsuka, R. Homma, Y. Hasegawa, *Estimation of Phonon and Carrier Thermal Conductivities for Bulk Thermoelectric Materials Using Transport Properties*, J. Electr. Mater. 46 (2017) 2752–2764.

[12] F.L.B.M. Redzuan, I. Mikio, T. Masatoshi, *Synthesis of Co-doped β-$FeSi_2$/Si composites through eutectoid decomposition and its thermoelectric properties*, J. Mater. Sci. 53 (2018) 7683–7690.

[13] V. Srivastava, Ojha. S.N, *Microstructure and electrical conductivity of Al–SiC_p composites produced by spray forming process*, Bull. Mater. Sci. 28 (2005) 125–130.

[14] M. Thesberg, H. Kosina, N. Neophytou, *On the Lorenz number of multiband materials*, Phys. Rev. B. 95 (2017) 1–14.

[15] X.W. Wang, H. Lee, Y.C. Lan, G.H. Zhu, G. Joshi, D.Z. Wang, J. Yang, A.J. Muto, M.Y. Tang, J. Klatsky, S. Song, M.S. Dresselhaus, G. Chen, Z.F. Ren, *Enhanced thermoelectric figure of merit in nanostructured n-type silicon germanium bulk alloy*, Appl. Phys. Lett. 93 (2008) 1–4.

[16] I. Yamauchi, A. Suganuma, T. Okamoto, I. Ohnaka, *Effect of copper addition on the β-phase formation rate in $FeSi_2$ thermoelectric materials*, J. Mater. Sci. 32 (1997) 4603–4611.

[17] I. Yamauchi, S. Ueyama, I. Ohnaka, *β-$FeSi_2$ Phase formation from a unidirectionally solidified rod-type eutectic structure composed of both α and ϵ*

phases, Mater. Sci. Eng. A. 208 (1996) 108–115.

[18] L. V. Zhigilei, *Introduction to the Science and Engineering : Phase Transformation*, http://people.virginia.edu/~lz2n/mse209/index.html (Online lecture notes), MSE 2090. (2010) 16.

[19] H. Zou, D.M. Rowe, G. Min, *Growth of p and n-type bismuth telluride thin films by co-evaporation*, J. Cryst. Growth. 222 (2001) 82–87.

Chapter 6

Kinetics of phase transformation in α-Fe_2Si_5 phase

6.1 Overview

In this chapter we tried to identify experimentally the phase transformation kinetics of α-Fe_2Si_5 phase yielding β-$FeSi_2$/Si heterogeneous phase. This enables us to provide indications in enhancing the study of nano-structuring in bulk thermoelectric materials, specifically β-$FeSi_2$ based TE material towards significant improvement of TE properties. We examined various annealing conditions for non-doped β-$FeSi_2$/Si composite and the enhanced synthesize rate of β-$FeSi_2$/Si composite with Cu in it as in previous chapter, where we discovered the complete decomposition of α-Fe_2Si_5 to occur at lower annealing temperature and shorter annealing time. As we plotted the annealing time and temperature with its phase transformation condition, we managed to estimate the characteristic of temperature-time-transformation (TTT) diagram. From this estimation, the fastest transformation rate can be observed providing beneficial hint to obtain microstructure desirable for TE performance enhancement, in this case a fine precipitations of Si within β-$FeSi_2$ able to suppress thermal conductivity.

6.2 Introduction

In chapter 5, we highlighted the successful attempt of enhancing phase transformation of high temperature α-Fe_2Si_5 phase yielding β-$FeSi_2$/Si composite phase by adding Cu. The enhancement was proved by the eutectoid decomposition to complete at lower annealing temperature and shorter annealing time when Cu is added. Nonetheless, the well balanced condition of annealing time and annealing temperature is yet to be discovered due to the limitations of conditions examined. Previous studies have shown the fastest decomposition rate of α-Fe_2Si_5 to complete at approximately 800℃ for 4 h by plotting the isothermal transformation diagram also known as the 'time-temperature-transformation' (TTT) diagram [2,4]. However, in our work, as revealed in previous chapters, we found that the complete decomposition of α-Fe_2Si_5 phase can occur at lower annealing temperature and shorter annealing time of 700℃ for 3 h even at the samples without Cu in them [7]. Therefore, it is essential to test experimentally on more of the annealing conditions to determine the possible fastest rate for α-Fe_2Si_5 phase to complete its decomposition. This may result in the nose position of the TTT diagram, indicating the complete phase transformation at the fastest rate, to be lower than that of the previous findings by J.X Xiang et al [2]. Therefore, we examine more than 10 of various annealing conditions for non-doped β-$FeSi_2$/Si composite. We also examine the n-type $FeSi_2$/Si composite with Cu in it which may indicate a different character of TTT diagram because Cu was proven to enhance the phase transformation yielding β-$FeSi_2$ single phase in previous studies [1,3,5,9–12], and we also revealed the enhanced decomposition yielding β-$FeSi_2$/Si composite as discussed in chapter 5. From these findings, we expect results as follows.

I Lower nose point of TTT diagram for non-doped β-$FeSi_2$/Si composite done in this work compared to the previous work [2].

II β-$FeSi_2$/Si composite exhibits further lower nose point of TTT diagram as Cu is added in it for Cu amount at 2 mass%.

From these results, we can estimate a character of transformation rate for β-$FeSi_2$/Si based composites with different composition that can be utilized as a basic reference for phase transformation control. Subsequently, we can also expect a fine precipitation of Si at these nose points causing possible enhancement of phonon scattering towards enhancing its TE properties.

6.3 Experimental Procedures

The experimental procedures of this work is divided to the synthesize process and properties analysis process as illustrated in Fig. 6.1. This time, as we focus on the evaluation of phase transformation, properties analyzed is the phase determination via XRD. From here, we observe the eutectoid decomposition from the high temperature α-Fe_2Si_5 metallic phase.

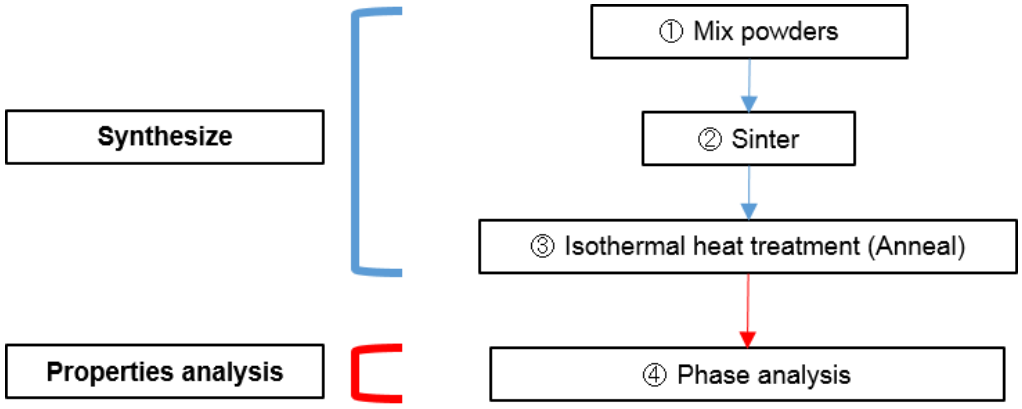

Figure 6.1 Graphical flow of experimental procedures

6.3.1 Synthesize process and its phase evaluation

Powders of Fe, Si, Co and Cu as described in Table 6.1 are mixed using the same method described in section 2.3.6 at atomic percent of $Fe_{28.49}Co_{0.59}Si_{70.5}$ with and without addition of Cu at 2 mass%. The mixed powders were then sintered and annealed through the same methods and equipments as described in section 2.3.6 and 2.3.7 respectively. The sintering conditions differ for Cu added samples with the sintering temperature of 1100℃ as described and discussed in section 5.3.1. Meanwhile, the annealing conditions are summarized in Table 6.2. Initially, the annealing conditions were set to 800℃ for 4

h due to its complete decomposition confirmed in previous chapters and their enhanced TE properties. From this initial condition, we change the following annealing conditions after evaluating its phase from XRD analysis each time.

Table 6.1 Description of powder types and amount used during mixing process.

Element	Size (purity)	Manufacturer	Amount (at%)
Iron (Fe)	150 μm (99.9%)	Wako Pure Chemicals Industries, Ltd	28.49
Silicon (Si)	150 μm (99.9%)		70.5
Cobalt (Co)	5 μm (99.99%)	Kojundo Chemical Laboratory Co., Ltd	0.51
Copper (Cu)	1 μm (99.99%)		2 mass%

Table 6.2 : Annealing conditions of sintered bodied (*reference from previous work)

Sample	Temperature (℃)	Time
No Cu added	500	1 h
	650	4 h
	700	1 h
	700	4 h
	750*	1 h*
	760	15 min
	770	15 min
	770	30 min
	800	4 h
	800*	8 h*
	800*	24 h*
	800*	48 h*
	900*	8 h*
	900	24 h
Cu at 2 mass%	500	10 h
	550	2 h
	550	3 h
	550	4 h

	600	1 h
	600	2 h
	650	2h
	650	4h
	700	3h
	700	4h
	800	3h
	800	4h

All mixed powders, sintered bodies and annealed samples were analyzed by XRD via the same method and equipment described in section 2.3.3 to evaluate their phases after each synthesis process.

6.4 Results and Discussion

6.4.1 Phase evaluation of annealed samples

Fig. 6.2 and Fig. 6.3 show the XRD patterns of annealed β-$FeSi_2$/Si composites under various conditions summarized in Table 6.2. In this section, both no element of dopant and no Cu addition is considered. We decide to focus on this phase to clarify the rate of eutectoid decomposition of initially produced α-Fe_2Si_5 yielding the composite phase of β-$FeSi_2$/Si. As shown in Fig. 6.2 (a), main peaks of the initial α-Fe_2Si_5 phase indicated that the decomposition did not progress in the annealing condition of 500℃ - 10 h. Meanwhile, we found that the annealing conditions of 650℃ - 4 h and 760℃ - 15 min as shown in and Fig. 6.2 (b) and Fig. 6.3 (b), respectively, indicated an incomplete phase transformation due to the co-existing of all α-Fe_2Si_5, ε-FeSi, and β-$FeSi_2$ phases. Other than that, the remaining annealing conditions as shown in Fig. 6.2 of (c) 700℃ - 3h, (d) 700℃ - 4h and in Fig. 6.3 of (a) 750℃ - 1h, (c) 770℃ - 15 min and (d) 770℃ - 30 min reveals the existence of β-$FeSi_2$ as main peaks and Si as secondary peaks. This indicates that the above annealing conditions are conducive for complete eutectoid decomposition of α-Fe_2Si_5 phase yielding the heterogeneous phase of β-$FeSi_2$/Si.

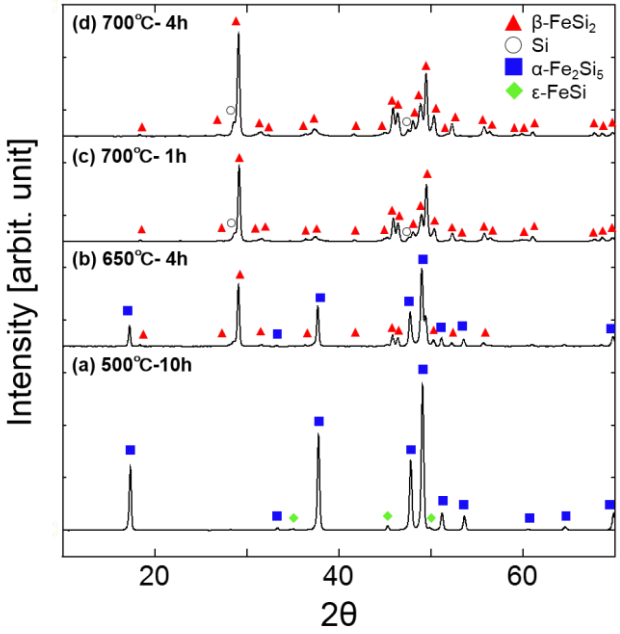

Figure 6.2 XRD patterns of $Fe_{29.5}Si_{70.5}$ with various annealing conditions of (a) 500℃ at 10 h, (b) 650℃ at 4 h, **(c)** 700℃ at 1 h, and (d)700℃ at 4 h.

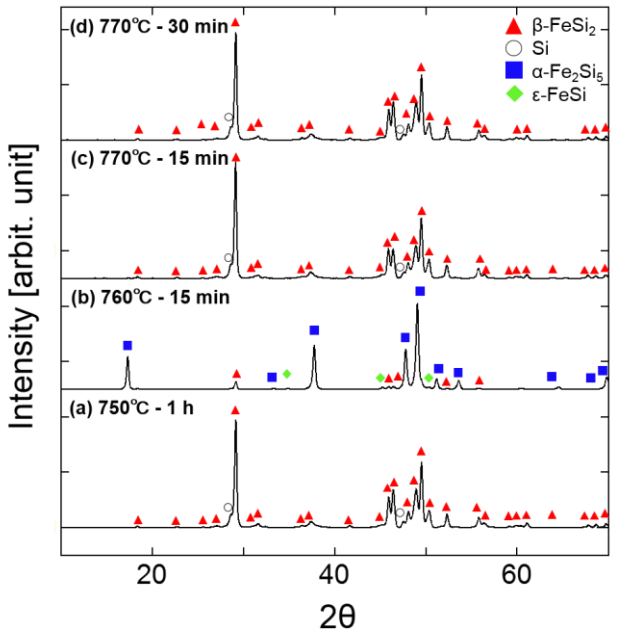

Figure 6.3 XRD patterns of $Fe_{29.5}Si_{70.5}$ with various annealing conditions of (a) 750℃ at 1 h, (b) 760℃ at 15 min, **(c)** 770℃ at 15 min, and (d)770℃ at 30 min.

Then we attempted to plot the phases obtained after various annealing process in a time-temperature graph to estimate the phase transformation rate as shown in Fig. 6.4. The x –axis is set as annealing time while the y-axis is set as the annealing temperature. The symbols of plots showing unchanged α-Fe_2Si_5 phase, midway α-Fe_2Si_5 + β-$FeSi_2$/Si phases and the complete β-$FeSi_2$/Si phases as final products are also expressed in this figure. From this figure, we try to estimate the 'Temperature-Time-Transformation' (TTT) diagram pattern and the position of 'nose' indicating the fastest rate for complete decomposition of α-Fe_2Si_5. This result will be discussed in detail in the next section. Before that, the phase evaluation of composites with added Cu will be discussed below.

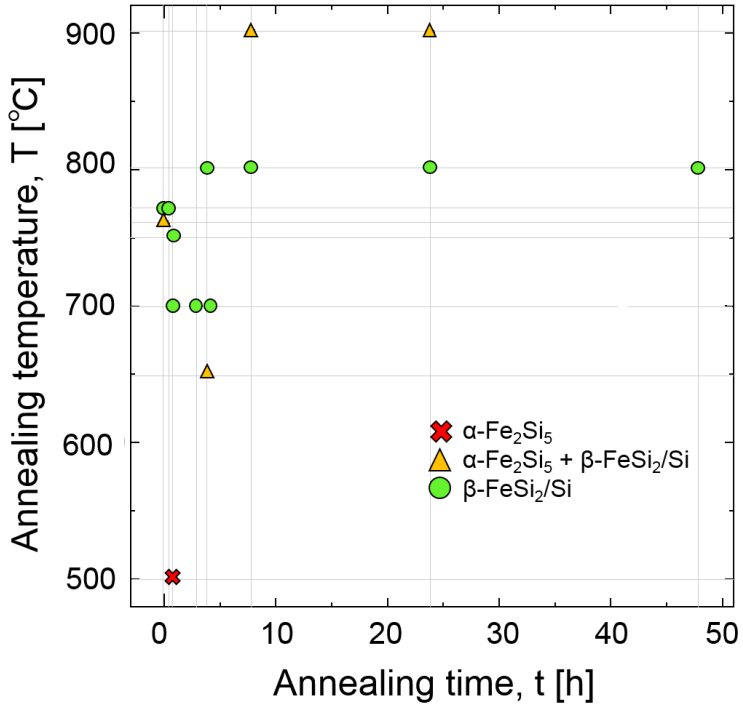

Figure 6.4 Plots of final product after annealing in the relation of annealing time-annealing temperature.

Fig 6.5 shows the XRD patterns of samples with Cu addition annealed at (a) 500℃ for 10 h, (b) 550℃ for 2 h, and (c) 550℃ for 3 h. From here, samples with annealing

conditions (Temperature - Time) of 500℃ - 10 h and 550℃ - 2 h showed incomplete phase transformation. As shown in Fig. 6.5 (a), only main peaks of α-Fe_2Si_5 followed by one peak of β-$FeSi_2$ is observed from these patterns. As the annealing temperature is increased to 550℃, even for a shorter time of 2 h, the phase transformation is enhanced and more progressed decomposition can be observed by major peaks of β-$FeSi_2$ and Si, followed by the minor peaks consisting of α-Fe_2Si_5. As the time is increased to 3 h at the same temperature, complete decomposition of α-Fe_2Si_5 is revealed as the XRD patterns shown in Fig. 6.5 (c) is consisted of main peaks β-$FeSi_2$ followed by the secondary peaks of Si only, indicating the final yield of β-$FeSi_2$/Si composite.

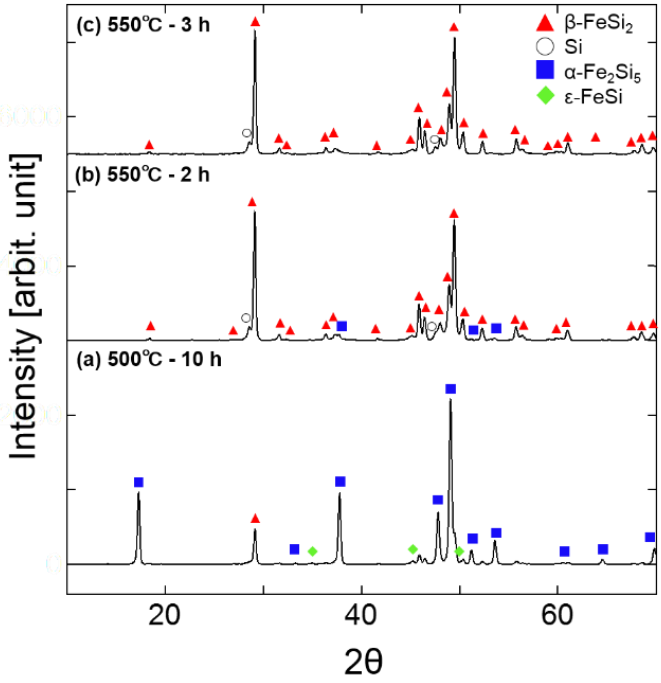

Figure 6.5 XRD patterns of $Fe_{28.49}Co_{0.59}Si_{70.5}$ + Cu at 2 mass% with various annealing conditions of (a) 500℃ for 10 h, (b) 550℃ for 2 h, and (c) 550℃ for 3 h

Fig. 6.6 shows the XRD patterns of samples with the same composition (2 mass% Cu addition) annealed at (a) 550℃ for 4 h, (b) 600℃ for 1 h, and (c) 600℃ for 2 h. From

these results, all samples annealed at these conditions show primary peaks of β-$FeSi_2$, followed by the secondary peaks of Si. This indicates that all samples annealed under these conditions are completely decomposed from the initial phase of α-Fe_2Si_5 to the heterogeneous phase of β-$FeSi_2$/Si.

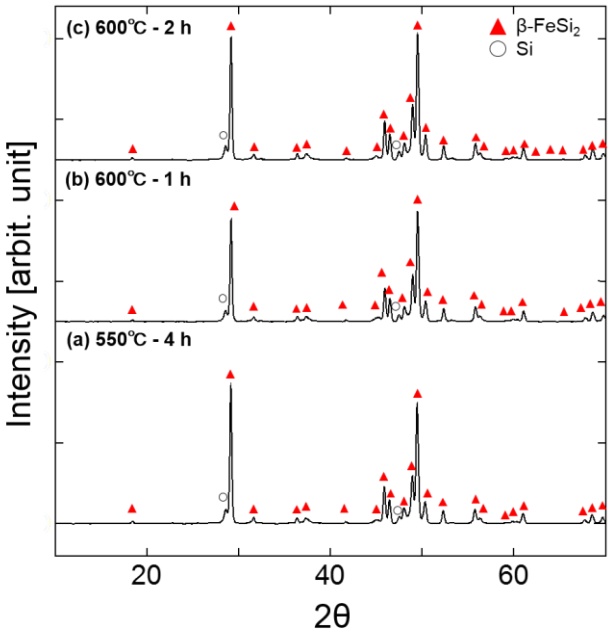

Figure 6.6 XRD patterns of $Fe_{28.49}Co_{0.59}Si_{70.5}$ + Cu at 2 mass% with various annealing conditions of (a) 550℃ for 4 h, (b) 600℃ for 1 h, and (c) 600℃ for 2 h.

Fig 6.7 shows the XRD patterns with the same composition annealed at (a) 650℃ for 2 h, (b) 650℃ for 4 h, and (c) 700℃ for 3 h, while Fig. 6.8 shows the XRD patterns with the same composition annealed at (a) 700℃ for 4 h, (b) 800℃ for 3 h, and (c) 800℃ for 4 h. From this results, all XRD patterns showed main peaks exhibited by β-$FeSi_2$ and secondary peaks exhibited by Si. This again indicates the complete decomposition of α-Fe_2Si_5 metallic phase yielding semiconducting β-$FeSi_2$/Si composite phase. In this current findings, we can say that n-type β-$FeSi_2$/Si composite with Cu addition underwent complete phase transformation at annealing temperature higher than

600℃, where β-$FeSi_2$/Si composite without Cu did not complete its phase transformation even at annealing conditions of 650℃ - 4h as discussed previously

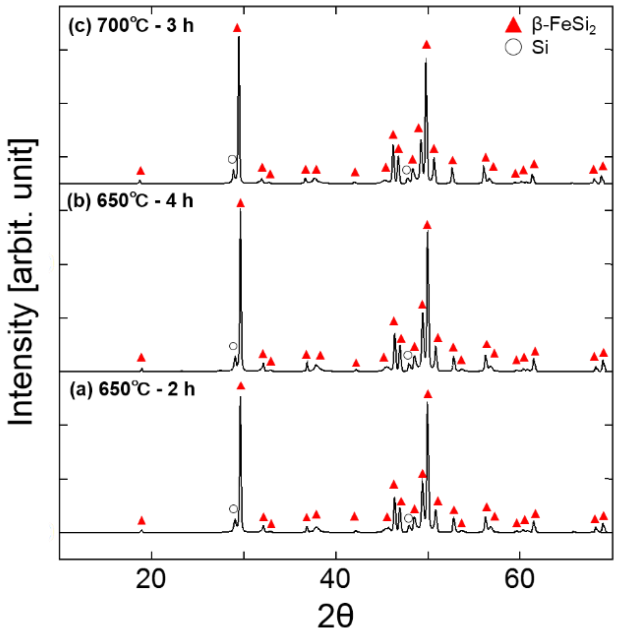

Figure 6.7 XRD patterns of $Fe_{28.49}Co_{0.59}Si_{70.5}$ + Cu at 2 mass% with various annealing conditions of (a) 650℃ at 2 h, (b) 650℃ at 4 h, and (c) 700℃ at 3 h.

We attempted to plot the phase obtained after annealing process in a time-temperature graph to determine the pattern of phase transformation analysis rate similar to the attempt done for non-doped β-$FeSi_2$/Si composites as shown in Fig. 6.9. Both of these plots form Fig. 6.4 of non-doped β-$FeSi_2$/Si composites and Fig. 6.9 of n-type β-$FeSi_2$/Si composites with 2 mass% Cu addition are then attempted to be further evaluated by setting their x-axis logarithmically in order to have a clearer observation on the possible pattern of TTT diagram as referred to previous work by J.X. Jiang et al. [2]. The approximate patterns of the TTT curves are estimated as illustrated in Fig. 6.10. The shape of the curves can typically be described by the character *'C'* and its nose temperature differs for each

composition.

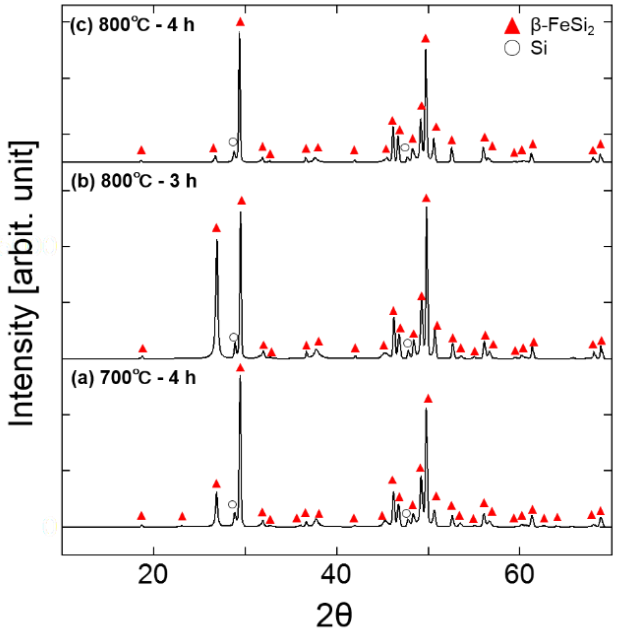

Figure 6.8 XRD patterns of $Fe_{28.49}Co_{0.59}Si_{70.5}$ + Cu at 2 mass% with various annealing conditions of (a) 700℃ at 4 h, (b) 800℃ at 3 h, and (c) 800℃ at 4 h.

.

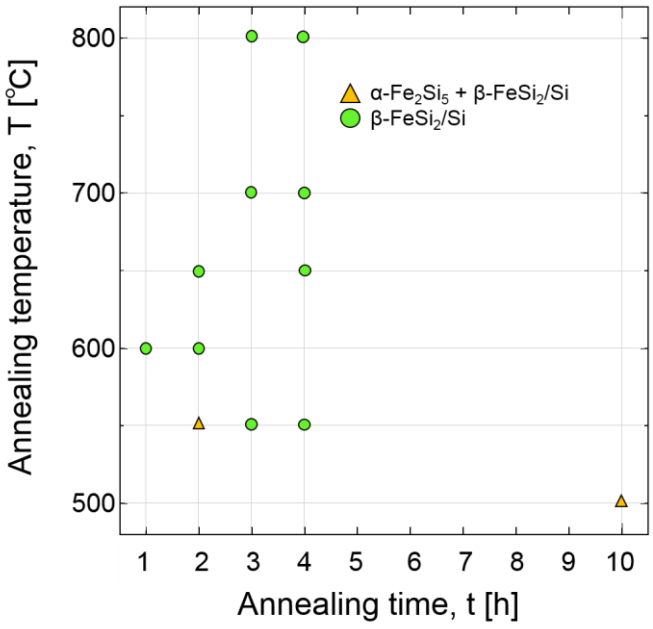

Figure 6.9 Plots of final product for n-type β-$FeSi_2$/Si composite with Cu 2 mass% after annealing in the relation of annealing time-annealing temperature.

Fig. 6.10 (a) shows the TTT curve for non-doped β-$FeSi_2$/Si composite. From here, the nose temperature is approximately at 770℃, indicating that the $Fe_{29.5}Si_{70.5}$ complete its decomposition yielding β-$FeSi_2$/Si composite at the fastest rate at this temperature. On the other hand, Fig. 6.10 (b) shows the TTT curve for n-type β-$FeSi_2$/Si composite with Cu addition at 2 mass%. From this result, the nose temperature is approximately at 620℃ for $Fe_{28.49}Co_{0.59}Si_{70.5}$ with Cu in it. Thus, it was found that the nose temperature of $Fe_{29.5}Si_{70.5}$ without Cu in it is higher than the nose temperature of $Fe_{28.49}Co_{0.59}Si_{70.5}$ with Cu at 2 mass%. This proves again that the addition of Cu clearly helps enhance the phase transformation or eutectoid decomposition of α-Fe_2Si_5 phase yielding β-$FeSi_2$/Si composite phase. Although the microstructure of these annealed samples are not evaluated, we can expect the precipitations of Si at both these nose points are at their finest condition. This estimation is considerably valid as discussed in previous chapter where the isothermal transformation rate is controlled by the nucleation and growth rates [4,6,8,13–15]. We can say that the nucleation rate increases rapidly while the growth rate decreases at lower temperature in a shorter time disallowing for growth to proceed, preserving its fine structure of Si. Therefore, the formation of Si can be expected to be its finest at this nose temperature.

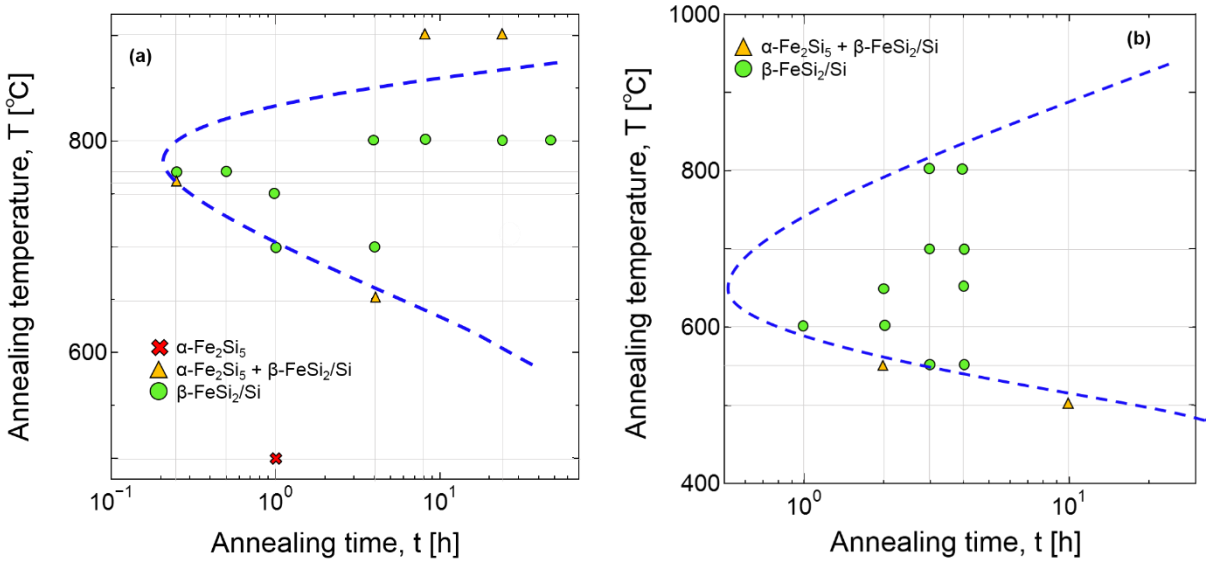

Figure 6.10 Estimated isothermal transformation diagram for (a) non doped β-$FeSi_2$/Si composite and (b) n-type β-$FeSi_2$/Si composite with Cu 2 mass% addition.

6.5 Conclusion

We summarize the findings in chapter 6 as follows

I The experimental estimation of TTT diagram for α-Fe_2Si_5 phase without Cu and α-Fe_2Si_5 with Cu were attempted to clarify the ideal annealing conditions to retrieve β-$FeSi_2$/Si heterogeneous phase and justify the effect of adding Cu as phase transformation accelerator partially proven in chapter 5. The attempt was considered successful by annealing of sintered bodies for each initial composition examined in conditions reaching more than 10 types of variations.

II The lower nose temperature of α-Fe_2Si_5 with Cu in it indicates clearly that the phase transformation occurs more rapidly. This means that Cu definitely helps accelerate significantly the decomposition of α-Fe_2Si_5 phase yielding β-$FeSi_2$/Si heterogeneous phase.

III The fastest transformation rate interpreted from the nose point of these *C* curves gives the microstructure estimation of finest Si precipitations, contributing beneficial hint for possible enhanced phonon scattering, leading to reducing thermal conductivity. Such further reduction in thermal conductivity is significant for vast enhancement of TE performance in the environmental friendly β-$FeSi_2$ based TE material.

6.6 References

[1] M. Ito, H. Nagai, D. Harimoto, S. Katsuyama, K. Majima, *Effects of Cu addition on the thermoelectric properties of hot-pressed β-$FeSi_2$ with SiC dispersion*, J. Alloys Compd. 322 (2001) 226–232.

[2] J. Jiang, K. Matsugi, G. Sasaki, O. Yanagisawa, *Resistivity Study of Eutectoid Decomposition Kinetics of α-Fe_2Si_5 Alloy*, Mater. Trans. 46 (2005) 720–725.

[3] N. Kiyoshi, K. Takuji, *Influence of Copper Addition on the Rapid Production of β-$FeSi_2$ by Spark-Plasma Sintering*, Mater. Trans. 41 (2000) 815–821.

[4] T. Nagase, I. Yamauchi, I. Ohnaka, *Eutectoid decomposition in rapidly solidified α-Fe_2Si_5-based thermoelectric alloys*, J. Alloys Compd. 316 (2001) 212–219.

[5] N. Niizeki, M. Kato, I.J. Ohsugi, Y. Isoda, H. Kohri, I. Shiota, *Effect of Aluminum and Copper Addition to the Thermoelectric Properties of $FeSi_2$ Sintered in the Atmosphere*, Mater. Trans. 50 (2009) 1586–1591.

[6] D.A. Porter, E.E. Kenneth, M.Y. Sherif, *Binary Phase Diagrams*, in : Phase Transform. Met. Alloy., 3rd ed., (2014) 31–40.

[7] F.L.B.M. Redzuan, I. Mikio, T. Masatoshi, *Synthesis of Co-doped β-$FeSi_2$/Si composites through eutectoid decomposition and its thermoelectric properties*, J. Mater. Sci. 53 (2018) 7683–7690.

[8] P.R. Rios, F. Siciliano Jr, H.R.Z. Sandim, R.L. Plaut, A.F. Padilha, *Nucleation and growth during recrystallization*, Mater. Res. 8 (2005) 225–238.

[9] H. Xie, X. Su, Y. Yan, W. Liu, L. Chen, J. Fu, J. Yang, C. Uher, X. Tang, *Thermoelectric performance of $CuFeS_{2+2x}$ composites prepared by rapid thermal explosion*, Nat. Publ. Gr. (2017) 1–12.

[10] I. Yamauchi, T. Nagase, I. Ohnaka, *Temperature dependence of β-phase*

transformation in Cu added Fe_2Si_5 thermoelectric material, J. Alloys Compd. 292 (1999) 181–190.

[11] I. Yamauchi, T. Okarnoto, H. Ohata, I. Ohnaka, *3 phase transformation and thermoelectric power in $FeSi_2$ and Fe_2Si_5 based alloys containing small amounts of Cu*, J. Alloys Compd. 260 (1997) 162–171.

[12] I. Yamauchi, A. Suganuma, T. Okamoto, I. Ohnaka, *Effect of copper addition on the β-phase formation rate in $FeSi_2$ thermoelectric materials*, J. Mater. Sci. 32 (1997) 4603–4611.

[13] L. V. Zhigilei, *Introduction to the Science and Engineering : Phase Transformation*, http://people.virginia.edu/~lz2n/mse209/index.html (Online lecture notes), MSE 2090. (2010) 16.

[14] *Introduction to Materials Science : Phase Transformations* in Metals, Univ. Tennessee, Dept. Mater. Sci. Eng.

[15] *Solid-State Phase Transformations and Reactions*, in : Ceram. Mater., Springer, New York, NY, (2007) 444–462.

Chapter 7 Conclusions and Future Perspectives

Earlier in chapter 1, the target of this work is thoroughly discussed where we aimed to clarify the processes feasible to improve both electrical and thermal properties of the β-$FeSi_2$/Si based composite towards enhancing its TE performance. Based on this aim and the attempts related, each attempt and its achievement of this work are summarized as follows.

I We attempted to synthesize β-$FeSi_2$/Si composite via the eutectoid decomposition of high temperature metallic α-Fe_2Si_5 phase, which can be obtained from annealing process. From here, we expected that the newly introduced β-$FeSi_2$/Si based composite with significantly accelerated time of synthesis to be consisting of fine Si precipitations within the main β-$FeSi_2$ phase. Subsequently, the fine precipitations may help further reduce thermal conductivity. We found that β-$FeSi_2$/Si composite can be synthesized by the annealing of high temperature metallic α-Fe_2Si_5 phase with its essential and well-balanced condition of annealing time and temperature. Furthermore, we revealed that sintered bodies of β-$FeSi_2$/Si composite are proven not only to be viable for evaluation in high temperature environment but also with improved electrical characteristic due to distinct reduction of cracks within the produced samples.

II We then tried to improve electrical properties of the β-$FeSi_2$/Si composite

without deteriorating its thermal properties by adding n-type dopants. First, doping of Co is expected to cause substitution of Co atoms for Fe atoms within the main phase of β-$FeSi_2$. This attempt was carried out by the annealing of high temperature metallic phase of α-Fe_2Si_5. Here, various annealing conditions were examined resulting to the most enhanced TE properties at annealing temperature of 800℃ and annealing time of 4 h. The significant enhancement of TE properties was dominated by the increased value of Seebeck coefficient, thus enhancing its TE properties with the ZT value enhancement from approximately 0.05 to 0.08, which is higher than that of the former Co doped β-$FeSi_2$ singular phase. Effects of Si dispersion within β-$FeSi_2$ phase matrix were then evaluated by the rule of mixture, indicating that the finely distributed secondary phase of Si helps reduce thermal conductivity, leading to the potential application for the future on enhancing thermoelectric performance of β-$FeSi_2$ system.

III Then, simultaneous doping of P to the Co doped β-$FeSi_2$/Si composites using the same process described above was tried. Here, P atoms were expected to be substituted with Si atoms in the secondary phase of precipitated Si. The attempt was found successful as the evaluation from the phase and microstructure analysis showed a complete decomposition from α-Fe_2Si_5 phase to β-$FeSi_2$/Si heterogeneous phase, annealed at 800℃ for 4h, and P was not found in the β-$FeSi_2$ main phase. However, P was found not to be distributed uniformly within the secondary phase of Si. On the other hand, P contributes to the further decrease in electrical resistivity of Co doped β-$FeSi_2$/Si composite while further revealing a reduction in thermal conductivity possibly

due to the reduced thermal conductivity of Si precipitates with P intervention in them. It was also found that the excessive amount of P contributes to grain coarsening of Si phase. The highest ZT value was obtained by the composite with the composition of $Fe_{28.49}Co_{0.59}Si_{70.5-x}P_x$ at x = 2.82 at%, indicating a distinct improvement compared to the Co doped β-$FeSi_2$/Si composites without P in them.

IV We tried to add Cu to the Co doped β-$FeSi_2$/Si composite to further improve its thermal properties from the possible reduction of Si size. We revealed that the addition of Cu helped accelerate the phase decomposition of α-Fe_2Si_5 phase yielding β-$FeSi_2$/Si phase, leading to finer precipitations of Si. This was proven by not only the complete decomposition of α-Fe_2Si_5 phase at a lower temperature and for shorter time of 650℃ - 2 h with reduced Si size, compared to the composites with less Cu in them, but also the enlargement of Si size after annealed at higher temperature and longer holding time of 800℃ - 4 h. We obtained the smallest size of Si phase within β-$FeSi_2$ phase (finest Si precipitations) in composite with maximum amount of Cu, in this case at 2 mass %. The thermal conductivity of β-$FeSi_2$/Si composite with Cu 2 mass%, annealed at 650℃ for 2 h exhibited a significant reduction, and was even lower than the thermal conductivity of Co doped β-$FeSi_2$ singular phase. This is proven to be influenced by the great reduction of Si size reaching lower than 100 nm.

V We tried tuning various annealing conditions in the effort not only to control the size of Si, but also to anticipate the annealing conditions that may result to reduced Si size contributing further to the reduction of thermal conductivity.

The significant reduction of Si was expected to enhance phonon scattering causing the reduction of thermal conductivity. We evaluated the phase transformation kinetics of α-Fe_2Si_5 phase by experimenting on various annealing conditions. From here, we discovered the approximate fastest rate of eutectoid decomposition for α-Fe_2Si_5 yielding β-$FeSi_2$/Si composite by estimating the characteristics of phase transformation rate from the TTT diagram. The nose point of the estimated TTT diagram is expected to exhibit the fastest rate for α-Fe_2Si_5 to be decomposed completely yielding β-$FeSi_2$/Si composite. Here, we estimate the microstructure of synthesized composite to have the finest precipitations of Si with the most reduced value of thermal conductivity, which needs further examinations.

In total, we successfully provide solid strategies possible to help improve both electrical and thermal properties of β-$FeSi_2$/Si composites, thus enhancing its TE performance.

From here, we propose possible future investigations to further enhance TE performance of the environmental friendly and low cost β-$FeSi_2$/Si based composite.

I Add phase transformation accelerator element (Cu) to the jointly doped β-$FeSi_2$/Si composites with P and Co to both retrieve distinct enhancement of electrical properties followed by suppression of thermal conductivities from the finer precipitations of Si.

II Examine more annealing conditions to determine the fastest rate for the decomposition of α-Fe_2Si_5. Finest precipitations of Si can be expected from the microstructure evaluation at the fastest phase transformation rate, thus leading to further reduction of Si small enough to suppress thermal conductivity.

We believe that these attempts are beneficial towards both properties enhancement and further expanding the route for nano-structuring of bulk β-$FeSi_2$ based TE materials. This is expected to be essential towards vast improvement of this material's performance itself, providing a promising future for its wide practical application in the TE research field.

List of Contributions

Publications

1. **F.L.B.M. Redzuan**, M. Ito, M. Takeda, '*Synthesis of Co doped β-$FeSi_2$/Si composites through eutectoid decomposition and its thermoelectric properties*', published in the Journal of Materials Science, vol. 53, issue 10, pp. 7683-7690, (doi : 10.1007/s10853-018-2066-1)
2. **F.L.B.M. Redzuan**, M. Ito, M. Takeda, '*Phosphorus doping in n-type β-$FeSi_2$/Si composites and its effects on thermoelectric properties*', published in the Journal of Intermetallics, vol. 108, pp. 19-24, (doi : 10.1016/j.intermet.2019.02.008)
3. **F.L.B.M. Redzuan**, M. Ito, M. Takeda, '*Effects of Cu addition to n-type β-$FeSi_2$/Si composite on the Si precipitation and its thermoelectric properties*', published in the Journal of Materials Science : Materials in Electronics, vol. 30, issues 13, pp 12234-12243, (doi : 10.1007/s10854-019-01582-9)

International Conference Presentations

1. **F.L.B.M. Redzuan**, M. Ito, M. Takeda, '*Influence of phosphorus addition to the microstructure of n-type β-$FeSi_2$/Si Duplex Composites*', 4th International Conference on Powder Metallurgy in Asia of the Japan Society of Powder and Powder Metallurgy (April 2017)
2. **F.L.B.M. Redzuan**, M. Ito, M. Takeda, '*Effects of Cu addition to Si precipitation in β-$FeSi_2$/Si composite and its thermoelectric properties*', 60th Anniversary International Conference in Powder and Powder Metallurgy of the Japan Society of

Powder and Powder Metallurgy (November 2017)

3. **F.L.B.M. Redzuan**, M. Ito, M. Takeda, '*Influence of Cu addition to Si precipitations in n-type β-$FeSi_2$/Si composite and its thermoelectric properties*', 5th International Conference on Material Science & Smart Materials (August 2018)
4. M.Ito, **F.L.B.M. Redzuan**, M. Takeda, '*Thermoelectric performance of heterogeneous β-$FeSi_2$/Si composites synthesized by eutectoid decomposition*', 5th Global Conference on Polymer and Composite Materials (April 2018)
5. M.Ito, **F.L.B.M. Redzuan**, M. Takeda, '*Effects of P doping on the thermoelectric performance of heteregenous β-$FeSi_2$/Si composites*', International Conference in Processing and Manufacturing of Advanced Materials, Processing Fabrication, Properties, Applications THERMEC 2018 (July 2018)

National Conference Presentations

1. **F.L.B.M. Redzuan**, M. Takeda, '*Themoelectric of Si precipitated β-$FeSi_2$ and its microstructure analysis*' 5th Micronano Engineering Symposium (November 2013)
2. **F.L.B.M. Redzuan**, M. Takeda, '*Thermoelectric properties and microstructure of β-$FeSi_2$/Si Composite'*, 154th Annual Spring Meeting of the Japan Institute of Metals and Materials. (March 2014)
3. **F.L.B.M. Redzuan**, M. Ito, M. Takeda, '*Synthesis of n-type β-$FeSi_2$/Si Composite by eutectoid decomposition and its thermoelectric properties*' 13th Annual Meeting of the Thermoelectrics Society of Japan (September 2016)
4. **F.L.B.M. Redzuan**, M. Ito, M. Takeda, '*Effects of fine Si Precipitation in the thermoelectric properties of n-type β-$FeSi_2$/Si Composites*', 118th Annual Autumn

Meeting of the Japan Society of Powder and Powder Metallurgy. (November 2016)

5. **F.L.B.M. Redzuan**, M. Ito, M. Takeda, '*Thermoelectric performance of phosphorus doped n-type heterogeneous β-$FeSi_2$/Si Composites*', 119th Annual Spring Meeting of the Japan Society of Powder and Powder Metallurgy. (May 2017)
6. **F.L.B.M. Redzuan**, M. Ito, M. Takeda, '*Thermoelectric properties of phosphorus and cobalt doped β-$Fesi_2$/Si composites and its microstructure*', 14th Annual Meeting of the Thermoelectrics Society of Japan. (September 2017)